2010-07-15

# Numerical Simulation of Atmospheric Internal Waves with Time-Dependent Critical Levels and Turning Points

Brian Patrick Casaday
*Brigham Young University - Provo*

# Numerical Simulations of Atmospheric Internal Waves with Time-dependent Critical Levels and Turning Points

Brian P. Casaday

A thesis submitted to the faculty of
Brigham Young University
in partial fulfillment of the requirements for the degree of

Master of Science

Julie C. Vanderhoff, Chair
Scott L. Thomson
Steven E. Gorrell

Department of Mechanical Engineering

Brigham Young University

August 2010

ABSTRACT

Numerical Simulations of Atmospheric Internal Waves

with Time-dependent Critical Levels

and Turning Points

Brian P. Casaday

Department of Mechanical Engineering

Master of Science

Just as water surface waves are found everywhere on the ocean's surface, internal waves are ubiquitous throughout the atmosphere. These waves constantly propagate and interact with other flows, but these interactions are difficult to observe due to inadequate current technology.

Numerical simulations are often utilized in the study of internal waves. In this work, ray theory is used to numerically simulate the interaction of atmospheric internal waves with time-dependent and time-independent background flows, specifically the interaction of small-scale internal waves and large-scale inertial waves. Parameters such as initial wavenumbers and amplitudes of both small internal waves and inertial waves are determined that will cause the small waves to reach a turning point or critical level, or in the case of time-dependent flows, a wavenumber that reaches a critical value. Other parameters that may cause the waves to become unstable are included in the analysis, such as wave steepness and shear instability. These parameters are combined to determine the spectrum of waves that will experience instability during the interaction.

Two principal interactions, small-scale internal waves propagating through an infinite wave train and small-scale internal waves propagating through an inertial wave packet, are simulated and compared. For the first interaction, the total frequency is conserved but is not for the latter. This deviance is measured and results show how it affects the outcome of the interaction. The interaction with an inertial wave packet compared to an inertial wave train results in a higher probability of reaching a Jones' critical level and a reduced probability of reaching a turning point, which is a better approximation of outcomes experienced by expected real atmospheric interactions.

Keywords: Brian Casaday, internal waves, ray theory, critical level

# ACKNOWLEDGMENTS

The author graciously acknowledges the assistance of his advisor, Dr. Julie Vanderhoff, and Dr. Scott Thomson and Dr. Steven Gorrell of his graduate committee, and fellow researchers in contributing to this research. He is also appreciative of the mentoring received from his graduate committee, for their encouragement and advice regarding general life educational pursuits.

TABLE OF CONTENTS

LIST OF FIGURES

LIST OF VARIABLES

| | |
|---|---|
| $x$ | Position in x – direction |
| $y$ | Position in y – direction |
| $z$ | Position in z – direction |
| $t$ | Time |
| $\rho$ | Density |
| $p$ | Pressure |
| $g$ | Gravity |
| $\vec{k}$ | Internal wave wavenumber, $\vec{k} = 2\pi / \vec{\lambda}$ where $\vec{\lambda}$ = internal wave wavelength |
| $k$ | Internal wave wavenumber in x – direction for small wave |
| $l$ | Internal wave wavenumber in y – direction for small wave |
| $m$ | Internal wave wavenumber in z – direction for small wave |
| $K$ | Internal wave wavenumber in x – direction for inertial wave |
| $L$ | Internal wave wavenumber in y – direction for inertial wave |
| $M$ | Internal wave wavenumber in z – direction for inertial wave |
| $k_H$ | Horizontal wavenumber, $k_H = \sqrt{k^2 + l^2}$ |
| $f$ | Coriolis frequency, $f = 2\Omega_E \sin\varphi$, where $\Omega_E$ = the rotational rate of the earth and $\varphi$ = latitude. |
| $N$ | Buoyancy frequency (also referred to as natural frequency or Brunt Väisälä frequency) |
| $\omega$ | Internal wave frequency |
| $\Omega$ | Internal wave total frequency |
| $c$ | Internal wave phase speed |
| $c_g$ | Internal wave group velocity |
| $c_{gx}$ | Internal wave group velocity in x – direction |
| $c_{gy}$ | Internal wave group velocity in y – direction |
| $c_{gz}$ | Internal wave group velocity in z – direction |
| $\vec{V}$ | Background wind velocity |
| $U$ | Background wind velocity in x – direction |
| $V$ | Background wind velocity in y – direction |
| $W$ | Background wind velocity in z – direction |
| $u'$ | Perturbation velocity in x – direction for internal wave |
| $v'$ | Perturbation velocity in y – direction for internal wave |
| $w'$ | Perturbation velocity in z – direction for internal wave |
| $A$ | Internal wave action density |
| $\varsigma_z$ | Vertical wave steepness, $\lvert\varsigma_z\rvert = k\left(\frac{2A}{\omega\rho}\right)^{1/2}$ |
| $Ri_g$ | Gradient Richardson number |
| $\forall$ | Volume |
| | Subscript $_0$ refers to initial condition |

# 1 INTRODUCTION

Internal gravity waves exist abundantly in stably-stratified fluids, such as the ocean and atmosphere. A stably-stratified fluid is one where the density of the fluid continuously decreases with increasing elevation. When a finite amount of fluid from a stratified environment is displaced from its equilibrium density location by moving it vertically, gravitational and buoyant forces will compel the fluid to return to its original location. Momentum forces will cause the fluid to move past its original location, inciting an oscillation at the natural, or buoyancy frequency of the fluid. If the fluid is forced to oscillate at any frequency below the buoyancy frequency, it will oscillate in the horizontal directions in addition to the vertical direction. These multidimensional oscillations are internal gravity waves. Internal wave propagation occurs throughout the fluid in three dimensions, without restriction to any horizontal plane of a liquid-gas interface like surface waves. Because the waves propagate in three dimensions, the wavelength consists of three spatial components. The internal wave phase propagation is orthogonal to the wave group velocity, which is also the direction of energy propagation.

Naturally occurring perturbations in stratified fluids create internal waves, such as air or water currents moving over topography, as shown in Figure 1.1. Other sources of internal wave generation include changes in temperature, storms and other fluid interactions, or the breakdown of large waves into smaller waves and turbulence. Internal waves in the atmosphere range widely in size, with vertical wavelength scales from meters to kilometers, and horizontal wavelengths of

tens of meters to thousands of kilometers. Due to their large size and prevalence, internal waves store and transport significant kinetic and potential energy.

These waves affect the dynamics of the ocean and atmosphere. Internal waves transport momentum and energy and can contribute to driving large-scale flows. Internal wave breaking contributes to the mixing of pollutants and heat in the ocean and atmosphere, maintaining environmental energy balances. Wave breaking also mixes the surrounding fluid, reducing the local stratification of the fluid, and causes fluid circulations and wave generation. Even though significant internal wave generation occurs near the earth's surface, the waves generally propagate toward the upper atmosphere where they are a principal contributor to mixing and circulation. In the ocean, waves generated at mid-depths can propagate into the deep ocean, mixing regions which would otherwise be stagnant. Many technical and environmental fields are affected by internal waves, and a better understanding is necessary for accurate climate models, pollution control, and for improving aerospace applications.

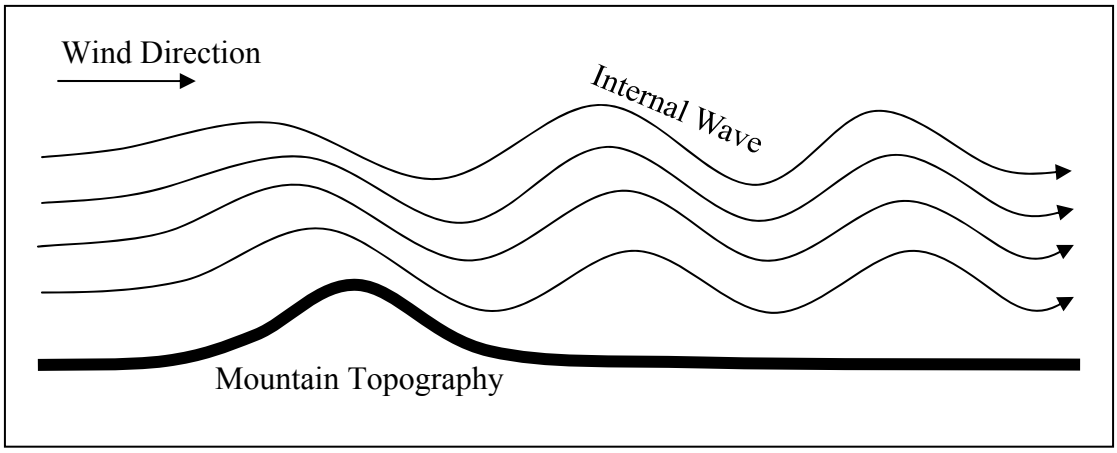


**Figure 1.1 Lines of constant density illustrate how flow over topography is a source of internal wave generation.**

When internal waves interact with other flows, properties of the internal waves may change, such as wavenumbers, frequency, and amplitude. Internal waves may also transfer their momentum and energy to the flow with which they interact, such as winds or other waves. Figure 1.2 shows three outcomes of internal waves approaching a mean wind, showing the energy propagation trajectories of multiple internal wave packets. The outcomes of interactions discussed in this thesis may be summarized by the following list.

- Free propagation indicates that the internal waves are able to propagate through the interacting flow. Properties such as wavenumbers, frequency, and amplitude may temporarily change during the interaction but typically are not significantly changed permanently.

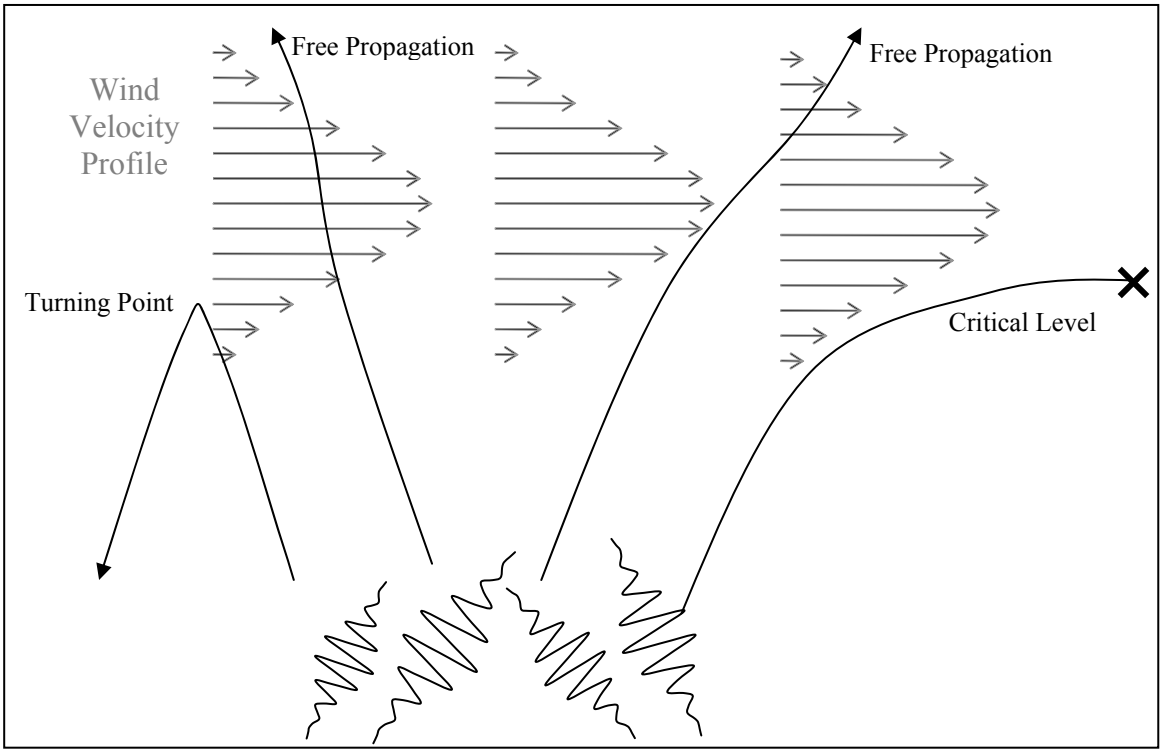


**Figure 1.2 Internal Waves propagate upward toward a mean wind. Waves may reach a critical level, turning point, or freely propagate through the wind.**

- A critical level represents a region where approaching internal waves transfer their energy to the flow with which they are interacting, referred to as the background flow. It is characterized by a region where wind in the same direction of internal wave propagation turns the waves horizontally and causes the frequency of the waves to diminish toward zero. The waves may become absorbed into the background flow, or the waves may become unstable and overturn, and hence cease propagation beyond this point. A critical level also represents a boundary where internal waves are unable to pass.
- A turning point is a region where internal waves are reflected and their vertical energy propagation direction changes sign. The horizontal propagation direction does not change for interactions discussed in this thesis. A turning point is characterized by a region where wind in the same opposite direction of internal wave propagation causes the frequency of the waves to increase toward the buoyancy frequency of the fluid, which is the maximum frequency at which internal waves may exist.
- A Jones' critical level (Jones 1967) is similar to a regular critical level in that it is a region where internal waves transfer their energy and become absorbed by the background flow or become unstable and overturn. It is different than a regular critical level in that it is characterized by internal waves reaching a critical wavenumber as opposed to a frequency that diminishes toward zero. This type of outcome occurs for time-dependent interactions and is later discussed in results section 3.2.
- Waves may also become unstable due to excessive wave steepness or excessive shear, which will be discussed in the results section.

More details about these outcomes will be discussed in subsequent sections.

## 1.1 Literature Review

Numerous obstacles hinder the study of atmospheric internal waves. The scales of practically applicable flows in the atmosphere range in size from hundreds of kilometers for global currents to millimeters or smaller for turbulence, creating a series of problems regarding observational data collection and the resolution of multidimensional nonlinear numerical models. To account for these complications, and to reduce computational cost, numerical models are often simplified by adopting linearized equations or resolving in only two dimensions. These simplifications result in limitations for which, with the onset of turbulence, linear models break down and two-dimensional models lose validity. However, simplified models are usually preferred when multiple interactions are analyzed or where the small-scale flow dynamics are not important for the study. Nappo (2002) explained that linear simulations were generally adequate and often preferred for many internal wave simulations in the middle and upper atmospheres. Winters and D'Asaro (1994) also showed that two-dimensional simulations are adequate for internal wave propagation and interaction prior to wave breaking and turbulence. One of these models utilizes ray theory, resulting in a linear model capable of simulating internal wave interactions at little computational cost.

Many researchers have used ray theory to study the propagation and interaction of internal waves, including Eckermann (1997), Vanderhoff (2008), Broutman and Young (1986), Bruhwiler and Kaper (1995) and Sartelet (2003). In ray theory, the Navier-Stokes equations are linearized and simplified to simulate internal wave propagation. Ray Theory approximates the internal wave properties, including wavenumbers and frequencies of internal waves, as they propagate through slowly varying background flows. This method bypasses the need to track

individual particle velocities or properties at all times and in space, significantly reducing the computational cost, and will be further discussed in the methods section.

Of particular interest are interactions of internal waves with other geophysical flows, such as the interaction between small-scale internal waves and a strong steady shear where the background wind continuously changes with altitude. These are common in the atmosphere due to basic winds and temperature variations over regions where internal waves are generated. One potential outcome of this interaction may be a critical level, where the frequency of the internal waves approach zero. Critical levels are common in the atmosphere. The background shear, or increase of horizontal velocity with elevation, alters the propagation of the internal waves such that the vertical velocity of the energy propagation decreases as the internal waves asymptotically approach the critical level, but do not actually reach it. (See Figure 3.3 in Results section) A critical level represents a boundary where instability is likely to occur, and linear theory predicts that internal waves are incapable of propagating beyond these regions. Other dynamics will be shown in the methods and results section.

Winters and D'Asaro (1989) numerically studied the interaction of an internal wave packet, or group of internal waves, approaching a mean flow with a critical level. They showed that if the amplitude of the waves is sufficiently small, energy from the wave packet approaching a critical level will be absorbed by the background flow, accelerating the flow near that region. Virtually no wave energy propagated beyond the critical level, and almost all wave energy was absorbed by the background from the internal wave packet in the form of horizontal momentum. They performed another numerical experiment where the amplitude of the waves was three times as large, and the waves would steepen as they approached the mean flow, analogous to surface water waves approaching a shore. This steepening caused the waves to overturn and break, as

discussed in greater detail in Winters and D'Asaro (1994). As these waves steepened and overturned, energy was lost to turbulence and viscous dissipation. Density perturbations due to overturning waves also generated new, smaller internal waves that propagated beyond the original critical level. These waves were not affected by the original critical level because their new properties define a different critical level. This phenomenon of internal waves approaching a critical level contributes to driving some mean circulations in the atmosphere.

In addition to creating new waves or accelerating the mean flow, another consequence of overturning waves near critical levels is turbulent mixing, which acts to mix the stratified environment and causes it to become homogenous within the mixed region. These results were confirmed by Javam and Redekopp (1998) who showed that instability was likely to occur in the vicinity of a critical level when the amplitude of the internal wave packet is relatively large in relation to the background flow. This instability caused the waves to break and mix the surrounding fluid.

Thorpe (1981) experimentally researched the interaction of internal waves and critical levels and found that numerical models were surprisingly accurate in predicting wave behavior. He concluded that linear approximations for internal wave propagation were valid until the local Richardson number, a ratio of the buoyancy frequency to the background shear, fell below a value of about 1.5. Gravitation instability became apparent with a background Richardson number of about 1.0, and Winters and D'Asaro (1989) confirmed that instability set in at a local Richardson number below about 0.25 due to both the background shear and internal wave shear. This research is advantageous in showing both where linear models remain valid, as well as predicting where instability may occur.

Godoy-Diana (2006) experimentally researched the interaction of an internal wave packet approaching a pancake dipole vortex (see paper for description). Although the complete interaction is complex, they showed that the internal waves propagating in the same horizontal direction as the dipole reached a critical level when the frequency of the waves diminished to zero. They also concluded that the waves experienced reflection when they propagated from the opposite horizontal direction as the dipole and the relative frequency of the waves approached the natural frequency of the fluid near the turning point. Similar scenarios are successfully predicted by ray theory in the results section.

Linear models are advantageous for internal wave propagation and critical level simulations due to significantly increased computational speed. This research is helpful in understanding large-scale energy budgets and knowing where critical levels exist, therefore knowing where wave energy is distributed or dissipated. Steady critical levels have been extensively studied, both numerically and experimentally, yet less research has been done with time-dependent background flows, which are very prevalent in the environment.

Particular interest exists in the interaction between small-scale internal gravity waves and large-scale gravity waves, referred to as inertial gravity waves due to their frequency being close to the Coriolis frequency, and thus defined by inertial effects. Despite difficulty in detecting large multidirectional flows far from the Earth's surface, numerous researchers have studied these waves through observation in the atmosphere, including Thompson (1978), Sato, O'Sullivan, and Dunkerton (1997), and Guest, Reeder, Marks, and Karoly (1999). All sources found similar properties of the inertial waves, with vertical wavelengths between 1 and 7 km and horizontal wavelengths on the scale of 1000 km. The frequencies of the inertial waves were near the Coriolis frequency, the phases of the waves propagated downward and the energy propagated

upward. Thompson (1978) showed the source of inertial waves is generally near the earth's surface, propagating upward and thus they are commonly found in the stratosphere. Sato, O'Sullivan, and Dunkerton (1997) detected inertial gravity wave packets 20 – 24 km over Shigaraki, Japan which had horizontal wind oscillations of about 2.5 to 3 m/s. Other background winds in the vicinity of the waves were relatively small. Because these inertial waves are common in the stratosphere, and internal waves are constantly being generated in the troposphere near the earth's surface, the interaction between upward propagating internal waves and inertial waves is expected to be a regular occurrence.

Various models have been used to predict the results of this type of interaction. Broutman and Young (1986), Sartelet (2003), Bruhwiler and Kaper (1995), and Vanderhoff (2007) used ray theory to study the interaction of small-scale internal gravity waves and large-scale inertial gravity waves, particularly in the oceans where the vertical phase speed of the inertial wave and small internal wave group velocity usually move in opposite directions. This research discussed regions, referred to as caustics, where the smaller internal waves experience strong refraction, or quick changes to wavenumbers and group velocity. The research successfully predicted the changes in wave frequency and propagation direction, as well as the changes in wave amplitude through space and time. Broutman and Young (1986) also explained that the total frequency of the waves, defined by equation 2.16, remains constant in time-independent background flows, but is not required to remain constant during time-dependent flows. This type of scenario is possible in the atmosphere, although the inertial waves and other internal waves typically propagate in the same direction.

Eckermann (1997) used ray theory to study the interaction between small-scale internal waves and both a time-independent background shear and a time-dependent background wave

where the vertical phase velocities of the interacting waves were in the same direction. Ray theory assumes that the background flow is not affected by the internal wave or its interaction. The large-scale waves were therefore not affected in Eckermann's simulations. He showed that for time-independent background shear, in addition to critical levels for certain interactions, there exists a critical vertical wavenumber for the small wave. This means that for a range of small waves, with differing frequencies or wavenumbers, all waves with a vertical wavelength smaller than a critical value would encounter either a critical level or a turning point when approaching the time-independent background wave of specified amplitude. He also showed in addition to this critical vertical wavenumber, there is also a critical horizontal wavenumber, which is a value near half of the vertical wavenumber. He confirmed that a critical level occurs when the frequency of the small wave approaches the local Coriolis frequency, and a turning point occurs when the frequency approaches the local buoyancy frequency. In these scenarios, like the scenarios in this research, there were no vertical background velocities, due to a background horizontal wavenumber of zero. For two-dimensional simulations such as these, the absence of vertical background velocities causes the horizontal wavenumbers of the small waves to remain constant throughout the interaction, and only the vertical wavenumber may change.

For the time-dependent background waves, Eckermann studied the interaction of upward propagating internal waves with inertial waves that had downward propagating phases. The background wave phases propagate with a speed equal to the Coriolis frequency divided by its vertical wavenumber. These time-dependent background flows significantly changed the interaction results for the small wave. One purpose of this study was to determine if the small waves encountered time-dependent critical levels, comparable to the time-independent case. Eckermann confirmed that the small waves did not encounter any critical level, for the

oscillations from the background flow did not cause the relative frequency of the small wave to decrease toward zero at any particular location, but would rather cause the small wave frequency to oscillate through periods of the background wave.

The small waves did, however, reach critical wavenumbers, which were large relative to the initial wavenumbers or fluid environment, and the small waves were assumed to overturn and be dissipated by turbulence at this point. This is referred to as a Jones' critical level. The waves in these simulations were also less likely to reach a turning point, compared to the time-independent simulations. Some of these results are shown in Figure 1.3, and are replicated and expanded in the results section. The figure shows the outcomes of numerous small internal waves interacting with an inertial wave with a phase speed of 0.1 m/s in the downward direction. The horizontal axis represents the initial vertical wavenumber of the small waves and the vertical axis represents the initial frequency of the small waves. The outcomes are indicated by symbols

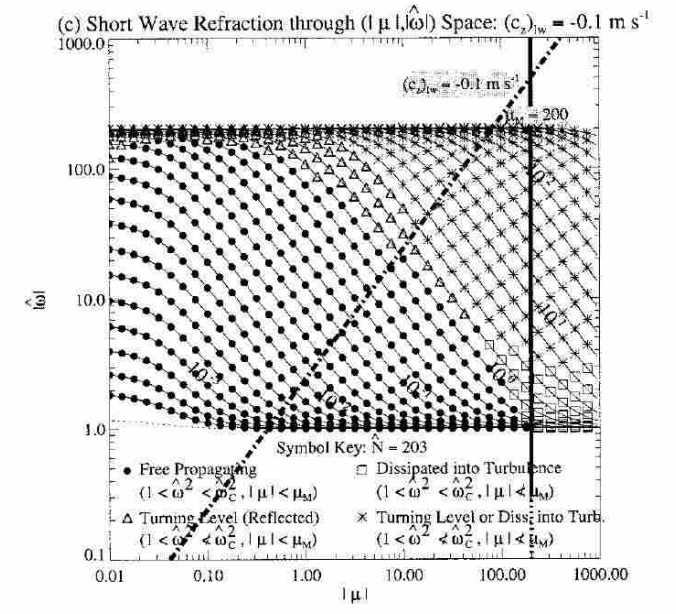


**Figure 1.3 Results of internal waves interacting with an inertial wave train, taken from Eckermann (1997) Figure 8c.**

on the plot, where squares represent waves that reached a Jones' critical level, triangles represent turning points, asterisks represent Jones' critical levels or turning points, and circles represent waves that freely propagate through the inertial wave. In all these simulations, the time-dependent background flows were assumed to be infinite wave trains, where small waves would propagate through sinusoidal background waves. In reality, however, atmospheric background waves exist as packets, or rather as spatial envelopes that contain a finite number of wavelengths.

Sartelet (2003) used ray theory to study the interaction of small waves with large background waves where the background waves exist as a wave packet contained within a spatial envelope. In ray tracing, internal waves are tracked using rays that show the position of the wave group in space and time. Sartelet showed that, with an infinite series of background waves as in Eckermann's research, these rays would all follow similar trajectories and never cross other rays except in situations where the waves are reflected. In simulating waves propagating through a finite wave packet, some rays would cross over other rays during the interaction with the

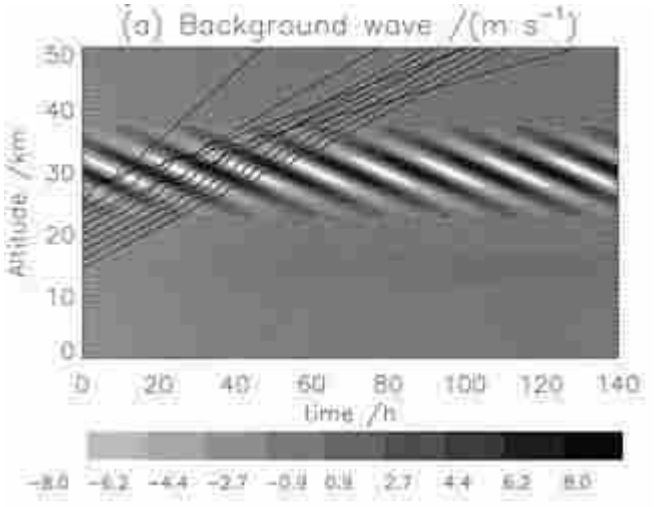


**Figure 1.4 Results of internal wave rays propagating through an inertial wave packet, taken from Sartelet (2003) Figure 2a. Most rays follow similar trajectories, but some do not because they are initialized in a nonzero background velocity.**

background flow, as shown in Figure 1.4. These rays did not follow similar trajectories and some waves were permanently changed after the interaction.

However, the rays that were permanently changed in these simulations were initialized in the background field with a nonzero background velocity. In other words, all of the rays were assumed to be identical waves at the beginning of the simulation, yet some rays were inserted into the background wave packet unaffected, and would have been altered had they propagated toward that location. Had the rays been initialized far below the background wave packet, where the background flow is near zero, it is the author's opinion that the rays would have all followed similar trajectories and experienced similar interactions, and thus differs from the results of Sartelet. The results section confirms that the rays follow similar trajectories but shows that some slight variance may exist between the rays and this variance is dependent on certain properties of the background wave.

This paper will further investigate the interaction between small-scale internal wave packets and background flows. Interactions with time-independent flows will be parameterized so that critical levels or turning points may be predicted based on the initial internal wave properties and the background flow field. These same parameters will be found for the interactions between internal waves and large-scale inertial waves, both in the form of infinite wave trains and inertial wave packets contained within a spatial envelope. In addition to predicting instability due to critical levels, other forms of instability, such as excessive wave steepening or shear-induced instability will be discussed. Interactions will principally adopt atmospheric conditions, where the buoyancy frequency is constant for a specified region and where both inertial phase speeds and small internal wave phases are propagating in the same vertical direction. Ray theory is used to determine if and where turning points or critical levels

occur both spatially and temporally. Differences between the types of scenarios will be discussed as well as whether the waves maintain a constant total frequency. In simulations where total frequency is not constant, results will measure the deviation and provide practical conclusions for the difference.

# 2 METHODS

This section discusses the equations used in ray theory to simulate the propagation of internal waves. It discusses the assumptions that are made to the governing fluids equations and the resulting simplified equations.

## 2.1 WKBJ Approximation

The WKBJ approximation (Wentzel, Kramer, Brullion, Jeffreys) is a set of assumptions that the waves' properties only slightly change over a wavelength or period of the internal wave during propagation. The result is applied to linear theory such that the energy of individual waves can be easily traced. This is commonly called ray theory. It can be used to simulate the interaction of internal waves propagating through a variety of background flow fields. This method is derived from the linearized Navier-Stokes equations and calculates the dynamic properties of the internal waves as they propagate through background flows. This theory follows the energy of the waves with the wave packet's group velocity. It does not account for individual crests, troughs, or particle motions of the wave, but treats each wave or wave packet as an individual ray containing wave properties, such as frequencies, amplitudes, and wavenumbers.

To use linear ray theory, the following assumptions, in addition to WKBJ, are made.

- The interaction of the internal waves does not affect or change the background flow field.
- Buoyancy frequency is constant.
- The theory is valid prior to wave breaking or reflection.

A ray tracing program was written in MATLAB, using the WKBJ approximation and a fourth order Runge-Kutta method for solving differential equations (See Appendix D). It applies the linear dispersion relation, which relates the frequency and wavenumbers, and ray equations to idealized background flows to simulate the propagations and interactions of internal waves. These defining equations will be shown in the next section.

## 2.2 The Linear Internal Wave Dispersion Relation

The linear dispersion relation defines the relationship between the frequency of internal waves and wavenumbers, and is necessary for determining the equations that define internal wave propagation. The linear dispersion relation for internal waves is defined by the Navier-Stokes equations and continuity equation. It is assumed that the fluid is both incompressible and inviscid, which are acceptable assumptions for atmospheric internal waves where the fluid particle velocities due to the wave are small. The dispersion relation is derived from the inviscid momentum and continuity equations listed below.

$$\rho \frac{Du'}{Dt} = \frac{-\partial p'}{\partial x} + \rho g_x \tag{2.1a}$$

$$\rho \frac{Dv'}{Dt} = \frac{-\partial p'}{\partial y} + \rho g_y \tag{2.1b}$$

$$\rho \frac{Dw'}{Dt} = \frac{-\partial p'}{\partial y} + \rho g_z \tag{2.1c}$$

$$\frac{\partial u'}{\partial x} + \frac{\partial v'}{\partial y} + \frac{\partial w'}{\partial z} = 0 \tag{2.2}$$

$$\frac{D\rho}{Dt} = 0 \tag{2.3}$$

Pressure and density are defined within a stratified fluid as follows.

$p = \overline{p} + p'$ where $p'$ is the perturbation pressure and the hydrostatic pressure $\overline{p} = \left(\rho_0 + \overline{\rho}\right)gh$.

$\rho = \rho_0 + \overline{\rho} + \rho'$ where $\rho'$ is the perturbation density, $\rho_0$ is a constant reference density and $\overline{\rho} = f(z)$, signifying that the average density is only a function of elevation. The Boussinesq approximation is applied here, which states that $\rho'$ is only significant when multiplied by gravity. A force balance on a fluid particle in a stably-stratified fluid results in the following equation for the natural frequency *N* of the resulting motion.

$$N^2 = \frac{\partial \overline{\rho}}{\partial z}\frac{g}{\rho_0} \tag{2.4}$$

According to the Boussinesq approximation, and assuming $\rho\frac{D\bar{u}'}{Dt} \approx \rho_0 \frac{D\bar{u}'}{Dt}$, the momentum equations become

$$\frac{\partial u'}{\partial t} + u'\frac{\partial u'}{\partial x} + v'\frac{\partial u'}{\partial y} + w'\frac{\partial u'}{\partial z} = \frac{-\partial p'}{\partial x}\frac{1}{\rho_0} \tag{2.5a}$$

$$\frac{\partial v'}{\partial t} + u'\frac{\partial v'}{\partial x} + v'\frac{\partial v'}{\partial y} + w'\frac{\partial v'}{\partial z} = \frac{-\partial p'}{\partial y}\frac{1}{\rho_0} \tag{2.5b}$$

$$\frac{\partial w'}{\partial t} + u'\frac{\partial w'}{\partial x} + v'\frac{\partial w'}{\partial y} + w'\frac{\partial w'}{\partial z} = \frac{-\partial p'}{\partial z}\frac{1}{\rho_0} + \frac{\rho'}{\rho_0}g_z \tag{2.5c}$$

Because the fluid is incompressible, the total fluid density is constant.

$$\frac{D\rho}{Dt} = 0 = \frac{\partial \rho}{\partial t} + u'\frac{\partial \rho}{\partial x} + v'\frac{\partial \rho}{\partial y} + w'\frac{\partial \rho}{\partial z} = \frac{\partial \rho'}{\partial t} + w'\frac{\partial \overline{\rho}}{\partial z} \tag{2.3b}$$

From here the equations are linearized, assuming that $u'$, $v'$, and $w'$, are small and any terms that include products of these terms will be removed.

$$\frac{\partial u'}{\partial t} = \frac{-\partial p'}{\partial x}\frac{1}{\rho_0} \tag{2.6}$$

$$\frac{\partial v'}{\partial t} = \frac{-\partial p'}{\partial y}\frac{1}{\rho_0} \tag{2.7}$$

$$\frac{\partial w'}{\partial t} = \frac{-\partial p'}{\partial z}\frac{1}{\rho_0} + \frac{\rho'}{\rho_0} g_z \tag{2.8}$$

$$0 = \frac{\partial \rho'}{\partial t} + w' \frac{\partial \overline{\rho}}{\partial z} \tag{2.9}$$

These are referred to as the linear Boussinesq equations, from which the perturbation, or wave density, pressure, and particle velocities may be determined.

Through manipulation shown in Appendix B, these equations become

$$\frac{\partial}{\partial t}\left(\nabla^2 \frac{\partial w'}{\partial t}\right) + \nabla_H^2 \left(N^2 w'\right) = 0 \tag{2.10}$$

At this point a wave solution may be assumed for *w*,

$$w' = w_0 e^{i(kx+ly+mz+\omega t)} \tag{2.11}$$

Where the real part is taken,

$$w' = w_0 \cos(kx + ly + mz + \omega t) \tag{2.11b}$$

By inserting equation 2.11 into equation 2.10, assuming *N* is constant, the dispersion relation is defined.

$$\nabla^2 \left(-\omega^2 w_0 e^{i(kx+ly+mz+\omega t)}\right) + \nabla_H^2 \left(N^2 w_0 e^{i(kx+ly+mz+\omega t)}\right) = 0$$

$$\left(k^2 + l^2 + m^2\right)\omega^2 w_0 e^{i(kx+ly+mz+\omega t)} - N^2\left(k^2 + l^2\right)\left(w_0 e^{i(kx+ly+mz+\omega t)}\right) = 0$$

$$\left(k^2 + l^2 + m^2\right)\omega^2 - N^2\left(k^2 + l^2\right) = 0$$

$$\omega^2 = \frac{N^2\left(k^2 + l^2\right)}{k^2 + l^2 + m^2} \tag{2.12}$$

This defines the frequency of the wave by the wavenumbers. This relation may be adjusted due to forcing terms, such as when the waves exist in a rotating fluid. When the Coriolis

force is important, such as for large atmospheric or oceanic internal waves, the frequency is adjusted to include the Coriolis frequency and the dispersion relation becomes

$$\omega^2 = \frac{N^2\left(k^2 + l^2\right) + f^2 m^2}{k^2 + l^2 + m^2} \tag{2.13}$$

Equation 2.13 defines the internal wave frequency in terms of limiting frequencies, *f* and *N*, and by wavenumbers. It shows that the frequency of the internal waves are constrained, such that $f \le |\omega| \le N$. Thus when objects are oscillated at frequencies greater than the natural frequency, internal waves are not generated.

## 2.3 The Ray Equations

In addition to the dispersion relation, the ray equations are necessary to define internal wave motion for these simulations. In ray theory, internal waves or internal wave packets are simulated as rays, where the wavenumbers, frequency, and amplitude are known, yet the individual particle velocities are ignored. The equations that govern the internal waves are given by equations 2.14 and 2.15 (Lighthill 1978 equations 148 and 149).

$$\frac{d\vec{k}}{dt} = -\nabla\left(\vec{k} \bullet \vec{V}\right) - \frac{\partial \omega}{\partial \vec{x}} \tag{2.14}$$

$$\frac{d\vec{x}}{dt} = \frac{\partial \omega}{\partial \vec{k}} + \vec{V} \tag{2.15}$$

For some simulations, such as internal waves propagating through time-independent flows, the total frequency is conserved. The total frequency is defined below, and the results section will show that this is only valid for certain simulations.

$$\Omega = \omega + \vec{V} \bullet \vec{k} \tag{2.16}$$

With these equations and the dispersion relation, it is possible to simulate internal waves through a background flow field.

## 2.4 The Idealized Problem

The principal scenarios in this paper involve small-scale internal waves propagating through a time-independent background flow field or a time-dependent idealized inertial frequency internal wave, which was described in the introduction. The inertial waves used in theses simulations have a finite vertical wavelength, and an assumed infinite horizontal wavelength, since $\lambda_V << \lambda_H \sim \infty$ for inertial waves. For simulations in this paper, the frequency of the inertial wave is equal to the Coriolis frequency, and the group velocity of the inertial wave packet is treated as negligible, because it is assumed that $K, L \approx 0$ and therefore $\vec{c}_g \approx 0$. The

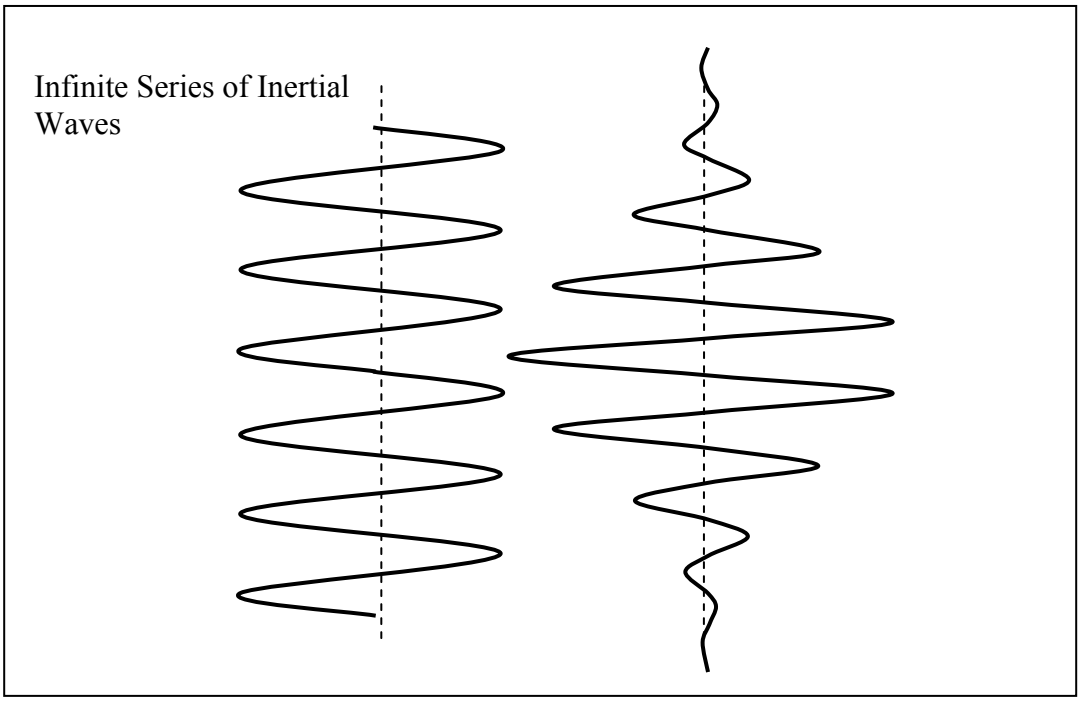


**Figure 2.1 Inertial wave horizontal velocity profiles showing an infinite wave train or waves contained within a Gaussian envelope.**

vertical phase speed is $\omega/M$, where $\omega = f$, and commonly propagates downward in the atmosphere. The inertial wave is simulated as either an infinite series of waves or as a wave packet as shown in Figure 2.1. In this setup, the wave packet is contained in an ideal Gaussian envelope, defined by $U_0 e^{-\frac{z^2}{L^2}}$, where $L$ is a characteristic vertical length of the packet, $U_0$ is the maximum horizontal velocity at the center of the packet, and $z$ is the elevation centered at the middle of the packet. $L$ is chosen so that the wave `packet contains at least 4 or 5 distinct wavelengths.

For the previous assumptions to hold, the horizontal wavelength must have an assumed infinite vertical wavelength. This assumption is validated by evaluating realistic inertial wave properties. The introduction discussed that for observed inertial waves, the ratio of horizontal to vertical wavelengths was typically about three orders of magnitude. For a ratio of buoyancy frequency to Coriolis frequency of 200, which is a typical value for the atmosphere, and a horizontal to vertical wavelength ratio of 1,000, the vertical group velocity magnitude of inertial waves is only 3.9% of the inertial wave phase speed. The vertical background particle velocities for these ratios are calculated from the polarization relations which define the perturbation velocities for internal waves, and are defined in Appendix A. The vertical background particle velocity is measured as

$$\frac{w'}{u'_H} = \frac{k_H}{m} \tag{2.17}$$

This results in vertical velocity magnitudes that are only one thousandth of the horizontal velocity, and may therefore be neglected. This leads to simplifying assumptions for the idealized background flow field, where the inertial wave is assumed to have an infinite horizontal wavelength.

- There is no vertical velocity caused by the inertial wave or other flow field, or $W = 0$.
- Buoyancy frequency and Coriolis frequency are constant at all elevations and horizontal locations.
- The scenarios are treated as two dimensional, where $l = 0$ and $\frac{\partial l}{\partial t} = 0$.

These assumptions allow the ray equations for the small wave to be simplified. Equation 2.14 may be expanded to show each component.

$$\frac{dk}{dt} = -k\frac{\partial U}{\partial x} - l\frac{\partial V}{\partial x} - m\frac{\partial W}{\partial x} - \frac{\partial \omega}{\partial x} \tag{2.14b}$$

$$\frac{dl}{dt} = -k\frac{\partial U}{\partial y} - l\frac{\partial V}{\partial y} - m\frac{\partial W}{\partial y} - \frac{\partial \omega}{\partial y} \tag{2.14c}$$

$$\frac{dm}{dt} = -k\frac{\partial U}{\partial z} - l\frac{\partial V}{\partial z} - m\frac{\partial W}{\partial z} - \frac{\partial \omega}{\partial z} \tag{2.14d}$$

Applying the assumptions above result in the following simplifications

$$\frac{dk}{dt} = 0 \tag{2.18}$$

$$\frac{dl}{dt} = 0 \tag{2.19}$$

$$l = 0 \tag{2.20}$$

$$\frac{dm}{dt} = -k\frac{\partial U}{\partial z} \tag{2.21}$$

These assumptions also simplify the equations that define the group velocity of the small internal waves, or velocity at which the energy propagates. Equation 2.15 describes the small wave group velocity and is shown below separated into each component.

$$\frac{dx}{dt} = c_{gx} = \frac{\partial \omega}{\partial k} + U \tag{2.15b}$$

$$\frac{dy}{dt} = c_{gy} = \frac{\partial \omega}{\partial l} + V \tag{2.15c}$$

$$\frac{dz}{dt} = c_{gz} = \frac{\partial \omega}{\partial m} + W \tag{2.15d}$$

Applying equations 2.18 – 2.21 and $W = 0$ result in the following simplifications.

$$c_{gx} = \frac{\partial \omega}{\partial k} + U \tag{2.22}$$

$$c_{gy} = V \tag{2.23}$$

$$c_{gz} = \frac{\partial \omega}{\partial m} = -\frac{\left(N^2 - f^2\right)k^2 m}{\left(N^2 k^2 + f^2 m^2\right)^{1/2}\left(k^2 + m^2\right)^{3/2}} \tag{2.24}$$

The amplitude of the small internal waves plays an important role in internal wave simulations, and affects the stability of waves. The wave action density is the square of the amplitude, and changes during wave interactions. The total wave action is the wave energy divided by the wave frequency, and does not change while linear ray theory remains valid. The total wave action is defined as the integral of the wave action density for a specified volume.

$$A_{TOT} = \int A \, d\forall \tag{2.25}$$

Ray tracing approximates internal waves as rays propagating through time and space, which may be analyzed as thin tubes. Because there are no vertical background velocities, and velocities do not change in the horizontal directions, the wave action density may be approximated as the vertical cross-sectional area, or relative volume, of the ray tube. It is thus defined as

$$\frac{A}{A_0} = \frac{\forall_0}{\forall} = \frac{1}{\partial z / \partial z_0} \tag{2.26}$$

The results section will further describe the wave action density, and how it affects the outcomes of internal wave interactions.

# 3 RESULTS

Ray theory was used to simulate the interaction of internal waves through time-independent background winds, through infinite inertial wave trains, and through inertial wave packets. During the interaction, the propagation direction of the internal waves may change permanently or temporally, and may cease propagation due to instability.

## 3.1 Wave Propagation through a Time-independent Wind

As internal waves propagate through a fluid, the waves' properties change with spatial or temporal changes in the medium, such as background wind shear. If an internal wave packet propagates upward into a region of wind moving in the same horizontal direction as the phase speed of the internal wave, (See Figure 3.1) the wave's frequency will decrease and its probability of reaching a critical level and overturning or becoming absorbed is increased. Alternately, if it propagates into a region of horizontal winds opposing the wave's phase speed, (See Figure 3.5) the wave frequency will increase and the wave packet may possibly encounter a turning point where the wave is reflected. For this paper, background winds in the same direction as the horizontal propagation direction of the small internal waves will hereon be defined as positive wind velocities and opposing winds will be defined as negative velocities, as all internal waves in these interactions will propagate in the positive horizontal direction.

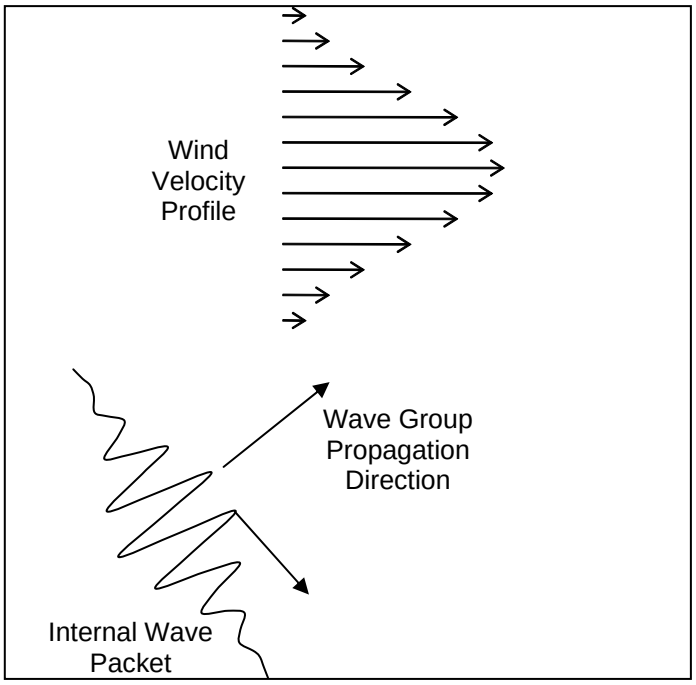


**Figure 3.1 Internal wave packet approaching a positive mean wind**

### 3.1.1 Critical Levels and Turning Points

The frequency of the internal waves will determine if they will encounter a critical level or turning point when propagating through a mean wind. By equation 2.13, this frequency is only a function of the vertical wavenumber *m* of the internal waves, for the other variables are all constant during the simulation. The relationship between the background wind velocity and the vertical wavenumber of the small waves may be calculated using equations 2.13, 2.21, and 2.24.

$$\omega = \pm\left(\frac{f^2 m^2 + N^2 k^2}{k^2 + m^2}\right)^{1/2} \tag{2.13}$$

$$\frac{\partial m}{\partial t} = -k\frac{\partial U}{\partial z} \tag{2.21}$$

$$c_{gz} = \frac{\partial z}{\partial t} = \frac{\partial \omega}{\partial m} \tag{2.24}$$

These equations are manipulated to find the relationships between the background wind velocities and internal wave frequencies and wavenumbers. A relationship may also be found for the wave action density and will be shown later. By combining equations 2.21 and 2.24

$$\frac{\partial m}{\partial t}\frac{\partial t}{\partial z}\frac{\partial \omega}{\partial m} = -k\frac{\partial U}{\partial z}$$

$$\partial m \frac{\partial \omega}{\partial m} = -k\partial U$$

$$\partial \omega = -k\partial U$$

Because $k$ is constant, integrating both sides yield

$$\omega = -kU + Cst$$

The total frequency for this type of time-independent flow field is defined as $\Omega = \omega + kU$ and is constant for this simulation according to ray theory. Because the internal wave begins propagation in a region of rest, with no background velocity, the total frequency when $U = 0$ *is* $\Omega = \omega_0$, and the resulting relationship is

$$U = \frac{1}{k}(\omega_0 - \omega) \tag{3.1}$$

Or

$$U = \frac{1}{k}\left[\left(\frac{N^2k^2 + f^2m_0^2}{k^2 + m_0^2}\right)^{1/2} - \left(\frac{N^2k^2 + f^2m^2}{k^2 + m^2}\right)^{1/2}\right] \tag{3.1b}$$

An internal wave approaches a critical level where $\omega$ approaches $f$, or where $m$ approaches $\infty$, and it ceases to be a wave. It reaches a turning point as $\omega$ approaches $N$ and $m$ must change sign for the wave to continue to propagate. The background wind velocities required for a critical level or turning point may be calculated by inputting $0$ or $\infty$ into equation 3.1, respectively.

$$U_{CL} = \frac{1}{k}\left(\frac{N^2k^2 + f^2m_0^2}{k^2 + m_0^2}\right)^{1/2} - \frac{f}{k} = \frac{\omega_0}{k} - \frac{f}{k} \tag{3.2}$$

$$U_{TURN} = \frac{1}{k}\left(\frac{N^2k^2 + f^2m_0^2}{k^2 + m_0^2}\right)^{1/2} - \frac{N}{k} = \frac{\omega_0}{k} - \frac{N}{k} \tag{3.3}$$

Figure 3.2 and Figure 3.3 show the results of internal waves approaching and propagating through a positive mean wind with a Gaussian profile. The internal waves are represented by the rays or lines in (a) showing elevation against time, with (b) showing the wind velocity profile. In Figure 3.2, a critical level is not present, and the internal waves propagate through the wind ultimately unaffected. The vertical group velocity decreases as the waves interact and propagate through the maximum background wind but returns to its original value after the interaction. The vertical wavenumber *m* increases in magnitude during the interaction, but similar to the vertical group velocity, decreases and returns to its original value after the interaction.

In Figure 3.3, the background wind is stronger and a critical level exists. The wave packet does not propagate beyond the critical level, but rather asymptotically approaches it until becoming unstable and overturning or becoming absorbed into the background (amplitude and shear considerations are necessary to determine which of these results will occur). The vertical wavenumber steadily increases and the frequency decreases toward *f*. As the frequency decreases, the wave action density increases. It should be remembered that ray theory is not valid after the waves become unstable.

When the wave frequency increases, energy from the background flow is transferred to the waves. Alternately, when the frequency decreases, wave energy is transferred to the background flow, and hence waves transfer their energy to the background near critical levels.

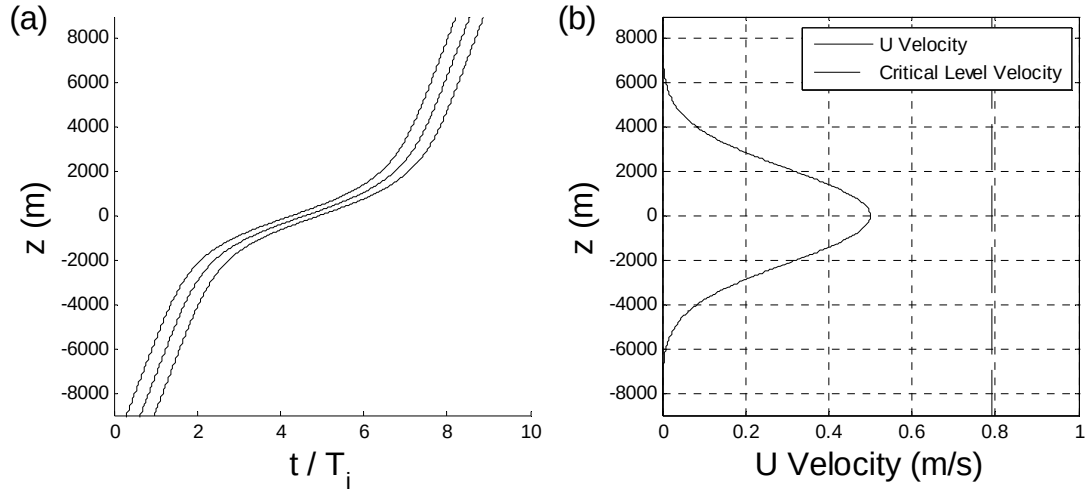


**Figure 3.2 Internal wave packet with $k = 2\pi/2500$ m$^{-1}$ and $m = -2\pi/250$ m$^{-1}$ approaches a mean wind with no critical level. (a) shows internal wave rays in elevation and time, and the waves freely propagate through the mean wind. The elevation is centered at the maximum horizontal velocity, and the time is nondimensionalized against the Coriolis period. (b) shows the horizontal velocity profile.**

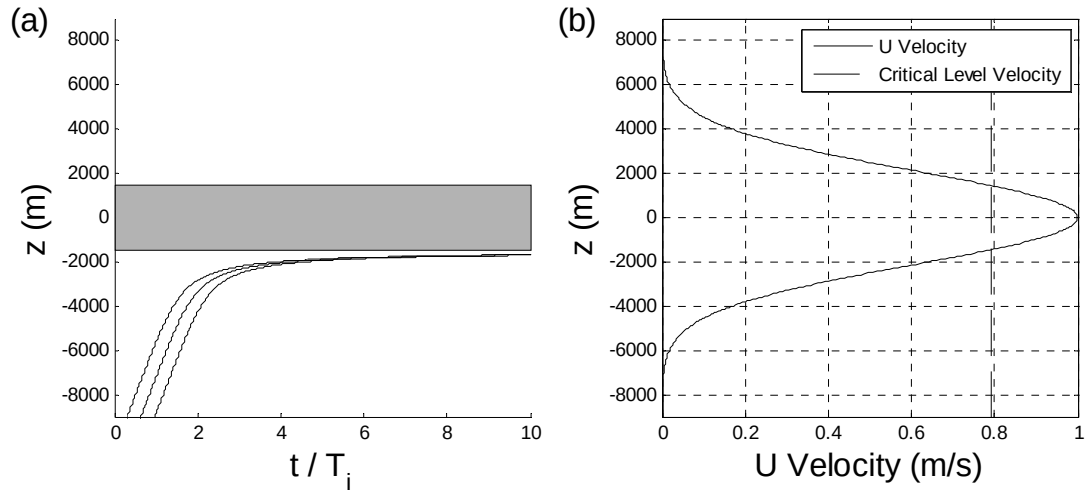


**Figure 3.3 Internal wave packet with $k = 2\pi/2500$ m$^{-1}$ and $m = -2\pi/250$ m$^{-1}$ approaches a mean wind with a critical level. (a) shows internal wave rays in elevation and time. The shaded region shows where the background velocities exceed the critical level velocity. (b) shows the horizontal velocity profile.**

For Figures 3.2 - 3.3 and 3.6 - 3.7, the initial wavenumbers of the small waves are $k = 2\pi / 2{,}500\ m^{-1}$ and $m = -2\pi / 250\ m^{-1}$, which are practical wavenumbers for atmospheric waves, though atmospheric waves may span a large range of wavenumbers, which will be shown hereafter.

The three waves, or rays, in Figure 3.2 and Figure 3.3 were initiated at the same horizontal location but at different vertical locations. Because the background wind does not change in the horizontal direction, waves do not experience any different results when initiated at different horizontal locations. The horizontal propagation does not affect the properties of the internal waves, and the path of propagation is similar to the z-t diagrams, for the horizontal group velocity is much more constant when compared to the vertical group velocity (for this simulation the horizontal group speed never varied by more than 1.0%). This is illustrated in Figure 3.4, which shows the simulation depicted in Figure 3.2.

If internal waves propagate through a region of negative horizontal winds, the vertical group velocity will increase with stronger background winds unless the waves reach a turning

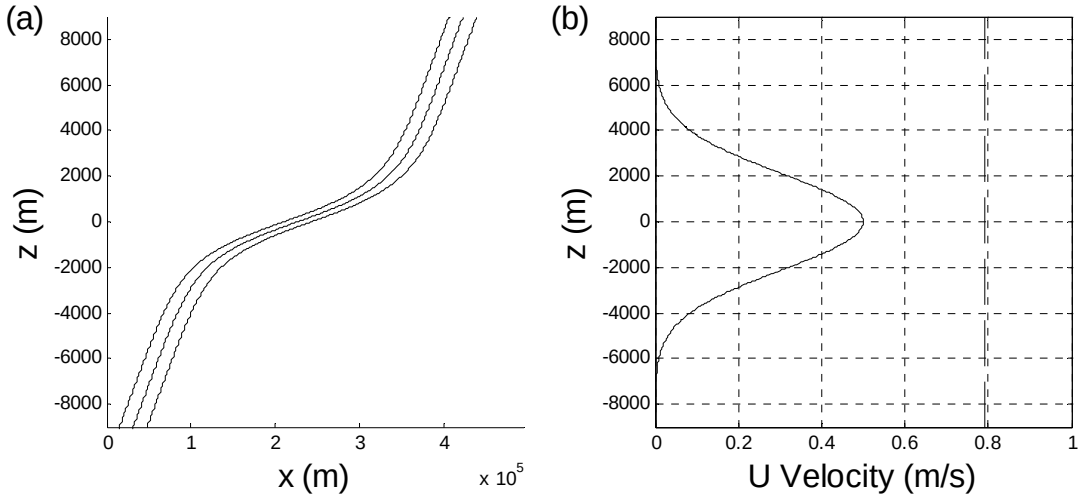


**Figure 3.4. Simulation identical to Figure 3.2 that shows path of propagation of internal waves.**

point. At this point the vertical group velocity quickly decreases and changes sign, causing the internal waves to become reflected. This occurs when the magnitude of the background velocity is larger than the velocity defined by equation 3.3. If the waves are not reflected, they will continue propagation through the background winds and will leave the interaction ultimately unaffected, similar to waves approaching a positive background wind without a critical level. These scenarios are depicted in Figure 3.5 – Figure 3.7.

Figure 3.6 shows waves that propagate through a negative velocity wind with a Gaussian profile. When the waves encounter the wind, the frequency decreases and the vertical group velocity increases. The wind isn't sufficiently strong to cause a turning point in Figure 3.6, but Figure 3.7 depicts an identical interaction with the only difference being that the background wind velocity is stronger. This results in a turning point in Figure 3.7.

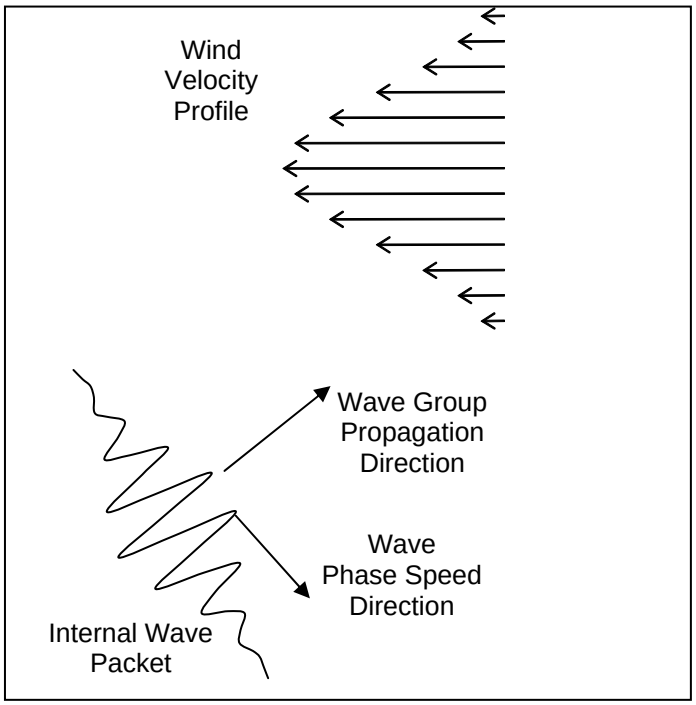


**Figure 3.5 Internal wave packet approaching a negative mean wind**

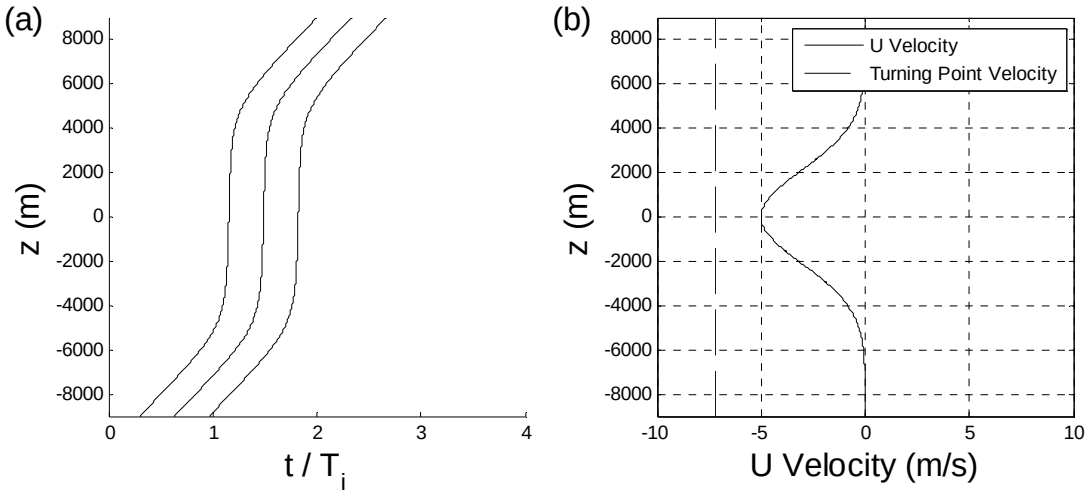


**Figure 3.6 Internal waves approaching a mean wind without a turning point. (a) shows internal wave rays in elevation and time. (b) shows the horizontal velocity profile.**

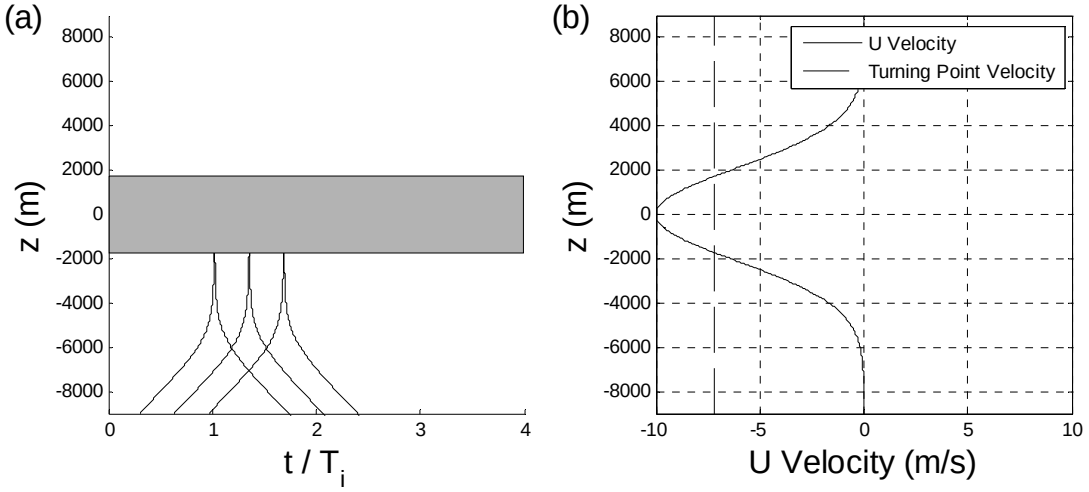


**Figure 3.7 Internal waves approaching a mean wind with a turning point. (a) shows internal wave rays in elevation and time. The shaded regions show where the magnitude of the background velocity exceeds the turning point velocity. (b) shows the horizontal velocity profile.**

Equations 3.2 and 3.3 show the background velocities that will cause a wave to reach a critical level or become reflected, but these velocities differ for different wavenumbers and frequencies. Internal waves in the atmosphere exist for a wide range of wavenumbers covering many orders of magnitude, (Fritts and Alexander 2003) at any frequency between *f* and *N*.

Ray theory allows many waves to be quickly analyzed, and the results may be shown in various ways. The parameters that affect the outcomes of this type of interaction are the wavenumbers of the internal waves, wave frequency, and velocity of the background flow, in addition to the buoyancy frequency and Coriolis frequency. The amplitude of the internal waves and average fluid density does not affect whether the internal waves will reach a critical level or turning point, but will affect other outcomes of interactions discussed in later sections.

Figure 3.8 and Figure 3.9 show the velocity required for a critical level or turning point in a time-independent flow field for a wide range of waves. Atmospheric internal waves may have wavelengths from meters to many kilometers, and the results figures cover all these practical ranges. In these plots, each of the black dots represents a distinct internal wave that was simulated for each interaction, with a total number of 969 waves. The horizontal axis represents the initial vertical wavenumber of the internal wave and the vertical axis represents the initial frequency, which is bounded by *f* and *N,* the Coriolis and buoyancy frequencies. The horizontal axis is normalized by a wavenumber $\mu = -2\pi / 2500\ m^{-1}$ (Eckermann 1997) for convenience in scaling, and covers vertical wavelengths from $2.5\ m$ to $250\ km$. The vertical axis is normalized by the Coriolis frequency. For this figure, and for all subsequent figures unless otherwise noted, $f = 0.0001\ s^{-1}$ and $N = 0.02\ s^{-1}$, which are typical values for the middle atmosphere at mid-latitudes. The initial horizontal wavenumber is defined by the initial frequency and vertical wavenumber by equation 2.13, and constant values of *k* are defined by diagonal lines that

connect adjacent dots from the upper left region to the lower right region. The colors on the plots represent the velocities required for the internal waves to reach a critical level or turning point. All axes, including the color contours, are defined in logarithmic scales, due to its ability to display a wide range of interactions, and its similarity to the figures in Eckermann (1997).

The red regions show where the internal waves will experience a critical level in Figure 3.8 with only a small background wind, below 1 m/s, and blue regions show where winds exceeding 10 m/s are required for a critical level to exist. If a background wind exceeding 100 m/s is required, which is unrealistic for atmospheric winds or currents, the region is white and it may be assumed that a critical level will not be reached for these waves in this type of interaction. The same is true for turning point velocities in Figure 3.9. Red regions indicate that small velocities will cause a turning point, and blue regions mean that larger velocities are required. White regions indicate that these waves will likely not encounter a critical level. For the same velocities, critical levels are generally more common than turning points.

The waves with a large initial vertical wavenumber are more likely to encounter a critical level at lower wind velocities. For example, if a large number of waves covering the whole spectrum propagated toward a mean wind with a positive velocity of 1 m/s, all waves that lie in the red or dark red regions of Figure 3.8 would encounter a critical level. All waves in white or other colored regions would freely propagate through the mean wind. Alternatively, waves with large initial horizontal wavenumbers are more likely to reach turning points at lower velocities. If a large number of waves propagated toward a mean wind with a negative velocity of 1 m/s, all waves that lie in the red or dark red regions of Figure 3.9 would encounter a turning point. All waves in white or other colored regions would freely propagate through the mean wind.

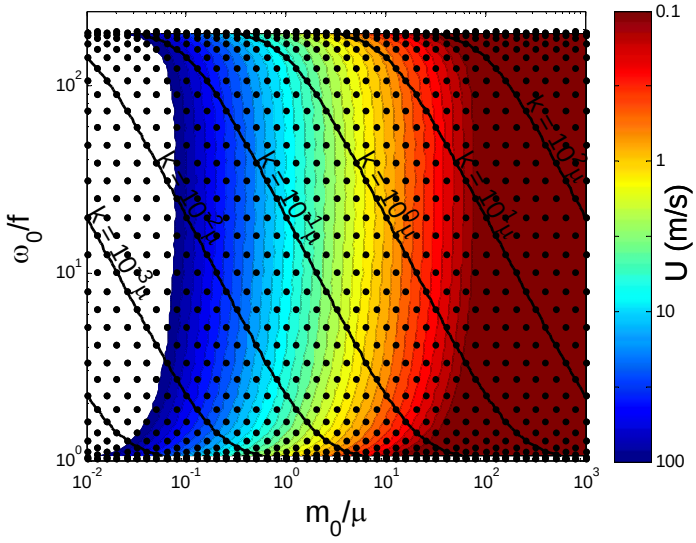


**Figure 3.8 Background critical level velocities. Color contours are horizontal background velocity in the same direction as internal waves' horizontal phase speed.**

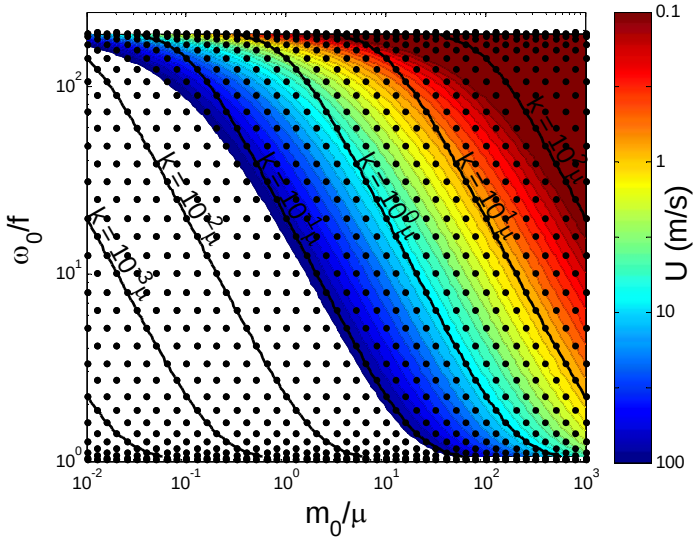


**Figure 3.9 Background turning point velocities. Color contours are horizontal background velocity in the opposite direction as internal waves' horizontal phase speed.**

### 3.1.2 The Mid-Frequency Approximation

Figure 3.8 and Figure 3.9 show regions where the relationships of critical level velocities or turning point velocities are linearly related to the initial horizontal or vertical wavenumbers, which occurs within the mid-frequency regions. Assuming $N^2 >> \omega^2 >> f^2$, and $m^2 >> k^2$ the dispersion relation and group speed equations simplify as follows, which is known as the mid-frequency approximation.

$$\omega \approx \pm \frac{Nk}{m} \tag{3.4}$$

$$c_{gz} \approx \frac{\pm Nk}{m^2} \tag{3.5}$$

The equations for the critical level velocity and turning point velocity simplify as well.

$$U_{CL} = \frac{\omega_0}{k} - \frac{f}{k} \tag{3.2}$$

$$U_{TURN} = \frac{\omega_0}{k} - \frac{N}{k} \tag{3.3}$$

$$U_{CL} \approx \frac{N}{|m_0|} \tag{3.6}$$

$$U_{TURN} \approx -\frac{N}{k} \tag{3.7}$$

From these simplified equations, an approximate value of *m* may be determined at any point within the background flow given the horizontal background velocity, by combining equations 2.21, 3.5, and 3.6.

$$\frac{\partial m}{\partial t} = -k \frac{\partial U}{\partial z} \tag{2.21}$$

$$\frac{\partial m}{\partial z} \approx \frac{m^2}{N} \frac{\partial U}{\partial z}$$

$$\frac{\partial m}{m^2} \approx \frac{\partial U}{N}$$

Multiply each side by equation 3.6.

$$U_{CL} m_0 \frac{\partial m}{m^2} \approx \partial U$$

$$m_0 \frac{1}{m} \approx -\frac{U}{U_{CL}} + Cst$$

When $U = 0$, then $m = m_0$, so $Cst = 1$:

$$\frac{m}{m_0} \approx \frac{1}{(1 - U/U_{CL})} \tag{3.8}$$

This simple model is valid for values where the buoyancy frequency is much larger than the Coriolis frequency (which is generally true for any stable region of the Earth's atmosphere) and where the initial horizontal wavelengths are larger than the vertical wavelengths.

### 3.1.3 Wave Steepness and Instability

The wave steepness of an internal wave, denoted as $\zeta_z$, is a good indicator of whether the small wave will remain stable or overturn and be dissipated by turbulence. When the wave steepness reaches a magnitude of unity, the isopycnals, or surfaces of constant density of the waves, are vertical, and any increase in wave steepness results in gravitational instability, and they are likely to overturn and break. When $\omega^2 << N^2$, the wave steepness is defined as

$$|\zeta_z| = k(2/\rho_0)\frac{A^{1/2}}{\omega^{1/2}} \tag{3.9}$$

The wave steepness for these simulations is proportional to the square root of the wave action density divided by the frequency, so an increase in the wave action density or amplitude will increase the steepness of the wave, and vice versa. Because there are no background velocity

changes in the x – direction or y – direction, but rather only in elevation changes, the relative change in wave action density is defined by equation 2.26, and the changes in volume may be defined by the following equations.

$$\frac{\partial\left(\partial z/\partial z_0\right)}{\partial t} = \frac{\partial^2 \omega}{\partial m^2}\partial m/\partial z_0 \tag{3.10}$$

$$\frac{\partial\left(\partial m/\partial z_0\right)}{\partial t} = -k\frac{\partial^2 U}{\partial z^2}\frac{\partial z}{\partial z_0} \tag{3.11}$$

For simulations where the internal waves begin propagation in a region of rest without any background wind or wind shear, which is true for these simulations where the waves are propagating from well below the mean wind, the initial values of $\partial z/\partial z_0$ and $\partial m/\partial z_0$ are shown below. These are known as the Hayes quantities.

$$\left(\frac{\partial m}{\partial z_0}\right)_0 = 0 \tag{3.12}$$

$$\left(\frac{\partial z}{\partial z_0}\right)_0 = 1 \tag{3.13}$$

This indicates that at the beginning part of the simulation, the vertical wavenumber does not change with elevation, and that the volume of a ray tube is unchanging, since the vertical group speed of the internal waves is constant, because the simulations are initiated in a region of rest. For time-independent background winds with no vertical background velocities, the wave action density can be defined as

$$\frac{A}{A_0} = \frac{c_{gz0}}{c_{gz}} \tag{3.14}$$

This is derived by combining equations 3.10– 3.13, 2.24, and 2.21, and the derivation is shown in Appendix C. From this derivation, we can find the equation that defines the change in the vertical wavenumber based on the background shear.

$$\partial m / \partial z_0 = \frac{-k}{c_{gz0}} \frac{\partial U}{\partial z} \tag{3.15}$$

$$\partial z / \partial z_0 = \frac{c_{gz}}{c_{gz0}} \tag{3.16}$$

$$\frac{A}{A_0} = \frac{c_{gz0}}{c_{gz}} \tag{3.14}$$

Or in terms of the wavenumbers

$$\frac{A}{A_0} = \frac{m_0 \left(N^2 k^2 + f^2 m^2\right)^{1/2} \left(k^2 + m^2\right)^{3/2}}{m \left(N^2 k^2 + f^2 m_0^{\,2}\right)^{1/2} \left(k^2 + m_0^{\,2}\right)^{3/2}} \tag{3.17}$$

In this way the change in wave action density can be determined at any point in the background flow field, for the vertical wavenumber is a function of the background velocity, and *A* is a function of *m*. The relative wave steepness may be determined by combining equations 3.9 and 3.14.

$$\frac{\zeta_z}{\zeta_{z0}} = \left( \frac{A \omega_0}{A_0 \omega} \right)^{1/2} = \left( \frac{c_{gz0} \omega_0}{c_{gz} \omega} \right)^{1/2} \tag{3.18}$$

The change in wave action density or wave steepness is all relative to the initial conditions according to linear ray theory. For this paper, the calculated wave action density and wave steepness will be given relative to the initial values.

The mid-frequency approximation may be used to simplify equations 3.14 and 3.18. The vertical wavenumber, action density, and steepness are all related to the background velocity that would cause a critical level in a time-independent flow field.

$$\frac{m}{m_0} \approx \frac{1}{\left(1 - U/U_{CL}\right)} \tag{3.8}$$

$$\frac{A}{A_0} \approx \frac{1}{\left(1 - U/U_{CL}\right)^2} \tag{3.19}$$

$$\frac{\varsigma_z}{\varsigma_{z0}} \approx \frac{1}{\left(1 - U/U_{CL}\right)^{3/2}} \tag{3.20}$$

When a critical level is present, the waves will asymptotically approach the critical level until overturning or becoming absorbed. Equation 3.20 shows how waves will steepen in the vicinity of a critical level. When a critical level is not present, equation 3.18 or 3.20 may be used to predict if the waves will overturn due to wave steepness, independent of a critical level. For example, even if the magnitude of the background wind is only 80% of the magnitude required for a critical level, the wave steepness will still increase by a factor of ten according to equation 3.20.

Mean winds and velocity gradients are common in the atmosphere, and internal waves are ubiquitous. Figure 3.8 and Figure 3.9 show how different waves will respond differently when encountering regions of wind, in that some may experience a critical level, some may become reflected and others will freely propagate through the mean wind. Internal waves contribute to the driving of currents and large flows in this manner. For example, if a large spectrum of internal waves propagate upward toward a wind current, waves that carry horizontal momentum in the same direction as the current, or whose phase speed is in the same direction may reach a critical level and deposit their momentum and energy with the current. This was shown by Winters & D'Asaro (1989). Waves that carry horizontal momentum in the opposite direction are more likely to freely propagate through the wind or become reflected, transporting energy and momentum away from the mean wind. The net effect is that the wind may become

accelerated by internal waves reaching a critical level in the same region, and contribute to driving large-scale flows. Waves that do not reach a critical level or become unstable will transport their energy elsewhere.

## 3.2 Wave Propagation through an Infinite Wave Train

These simulations involve internal waves propagating through an infinite inertial wave train, meaning an inertial wave with an infinite number of wave phases, as shown in Figure 3.10. For this idealized inertial wave, the horizontal wavelength is assumed infinite, the vertical wavelength is finite and constant, and the frequency is equal to the Coriolis frequency. The phases of the inertial wave propagate downward, meaning that $M$ is negative, and because $K_H = 0$, the inertial wave group velocity is $0$. The vertical wavelengths and frequency in this section reflect real, observational values noted in the introduction. However, real inertial waves exist as packets, which will be discussed in later sections.

Figure 3.11 shows an internal wave ray propagating through an infinite inertial wave train. When small amplitude waves interact with a large inertial wave, they will encounter moving envelopes of positive and negative horizontal background winds. If the positive wind is sufficiently strong, the wave may become unstable similar to a critical level. If the negative wind is sufficiently strong, it may cause the wave to reach a turning point like the previous scenario and change its propagation direction. If the wave does not encounter a turning point or become unstable, the internal wave will freely propagate through the inertial wave, like in Figure 3.11.

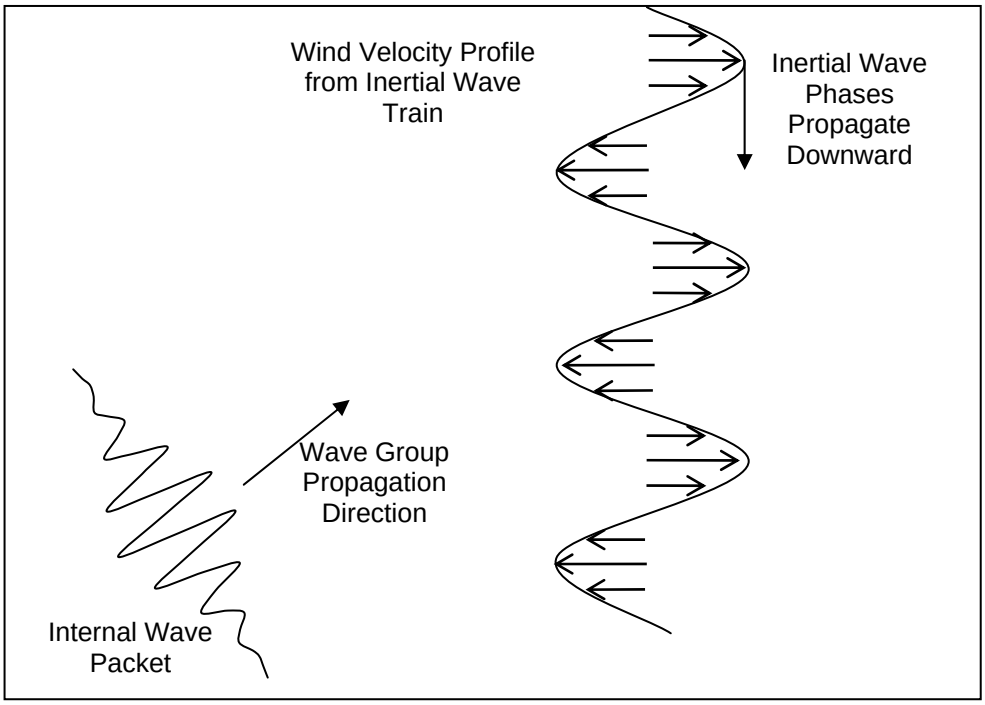


**Figure 3.10 Internal wave packet propagating through an infinite inertial wave train.**

The properties of the small waves may be calculated at any location of the time-dependent background inertial wave. The frame of reference of the small waves may be changed by subtracting the inertial phase speed from the vertical group speed of the small waves, as shown below.

$$\frac{\partial z}{\partial t} = c_{gz} - c_{LW} \tag{3.21}$$

$$c_{LW} = \frac{f}{M} \tag{3.22}$$

Combining these equations with equation 2.21 shows that the total frequency is constant according to equation 2.16. This can then be used to determine the properties of the small waves at any point in the background flow.

$$\Omega = \omega + Uk - Cm = Cst\,. \tag{2.16}$$

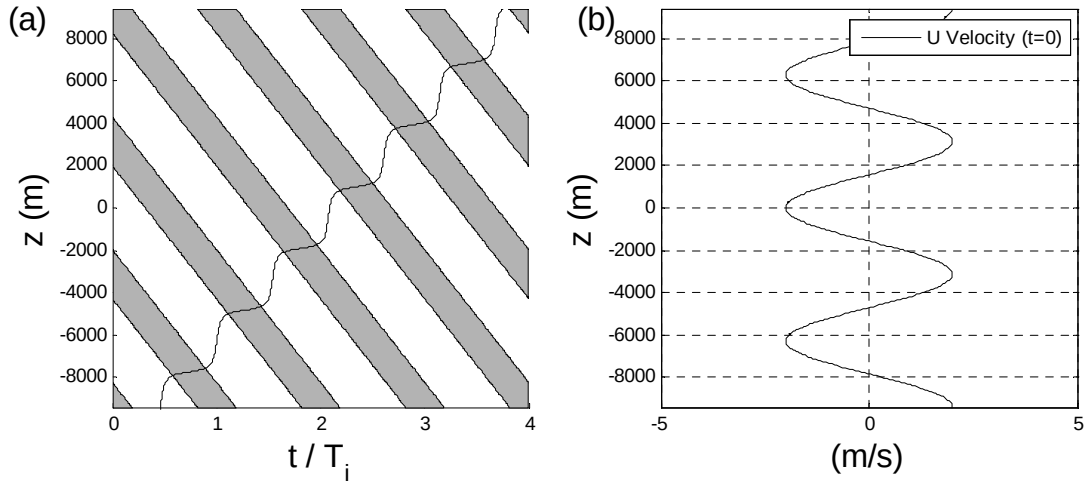


**Figure 3.11 (a) Internal wave packet ray propagating through an inertial wave train. The shaded regions show where the background velocities exceed the time-independent critical level velocity. (b) shows the horizontal velocity profile at the initial time.**

At $U = 0, \quad m = m_o$ and $\omega = \omega_o$

$$\omega + Uk - Cm = \omega_0 - Cm_0$$

$$U = \frac{1}{k}(\omega_0 - \omega) + \frac{f(m - m_0)}{Mk} \tag{3.23}$$

This agrees with equation 35 of Eckermann (1997) and may be rewritten as

$$U = \frac{1}{k}\left[\left(\frac{f^2 m_0^2 + N^2 k^2}{k^2 + m_0^2}\right)^{1/2} - \left(\frac{f^2 m^2 + N^2 k^2}{k^2 + m^2}\right)^{1/2}\right] + \frac{f(m - m_0)}{Mk} \tag{3.24}$$

A critical level where $m = \infty$ or $\omega = f$ does not exist without a velocity that also approaches infinity. However, turning points can occur where $m = 0$, and is calculated as follows.

$$U_{TURN} = \frac{1}{k}\left(\omega_0 - N - \frac{fm_0}{M}\right) = \frac{1}{k}\left(\frac{N^2 k^2 + f^2 m_0^2}{k^2 + m_0^2}\right)^{1/2} - \frac{N}{k} - \frac{fm_0}{Mk} \tag{3.25}$$

Although a velocity where *m* is equal to infinity does not exist, it is possible to denote a critical wavenumber where the vertical wavelength becomes so small that the wave is unlikely to exist with a vertical wavenumber larger than this value. In this sense, the critical level is estimated by an unrealistically small vertical wavelength, and this is referred to as a Jones' Critical Level (Jones 1967). A typical critical value for the atmosphere is

$$m_{CR} = 200\mu = -\frac{2\pi}{12.5} meters^{-1} \text{ (Eckermann 1997)}$$

The velocity required to reach this type of critical level is

$$U_{CL} = \frac{1}{k}\left[\left(\frac{f^2 m_0^2 + N^2 k^2}{k^2 + m_0^2}\right)^{1/2} - \left(\frac{f^2 m_{CR}^2 + N^2 k^2}{k^2 + m_{CR}^2}\right)^{1/2}\right] + \frac{f\left(m_{CR} - m_0\right)}{Mk} \tag{3.26}$$

To illustrate the practicality of this critical wavenumber, it may be compared against actual critical levels in time-independent background flows. This is simple, for equation 3.26 may be used with an inertial phase speed of zero, or $M = \infty$. Figure 3.12 shows the difference in critical level velocities for time-independent flows. The left plot uses a critical wavenumber and the right plot shows an actual critical level velocity, or $m_{CR} = \infty$. They are nearly identical, and

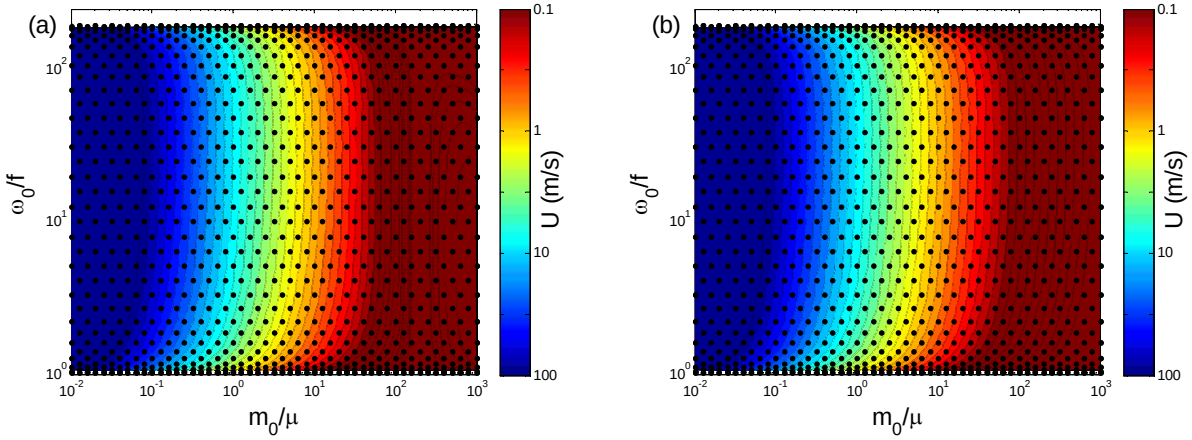


**Figure 3.12 Comparison of critical level contours for time-independent background flow. (a) shows velocities that are required for a Jones' critical level, and (b) shows actual critical level velocities.**

the largest difference in required background velocity is only 0.038 m/s, indicating that a critical wavenumber is valid for these scenarios.

### 3.2.1 Scale Separation

For ray theory to be valid, it must be assumed that the changes in the internal wave properties occur slowly during the interaction. This requires that the small waves and the inertial wave be scale separated, or that the horizontal and vertical wavelengths of the small waves are significantly smaller than the wavelengths of the inertial wave. Because it is assumed that the small waves do not affect the background flow field, the amplitude of the small waves must also be much smaller. In these idealized scenarios, $K_H$ is zero, or rather the horizontal wavelength of the inertial wave is assumed as infinite, and therefore the small wave is always scale separated in the horizontal direction. In the vertical direction, $M$ is finite, and in order to be scale separated, $m$

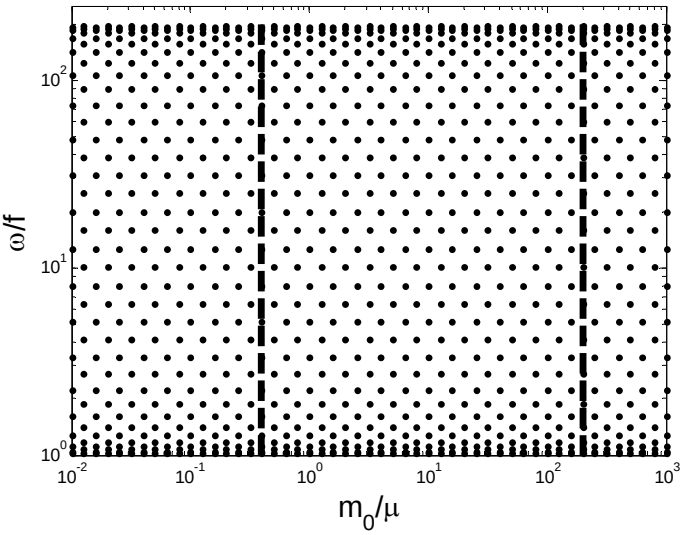


**Figure 3.13 Bounds of validity for internal wave interaction. The dashed line to the left shows where the vertical wavenumber of the small wave is identical to the vertical wavenumber of the inertial wave. The dashed line to the right represents the critical wavenumber, where all waves to the right are assumed initially unstable.**

must be larger than $M$. The internal wave frequencies must also be between $f$ and $N$, for internal waves may not exist at frequencies outside of these bounds.

For the scenarios in this section, the vertical wavenumber of the large wave is kept constant at $M = -0.001\, m^{-1}$ unless otherwise noted. This is a probable value for an atmospheric inertial wave with a vertical wavelength of $6.28\, km$, agreeing with observed inertial waves noted in the introduction.

Figure 3.13, showing the same domain as Figure 3.8 and Figure 3.9, shows the bounds of validity set by this scale separation. On the figure, the left dashed black line indicates where the initial vertical wavelength of the small wave matches the vertical wavelength of the inertial wave, at $M = -0.001\, m^{-1}$. Any simulations near or to the left of this line are not scale separated and the results may not be completely accurate. The dashed black line on the right indicates the value of the critical wavenumber, and any data to the right of this line is initialized in a Jones' critical level. These waves are therefore assumed to become unstable with to any interaction with the background. Therefore, only data between the dashed black lines should be considered valid for these simulations. Conveniently, this region contains waves that will experience a variety of outcomes, including critical levels, turning points, large wave steepening, or free propagation with no permanent change. Although scale separation is important for ray theory simulations, results from interactions that are not scale separated may still be accurate or generally give accurate outcomes (Sartelet 2003). Because these results may still be accurate, and these bounds of scale separation are unique for different values of $M$ or $m_{CR}$, and may change for different simulations or environments, the results on subsequent figures will be shown over the entire domain. Unless otherwise noted, subsequent figures will have identical regions of validity.

### 3.2.2 Jones' Critical Level and Turning Point Solutions

Using equations 3.25 and 3.26, the outcomes may be predicted for any interaction of small internal waves and a large inertial wave train. Figure 3.14 shows the potential outcomes of a wide range of waves interacting with inertial wave trains. The format is similar to those of Eckermann (1997) and shows interactions with wave trains of different maximum background velocities, (a) 1.5 m/s, (b) 5.0 m/s, and (c) 8.3 m/s, respectively. The horizontal and vertical axes are identical to those in Figure 3.13. In all cases, *f*, *N*, and the vertical wavenumber of the inertial wave, $M = -0.001\ m^{-1}$, were kept constant. An increase in the inertial wave amplitude increases

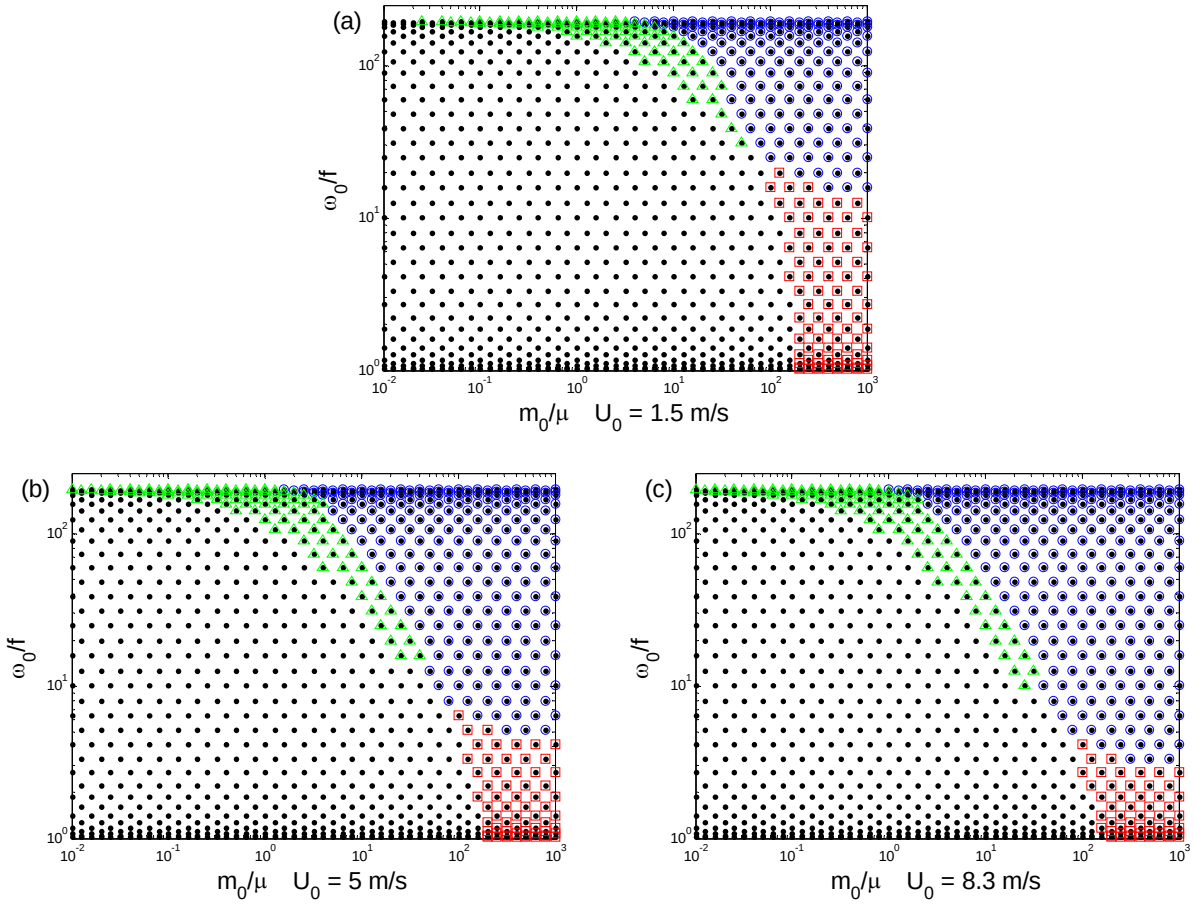


**Figure 3.14 Summary of end results of internal waves interacting with a background inertial wave. The magnitude of the inertial wave background velocities are the only parameter that is different for each plot, (a) 1.5 m/s (b) 5.0 m/s, and (c) 8.3 m/s. Green triangles depict waves that reach a turning point, red squares represent waves that reach critical levels, and blue circles represent waves that reach either a turning point or critical level.**

the size of the critical level and turning point regions, or rather a wider variety of waves will experience a critical level or a turning point for such interactions. The green triangles represent interactions where small wave will reach a turning point, the red squares represent a critical level interaction (based on a critical wavenumber), and the blue circles represent either a critical level or a turning point depending on whether the wave propagates first through positive or negative background velocities. The other dots without surrounding shapes represent regions of free propagation of the small waves.

Any wave where $m$ exceeds the value of $m_{CR}$ during the interaction will experience a Jones' critical level, so it is safe to assume that waves with initial wavenumbers near (or above) this value are more likely to experience a critical level compared to other waves. Waves with higher initial frequencies are also more affected than those with lower frequencies. Similarly, waves with initial frequencies near $N$ are more likely to reach a turning point, and waves with large initial wavenumbers are more strongly affected. Realistic waves may exist anywhere in this spectrum provided they are within the limits from Figure 3.13.

Figure 3.15 and Figure 3.16 show the required velocity for a critical level or turning point for a wide range of small waves, according to equations 3.25 and 3.26. The red regions show waves that will reach a critical level or turning point with a weak inertial wave, and yellow and blue regions show outcomes for stronger inertial waves. If the required velocity is greater than 15 m/s, which is much larger than any observed inertial waves noted in the introduction, the region is left white and those waves can be assumed to propagate freely through the inertial wave. These differ significantly from Figure 3.8 and Figure 3.9 and show that many waves will experience a critical level or a turning point in a time-independent flow for the same velocity, but will not experience a turning point or velocity for this type of time-dependent interaction.

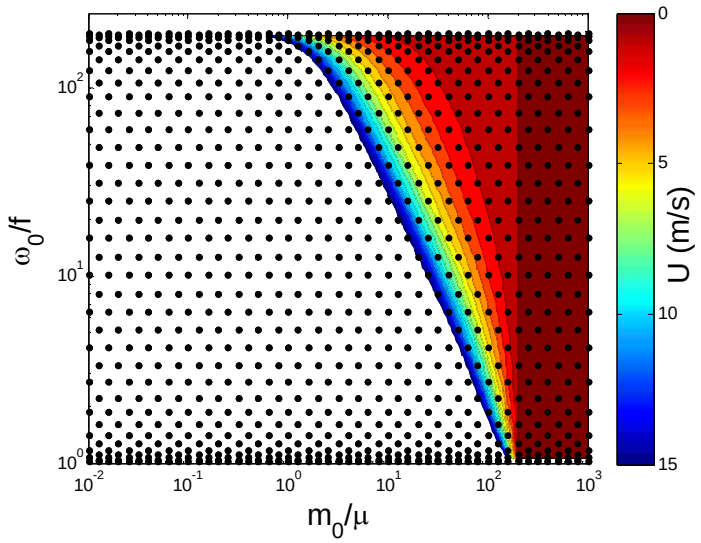


**Figure 3.15 Background velocities required for internal waves to reach a critical level. Color contours are in m/s. If the required velocity is larger than 15 m/s, the region is white.**

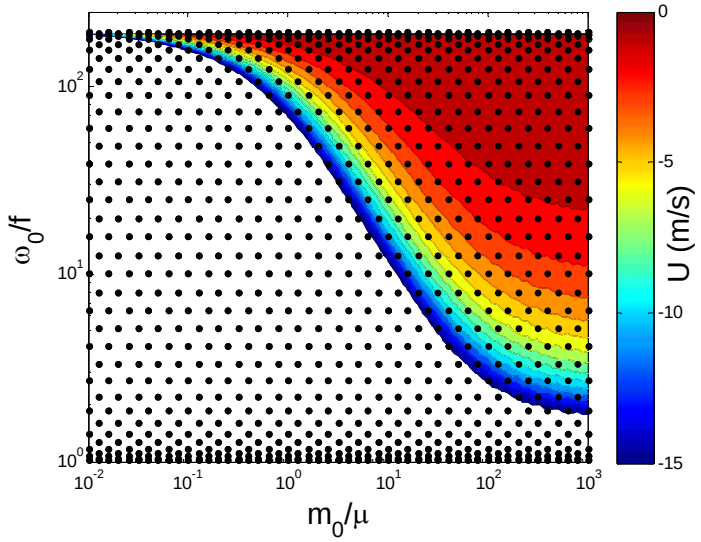


**Figure 3.16 Background velocities required for internal waves to reach a turning point. Color contours are in m/s. If the required velocity is larger than 15 m/s, the region is white.**

Figure 3.15 differs significantly from Figure 3.8. While the critical level velocity for the time-independent interaction was principally a function of the initial vertical wavenumber, the critical level velocity for the interaction with an infinite wave train is strongly dependent on the initial frequency. Figure 3.16 is only slightly different from Figure 3.9, indicating that time-dependence has a smaller effect on turning points compared to critical levels.

If properties of the inertial wave, such as $M$, are changed, then the chances of a critical level or turning point are altered. Because the phase speed of the inertial wave is equal to $f/M$, as the magnitude of $M$ increases, the phase speed of the inertial wave decreases. As the phase speed decreases, the inertial wave interaction becomes more like a time-independent flow interaction, where real critical levels exist. This reasoning shows that as $M$ increases or $f$ decreases, the probability of a Jones' critical level should increase toward the required probability of a critical level in a time-independent flow field. Incidentally, the probability of turning points also increases. The alternate is also true, in that if $M$ decreases or $f$ increases, the probability of a critical level or turning point decreases, as is shown in Figure 3.17 and Figure 3.18. These plots show the critical level velocities and turning point velocities for different values of $M$, and show different scale separation lines. As the phase speed of the inertial wave increases, the small wave has less time to be affected by the interaction, ultimately reducing the severity of the interaction.

Changes $f$ or $N$ will also affect the outcome of the interaction. Because free propagating waves must have frequencies between $f$ or $N$, any change in $f$ or $N$ will change the range in which waves may exist in the environment. The general patterns for other values of $f$ or $N$ are similar to those shown in Figure 3.15 - Figure 3.18, where waves with initial frequencies near $N$ are more likely to experience a turning point and waves with large initial wavenumbers are more likely to reach a Jones' critical level.

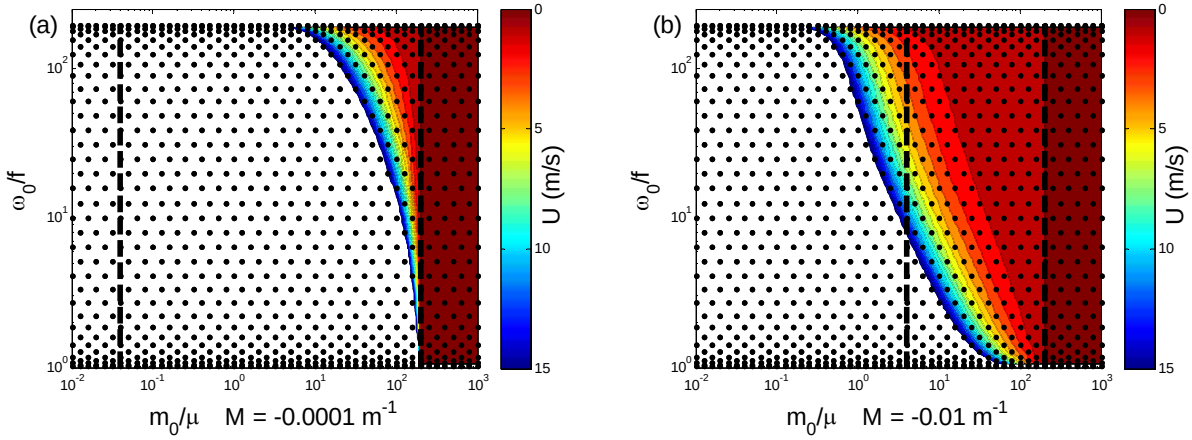


**Figure 3.17 Changes in *M* affect the velocities required for internal waves to reach a critical level. Smaller values of *M* result in larger required velocities. If the required velocity is larger than 15 m/s, the region is white.**

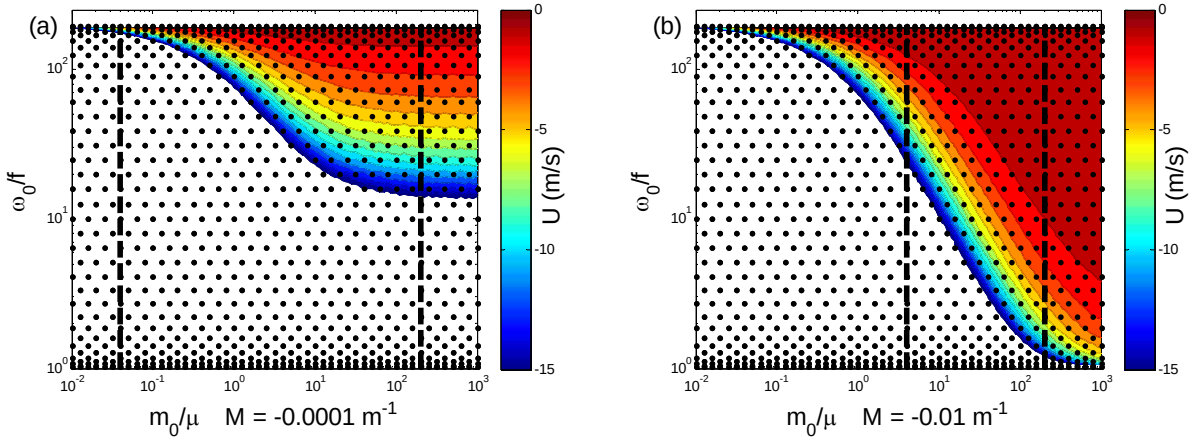


**Figure 3.18 Changes in *M* affect the velocities required for internal waves to reach a turning point. Smaller values of *M* generally result in larger required velocities. If the required velocity is larger than 15 m/s, the region is white.**

For all these scenarios, the critical wavenumber is kept constant, at $m_{CR} = -2\pi / 12.5\ m^{-1}$. This value was used by Eckermann (1997), who also displayed nearly identical results to those shown in Figure 3.14c. This value of $m_{CR}$ is practical for atmospheric interactions of these kinds, but may change with different interactions or environments. Also, it should be remembered that wave breaking may occur in other ways besides reaching a Jones' critical level.

### 3.2.3 Wave Action Density and Steepness

The internal waves may become unstable due to changes in wave action density or steepness. The wave action density can be calculated in the same manner as the time-independent case, by combining equations 3.21 and 3.14. This agrees with equation 27 of Eckermann (1997).

$$\frac{A}{A_0} = \frac{c_{gz0} - f / M}{c_{gz} - f / M} \tag{3.27}$$

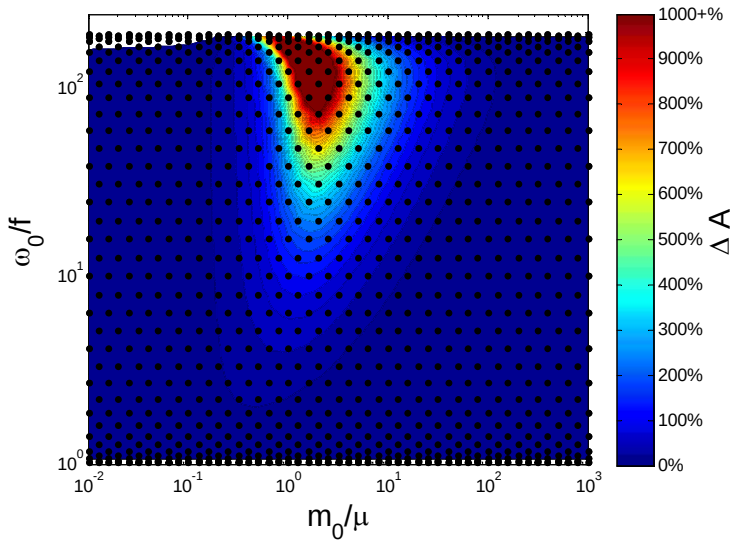


**Figure 3.19 Contours of maximum increase in wave action density. The maximum positive background velocity is 5 m/s**

From this the wave action density may be calculated from any wavenumber *m* or any velocity *U*, provided the wave hasn't been reflected. Figure 3.19 shows the maximum relative change in wave action density during an interaction with an inertial wave with background velocity magnitudes of 5 m/s. This maximum change occurs when the small internal wave propagates through the maximum positive background velocity.

The waves that will experience the largest change in wave action density are those that have initial frequencies near *N* and initial vertical wavenumbers between $\mu$ and *10* $\mu$. Although this region is not necessarily regular or intuitive, the region is found to be bounded by limits inherent to the interaction. Equation 3.27 indicates that there is a maximum change associated with an infinite velocity and therefore an infinite vertical wavenumber. This is done by setting $U = \infty$ and subsequently, $c_{gz(U=\infty)} = 0$. Understanding this maximum potential change is beneficial for understanding the actual change in wave action density associated with a finite background velocity, as is shown in Figure 3.20.

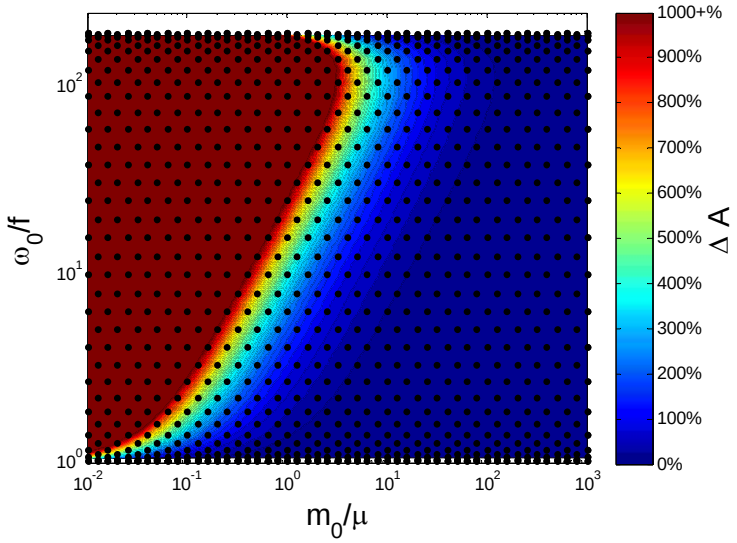


**Figure 3.20 Contours of maximum change in wave action density with an infinite background velocity and finite inertial phase speed.**

The waves with small initial wavenumbers will experience large changes in wave action density, whereas waves with larger initial wavenumbers will have a small, finite change, even with a background velocity approaching infinity. This indicates a maximum change in wave action density which diminishes with larger wavenumbers. Interestingly, this limit is approximately defined by the phase speed of the inertial wave, which in this case is 0.1 m/s. The other limit may be taken from Figure 3.8, which illustrates that a critical level velocity exists for each type of wave in a time-independent flow field. Waves that do not experience a critical level in a time-independent flow field are not likely to experience a large change in wave action density for the same background velocity in an inertial wave. Internal waves that require larger critical level velocities will therefore experience smaller changes in wave action density. Both limits are shown in Figure 3.21, where the change in wave action density is depicted for two scenarios with different background velocity amplitudes and inertial phase speeds, jointly with white lines that indicate the inertial phase speed, plotted in frequency and wavenumber space, and time-independent critical level velocity. Because these lines are farther apart for Figure

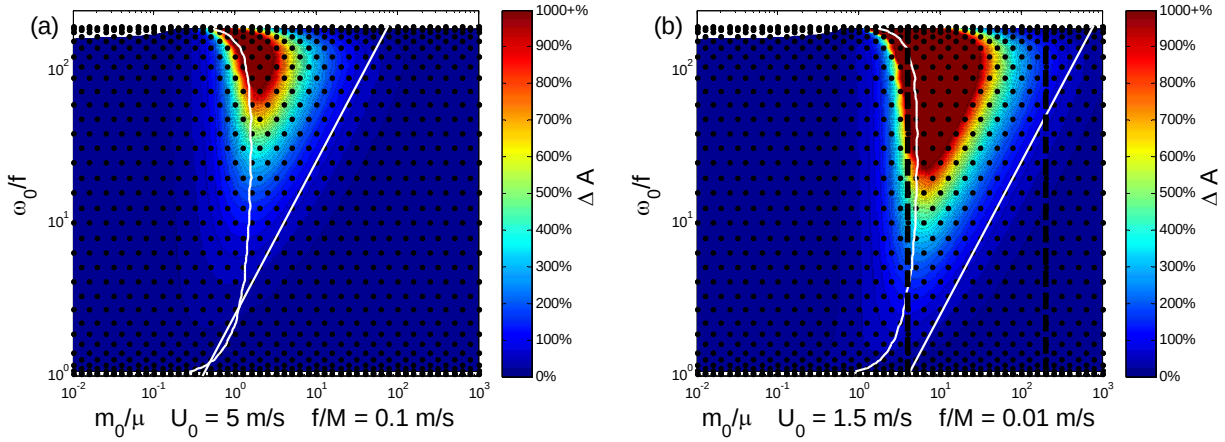


**Figure 3.21 Contours of maximum change in wave action density showing bounds of large change for two scenarios with different background velocities and inertial phase speeds. The white line to the left shows the critical level boundary for a stationary background, and the white line to the right shows the value of the inertial wave phase speed.**

3.21*b*, waves will experience a larger change in wave action density than Figure 3.21*b*. Waves with small initial frequencies will not experience large changes in wave action density, for the white lines converge in Figure 3.21 at lower frequencies.

Waves that exist to the right of the phase speed line will experience very little change in wave action density, as well as waves that exist far to the left of the left line. Waves in between the lines, and especially those that exist far from the right line, will experience large changes in wave action density.

The wave action density influences the probability of wave breaking by contributing to the change in wave steepness. An increase in wave action density results in an increase in wave steepness. Equation 3.18 is valid for this scenario in calculating the change for wave steepness.

$$\frac{\varsigma_z}{\varsigma_{z0}} = \left( \frac{A\omega_0}{\omega A_0} \right)^{1/2} \tag{3.18}$$

The changes in wave steepness depend on the frequency and action density, with the maximum steepness occurring when the action density is a maximum and the frequency is a

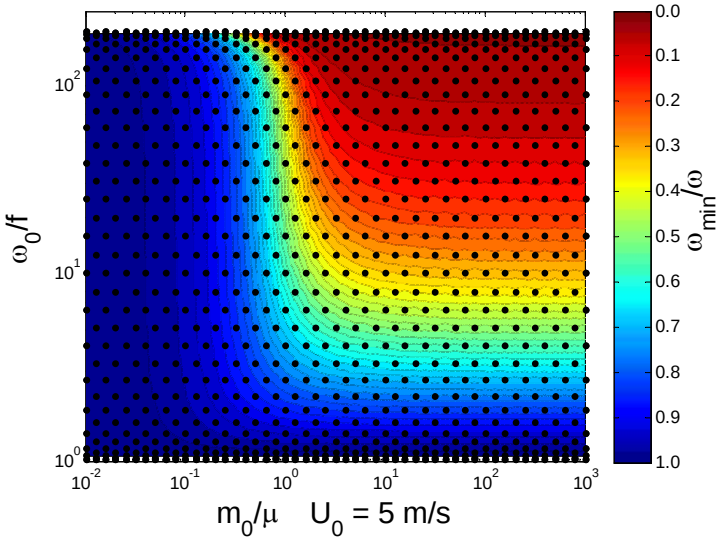


**Figure 3.22 Contours of maximum change in wave frequency.**

minimum. Figure 3.22 shows the maximum changes in wave frequency associated with waves propagating through an inertial wave with properties identical to those in Figure 3.20. The region that experiences the largest changes in frequency is nearly rectangular in the upper right portion of the figure, bounded on the left by the time-independent critical level velocity, and bounded on the bottom by the Coriolis frequency, for the change in frequency of the waves can never decrease below *f*. Because the wave steepness is a function of frequency and wave action density, it will experience the largest change in regions where both the frequency and wave action density experience large changes. For these interactions, the largest change in wave action density and wave steepness occur at the same location during the interaction, which is where the background velocity is at a maximum positive value. Figure 3.23 shows the resulting change in wave steepness by equation 3.18.

This wave steepness plot shows a defined region where the waves experience a large relative change in wave steepness, and have a higher likelihood of wave breaking. When internal waves reach excessive wave steepness, defined by a value of $\zeta_z = 1.0$ by equation 3.9, the

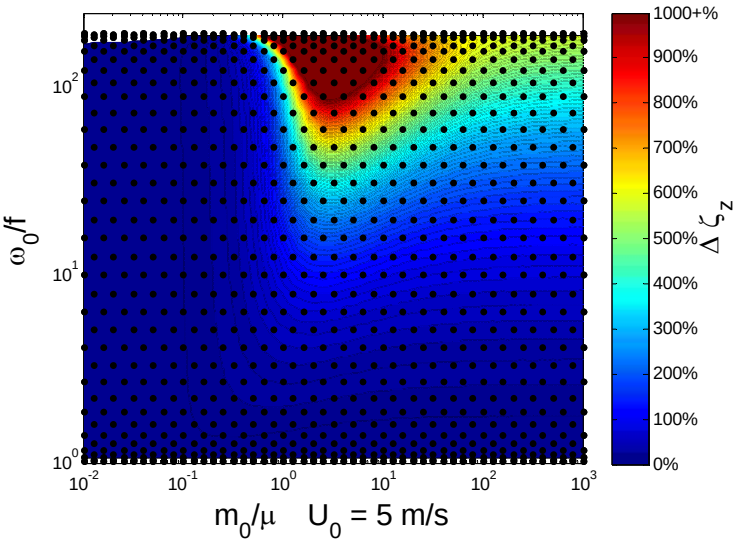


**Figure 3.23 Contours of maximum change in wave steepness.**

waves become unstable and are likely to overturn, break, and be dissipated by turbulence. This may be the same result as when internal waves approach a critical level or Jones' critical level, yet the waves that will experience the largest change in wave steepness do not necessarily correspond to the waves that will reach a critical level for the same interaction.

The most severe change in wave steepness in Figure 3.23 occurs for waves that have large initial frequencies and initial vertical wavenumbers between $\mu$ and $10\ \mu$. Because wave steepness is given as a relative change, it would be necessary to know an initial steepness of the internal waves to predict whether they would become affected by excessive wave steepening. For example, if the waves had an initial steepness magnitude of 0.1, an increase multiplier of 10 would result in a value of unity and the waves would become unstable and possibly overturn. This refers to any waves in the dark red region in Figure 3.23. Background velocities that cause wave steepness to increase by a factor of 10 are shown in Figure 3.24. Comparing this region to Figure 3.14b or Figure 3.15 shows that these waves may not experience a Jones' critical level,

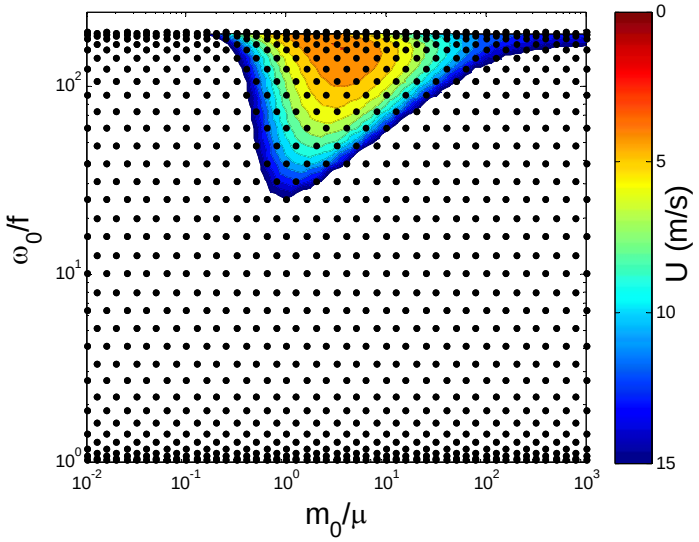


**Figure 3.24 Background velocity contours required to increase wave steepness by a factor of 10. Compare with Figure 3.15.**

but rather are more likely to experience reflection or possible free propagation if wave steepness is ignored. Therefore, the waves in this region may possibly overturn due to excessive steepness yet not approach any critical wavenumber. It may also be concluded that wave instability may be caused by multiple sources, such as reaching a critical wavenumber or excessive wave steepening, and in some cases the wave may become reflected in place of or in combination to other results. This paper will not discuss in detail which outcome is most likely, as such details require nonlinear simulations.

It should be noted that for linear ray theory, the amplitude, which affects the initial wave steepness, has no effect on the probability of reaching a critical wavenumber or reflection, so each potential outcome is independent of the other. Figure 3.25 illustrates the change in wave steepness jointly with the waves that will experience a Jones' critical level or turning point for two different inertial wave amplitudes, showing how the some waves will steepen without approaching a Jones' critical level. In the regions where waves will experience large changes in wave steepness, those waves may be otherwise expected to freely propagate or become reflected.

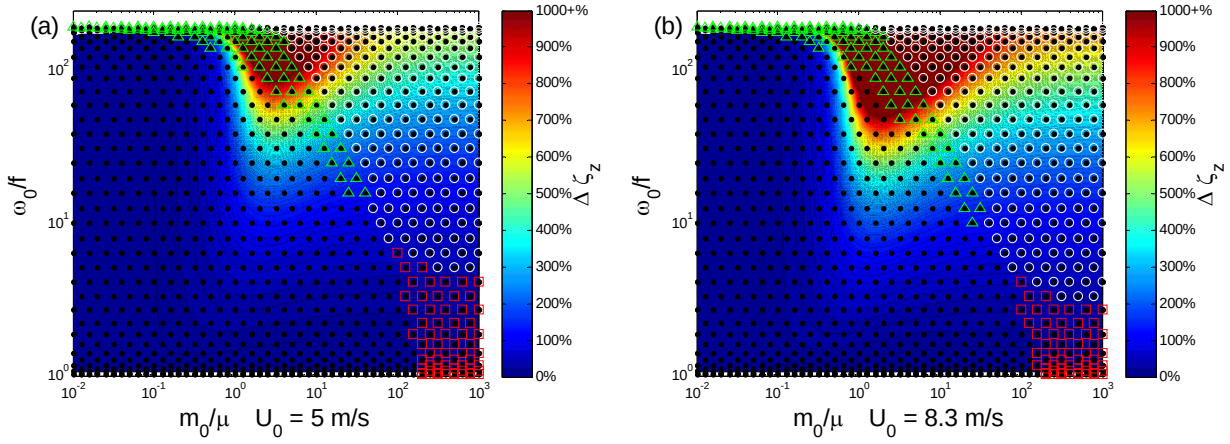


**Figure 3.25 Summary of end results of internal waves interacting with a background inertial wave, combined with relative changes in wave steepness. Waves may be impacted by changes in wave steepness or critical levels and turning points. Green triangles depict waves that reach a turning point, red squares represent waves that reach critical levels, and white circles represent waves that reach either a turning point or critical level.**

Nonlinear simulations are required to determine which outcome would occur, or whether a combination of both might occur. Figure 3.25b has a larger dark red region than Figure 3.25a where the waves will not experience a critical level or turning point. This indicates that waves that become unstable due to steepness are more necessarily analyzed when background velocities are large.

### 3.2.4 Shear-induced Instability

In addition to reaching a Jones' critical level or excessive wave steepness, internal waves can become unstable due to background shear. As mentioned in the introduction, wave instability occurs when the background gradient Richardson number falls below about 1.0 and is calculated by equation 3.28.

$$Ri_g = \frac{N^2}{\left(\frac{dU}{dz}\right)^2} \tag{3.28}$$

Because the small internal waves are scale separated from the large inertial wave, and the small waves are assumed to have no affect on the background flow field, most of the shear will come from the background wave. If the local $Ri_g$ calculated from the background is near a value of 1.0, internal waves may become unstable at this location. The strongest background shear occurs near the nodes of the inertial wave, where the background velocity is near zero, and has a magnitude of $|U_0 M|$ for a sinusoidal inertial wave. This indicates that the background shear increases with larger background velocities or smaller inertial wavelengths.

Figure 3.26 shows that in order for $Ri_g$ to approach a value of 1.0, maximum background velocities near 20 m/s are required for the inertial wavelength used in previous simulations.

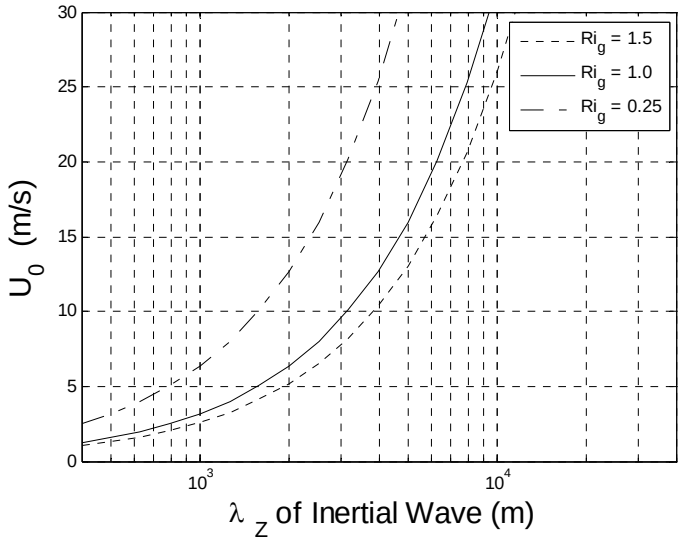


**Figure 3.26 Required background velocities to reach low Richardson numbers. Linear ray theory becomes invalid when $Ri_g$ falls below about 1.5, and waves become unstable when $Ri_g$ falls below about 1.0.**

Shear-induced instability is therefore unlikely for internal waves interacting with inertial waves of this size, for 20 m/s may be excessively large. However, for inertial waves with smaller vertical wavelengths such as inertial wavelengths of 1.0 km, or $M = -2\pi/1000\ m^{-1}$ (observed inertial waves noted in the introduction had wavelengths of 1-7 km), background velocities of only 3.0 m/s will result in small values of $Ri_g$. Internal waves interacting with these inertial waves will experience even lower values of local $Ri_g$ due to added wave-induced shear, and may become unstable and overturn. It is interesting to note that this type of instability occurs where the background velocity magnitude is near zero, and other forms of internal wave instability, such critical levels and wave steepening, occur when the background velocity is at maximum positive value.

Richardson numbers measure stability, not only for interacting internal waves but also for the background itself. If the local background Richardson number falls below about 0.25, the

background itself may become unstable and some overturning and mixing may occur, independent of small internal waves. Therefore, there exists a maximum background velocity shear for a stable inertial wave, which is twice the value of the velocity that causes a $Ri_g$ of 1.0. In other words, there exists a range of inertial background velocities that will allow for shear-induced instability for interacting internal waves. Also, the introduction noted that linear theory was only valid for local Richardson numbers above about 1.5. If the background Richardson number falls below about 1.5, but not below 1.0, the ray tracing simulation may not accurately predict the outcome.

### 3.2.5 Time to Breaking

It may be beneficial to know the approximate time between wave generation and wave breaking. This can be calculated using ray theory if simplifying assumptions are made. If the internal waves are assumed to break upon reaching a critical wavenumber, and that a wind shear is constant, the time to breaking may be determined for both time-independent flows and time-dependent flows. Equation 2.21 is used to determine the time to wave breaking.

$$\frac{\partial m}{\partial t} = -k\frac{\partial U}{\partial z} \tag{2.21}$$

$$\frac{\partial U}{\partial z} = Cst$$

$$dm = -k\frac{dU}{dz}dt$$

$$m_{CR} = m_0 + dm$$

$$dt = \frac{m_0 - m_{CR}}{k\dfrac{dU}{dz}} \tag{3.29}$$

The time required to reach a critical wavenumber is shown in Figure 3.27, and the velocities are given by equations 3.2 or 3.24. It is interesting to note that, given the same background shear, the required velocities and the required time to breaking may be very different. This is because $m$ changes at rates proportional to the value of $k$, according to equation 2.21. For a majority of the domain, where the magnitude of $m_{CR}$ is much larger than the magnitude of $m_0$, the time required is inversely proportional to the value of $k$.

As expected, the time required for initial wavenumbers near the critical wavenumber is small. Any waves that have initial vertical wavenumbers larger than $m_{CR}$ do not require any time, as is shown by the dark red rectangular region in the figure.

Although a background wind profile with a constant wind shear is not very realistic, Figure 3.27 still offers important information. Real scenarios are rarely constant, and a background wind velocity profile may exist for a finite amount of time before changing. Similarly, inertial waves may only exist for finite periods of time. The inertial wave packets that

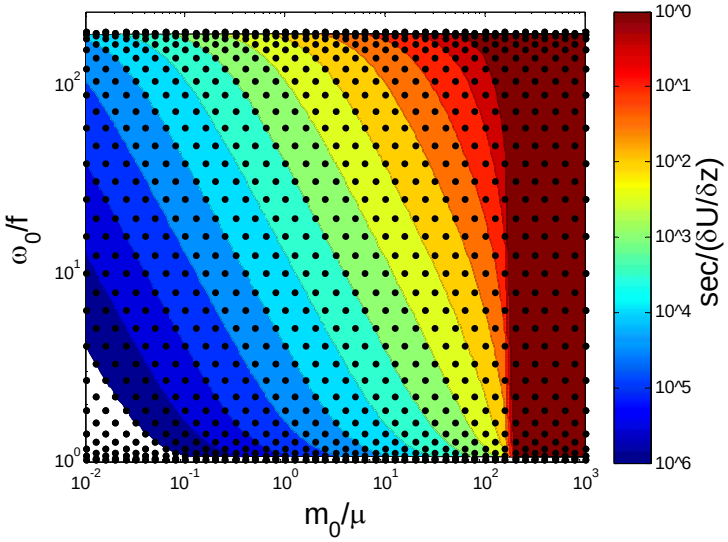


**Figure 3.27 Time required to reach a critical level for a time-independent or time-dependent flow, assuming a constant background wind shear. Color contours are in seconds divided by the background shear.**

were detected by Sato, O'Sullivan, and Dunkerton (1997) only existed, or were at least identifiable, for a few inertial periods at a time. If internal waves are expected to reach a critical level or turning point, either in a time-independent or time-dependent background flow, it is necessary that the background flow persist for sufficient time for the internal waves to be affected. From Figure 3.27, waves with larger initial frequencies will approach a critical level faster than lower frequency waves that require the same background velocities. More of these waves may therefore reach a critical level when the background flow is temporary.

The role of time-dependence is very important in predicting the outcomes of internal wave propagation. Waves may become unstable due to encountering a Jones' critical level, excessive wave steepening, or excessive shear. The probability of reaching a Jones' critical level is significantly reduced for time-dependent flows, and the difference is enhanced with increased phase speeds of the inertial wave. The probability of turning points is only slightly reduced for time-dependent interactions, unless the phase speed is significantly large compared to the maximum background velocities, in which case the probability of turning points is significantly reduced. Wave steepness and shear may also affect the stability of internal waves during interactions, so all stability factors should be used in predicting interaction outcomes.

The equations discussed in this section, and velocities required for a critical level or turning point, do not require that the inertial wave have more than one phase of positive horizontal velocity and one phase of negative horizontal velocity. For this reason, the equations are valid for phases of different magnitudes of velocity. The phases are also not required to be sinusoidal in shape, but may take any form (except for Figure 3.26 which assumes a sinusoidal wave. The only requirement is that the phases move vertically at a constant phase speed and propagate as non-deforming envelopes of wind.

## 3.3 Wave Propagation through an Inertial Wave Packet

The interaction with an infinite wave train provides valuable information regarding how internal waves interact with time-dependent background flows, specifically interactions with vertically moving, yet non-deforming, envelopes of background wind. Although it is beneficial to understand the interaction between internal waves and an infinite inertial wave train, such an interaction is not realistic in that internal waves, including inertial waves, exist as packets. It is therefore more beneficial to understand the interaction between small internal waves and an inertial wave packet, and how it differs from the interaction with an infinite wave train. This section describes the results from internal waves interacting with an idealized inertial wave packet contained within a Gaussian envelope, which is shown in Figure 3.28 and Figure 3.29. It will describe the differences in results from previous simulations with an infinite inertial wave train. The inertial wave packet is defined as a sinusoidal wave contained within a Gaussian

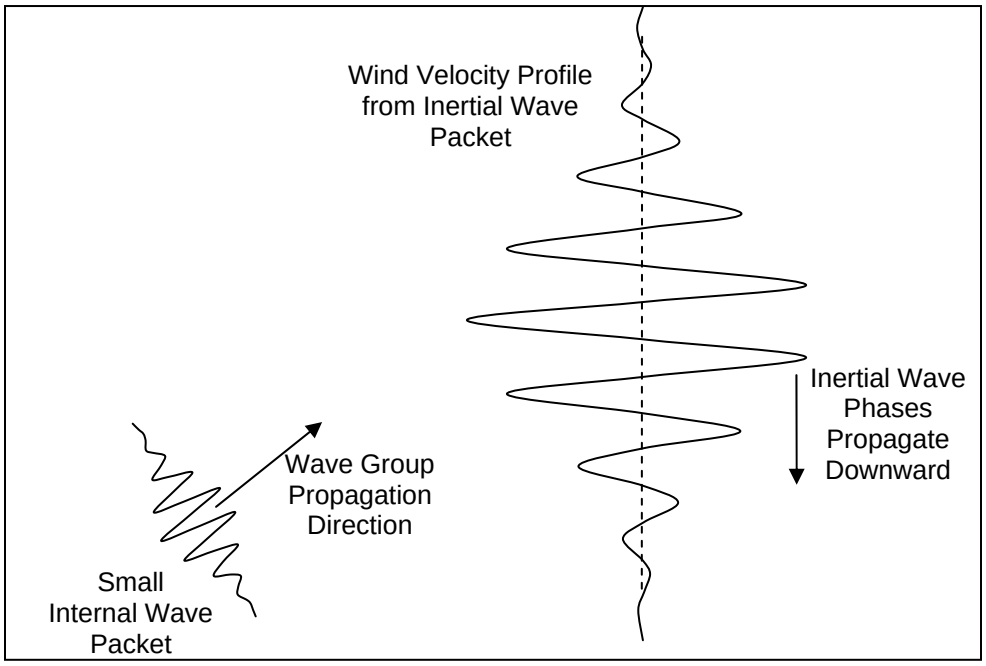


**Figure 3.28 Internal wave packet propagating through an inertial wave contained within a Gaussian envelope.**

envelope, but this section will show that the shape of the envelope does not significantly affect the outcomes of the interaction.

### 3.3.1 Influence of Envelope and "Zero Shift"

The propagation of an internal wave through an inertial wave packet contained within a Gaussian envelope presents some complicated adjustments to the changing properties of the wave during the interaction. The general trend is similar to the interaction with an infinite wave train, in that the vertical wavenumber and wave steepness increase in regions of positive background velocity and decrease in regions of negative background velocity. Figure 3.29 shows freely propagating waves whose vertical group velocity decreases in positive velocities and increases in negative velocities, but returns to its initial value after the interaction, similar to freely propagating waves in previous interactions.

In order to solve the infinite wave train interaction analytically, it was necessary to

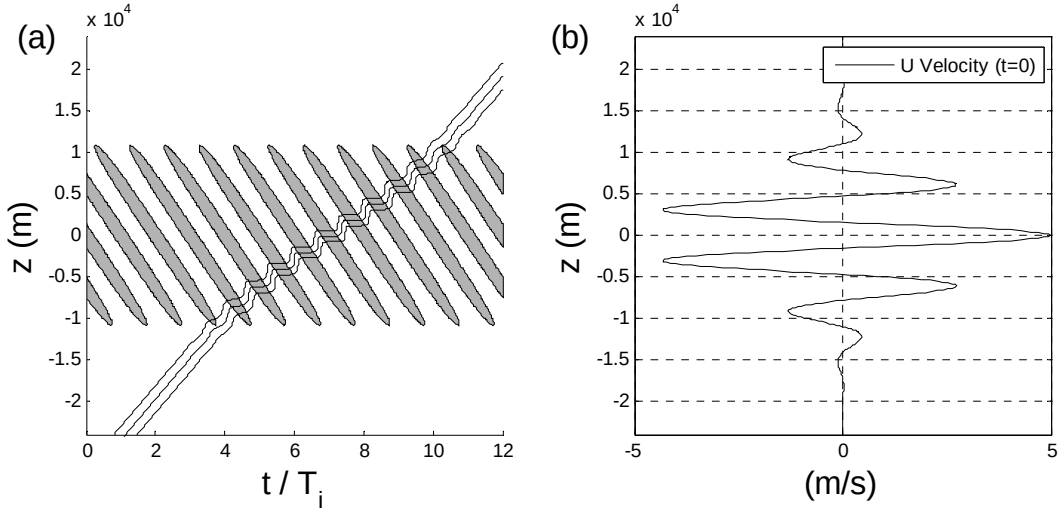


**Figure 3.29 (a) Internal wave packet rays propagating through an inertial wave packet. The shaded regions show where the background velocities exceed the time-independent critical level velocity. (b) shows the horizontal velocity profile at the initial time.**

change the frame of reference by subtracting the phase speed of the inertial wave from the vertical group velocity of the small wave. The background flow field was then considered time-independent as "seen" by the small waves. In the case of an inertial wave packet, contained in a Gaussian envelope, the phases of the inertial wave are continually deforming as the phases propagate through the inertial envelope. On the side of the envelope for which the small waves initially interact, the background velocity magnitudes are diminishing as the phases move away from the center of the packet. Conversely, the background velocity magnitudes for the closing of the envelope are growing. If the frame of reference is changed as before, where the phase speed of the inertial wave is subtracted from the group speed of the small waves, the small waves will initially propagate through diminishing phases until reaching the center of the envelope, followed by growing phases.

According to the ray equations, the properties of internal waves do not change when the background wind changes velocity with time but without shear, except that the horizontal group velocity of the small waves will be accelerating with the wind. The changing phase amplitudes of an inertial wave act as accelerating winds, and as such shift the "zero velocity" of the small waves, designated as $U_{ZERO}$. The variable $U_{ZERO}$ is defined as the velocity at which the properties of the small wave are identical to its initial conditions prior to the interaction, or $U_{ZERO} = U_{(\omega=\omega_0, m=m_0)}$, or may also be defined as the difference between the local background velocity and the predicted velocity from equation 3.24. $U_{ZERO}$ results in changes to the total frequency of the small wave, and is defined as

$$\Delta\Omega = kU_{ZERO} \tag{3.30}$$

For simulations involving an infinite wave train or a time-independent background flow field, this value has remained constant at $U_{ZERO} = 0$. In the previous scenarios, it was

theoretically possible to determine the wavenumbers, frequency, and wave action density of the small waves for any given background velocity and initial wave properties through the constancy of the total frequency. This is not the case for an inertial wave packet interaction. During the interaction, the small waves will spend less time in negative background velocities and more time in positive background velocity, due to the vertical group velocity of the small waves growing in positive shear and decreasing in negative shear. During the first half of the interaction, the background velocity magnitudes are diminishing as they propagate downwards, and as such $U_{ZERO}$ will generally be shifted downward. During the peak interaction, at the center of the Gaussian envelope, the frequency and wavenumbers of the small waves only return to their initial values at a background velocity between zero and the maximum negative velocity. Similarly, as the waves propagates out of the envelope, $U_{ZERO}$ is shifted upward towards its original value prior to the interaction, and assuming that a critical level or reflection have not occurred, the small waves propagate out of the inertial wave packet with no permanent changes. $U_{ZERO}$ returns to a value near zero after the interaction, and hence the properties of the small waves will be nearly identical to their initial conditions.

The ray tracing method of ray theory accounts for this shift, for it assumes that properties of the internal waves do not change with uniformly accelerating winds. When small waves propagate through an inertial wave packet, the largest shift occurs near the center of the packet envelope. At this point, the wave no longer "sees" background wind oscillations equal to the maximum velocities of the inertial wave, but rather the background velocities offset by $U_{ZERO}$. For example, if a short wave is propagating through an inertial wave with maximum oscillations of 5 m/s, and the short wave experiences a shift of 2 m/s, the short wave would then be experiencing oscillations of -3 to +7 m/s according to predicted property values defined by

equation 3.24. Figure 3.30 and Figure 3.31 show how *m* changes with the local background velocity as a small wave propagates through an inertial wave packet. The first is an interaction with an infinite wave train and the other is an interaction with an inertial wave contained within a Gaussian envelope. The small wave and inertial wave properties are identical to those defined for Figure 3.14b, with the only difference being that Figure 3.31 involves an inertial wave packet.

The shift is seen in Figure 3.31 which shows the vertical wavenumber plotted against the local background velocity during the entire interaction. At the beginning of the simulation, *m* only matches its initial value with background velocities near zero. During the interaction with the inertial wave packet, *m* passes its initial values with background velocities below zero. The largest shift occurs at the center of the envelope, with a magnitude of about 2.5 m/s. This means that in comparing the interaction to that of one with an infinite wave train, the small wave is experiencing background oscillations of -2.5 and 7.5 m/s. The curves in Figure 3.31 are nearly parallel to the curves in Figure 3.30, only shifted along the horizontal axis. This shows how

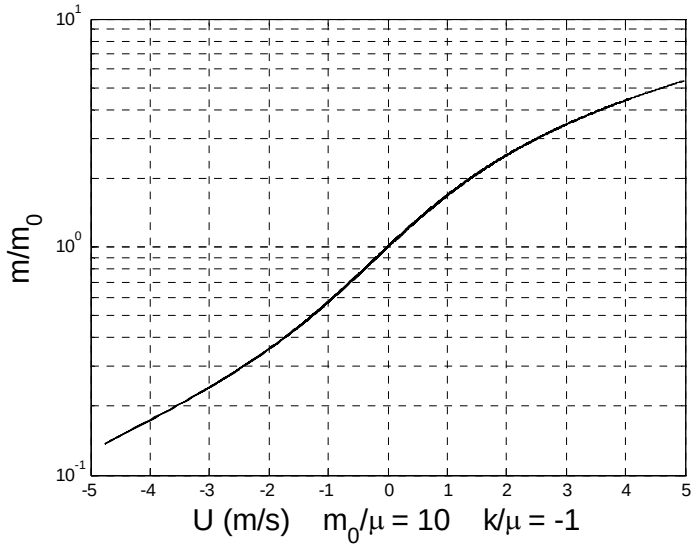


**Figure 3.30 Single internal wave propagating through an infinite inertial wave train, showing vertical wave number against the local background velocity. This plot agrees with equation 3.24.**

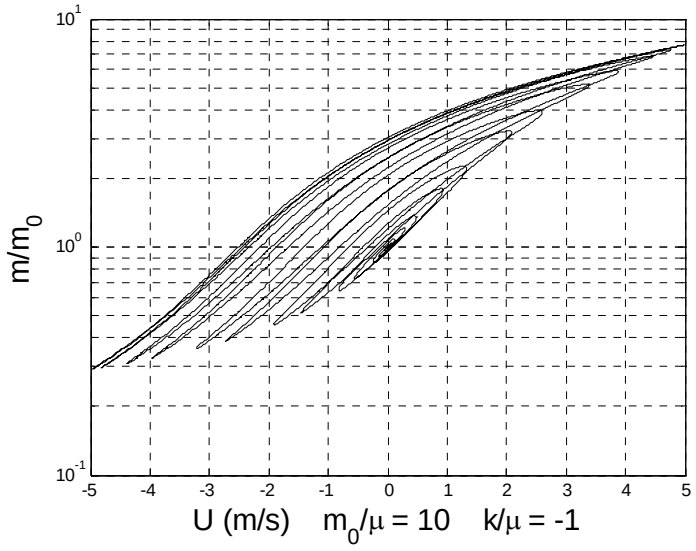


**Figure 3.31 Single internal wave propagating through an inertial wave contained within a Gaussian envelope, showing vertical wave number against the local background velocity. This illustrates divergence from equation 3.24.**

$U_{ZERO}$ is shifted during the opening and closing of the envelope, and it can be seen that when the envelope is opened to where the maximum background velocities are about 3.0 m/s, $U_{ZERO}$ has shifted about 1.0 m/s.

$U_{ZERO}$ is not significantly affected by $L$, the length of the inertial envelope, which is an indicator of how many inertial wavelengths exist within the envelope. While Figure 3.31 represents an interaction where about four or five distinct crests and troughs exist within the inertial wave packet, Figure 3.32 shows the same interaction with a value of $L$ that is twice as large as the original packet, and about nine or ten distinct wavelengths exist within the envelope. Both figures indicate the same total shift independent of the value of $L$.

$U_{ZERO}$ has a significant impact on the outcome of the interaction. As mentioned previously, background velocities opposing the horizontal phase speed of the small wave lead to reflection and background velocities in the same horizontal direction lead to critical levels. Because $U_{ZERO}$ causes the waves to experience larger positive background velocities, the ultimate result of $U_{ZERO}$ is that the small wave is less likely to experience a turning point and is more likely to experience a Jones' critical level. Comparing Figure 3.30 and Figure 3.31 shows that these waves propagating through an inertial wave packet will experience maximum values of *m* that are about 50% larger for an inertial packet when compared to an infinite wave train. Conversely, the minimum value of *m* is twice as large for an inertial packet when compared to an infinite wave train. Although the interactions of Figure 3.31 or Figure 3.32 do not experience a Jones' critical level or turning point, they are illustrative of how the inertial envelope changes the possible outcomes of the interactions. Waves that come close to experiencing a Jones' critical

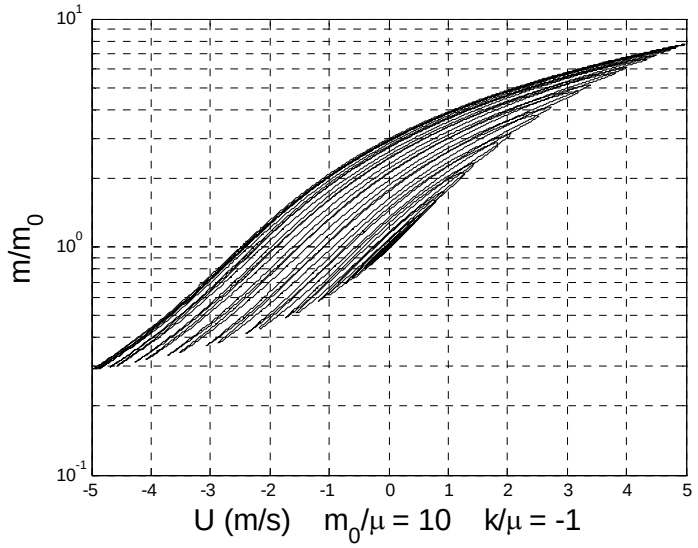


**Figure 3.32 Single internal wave propagating through an inertial wave contained within a Gaussian envelope, showing vertical wave number against background velocity. The same shift occurs when compared to Figure 3.31**

level in an infinite wave train are likely to experience a critical level when dealing with an inertial wave packet.

$U_{ZERO}$ may be determined by tracking the background wind acceleration from a frame of reference moving at the inertial phase speed in the downward direction. The acceleration of the local wind from this frame of reference as seen by the small wave is shown below, as well as how it affects the change in total frequency.

$$\frac{dU_{ZERO}}{dt} = \frac{\partial U_{ENV}}{\partial z}\frac{f}{M}\frac{U}{U_{ENV}} \tag{3.31}$$

$$\frac{d\Omega}{dt} = k\frac{\partial U_{ENV}}{\partial z}\frac{f}{M}\frac{U}{U_{ENV}} \tag{3.32}$$

The term $\frac{\partial U_{ENV}}{\partial z}$ is the slope of the inertial wave envelope relative to the vertical direction and $f/M$ is the inertial phase speed. $U$ is the local background wind and can be defined as $U = U_{ENV}\cos\theta$, where $\theta$ is the local phase of the inertial wave. The value of $U_{ZERO}$ can also be represented relative to the size of the envelope, by equation 3.33.

$$\frac{dU_{ZERO}}{dU_{ENV}} = f/M\,\frac{\cos\theta}{c_{gz}} \tag{3.33}$$

Because $c_{gz}$ of the small waves is a function of *m* in these scenarios, and *m* is a function of both *U* and $U_{ZERO}$, the analytical solution to this equation is nonlinear and difficult to display, though the trend can be seen in Figure 3.33b and Figure 3.34b. The average value of $U_{ZERO}$ is related to the size of the envelope, in a nearly hyperbolic trend. This hyperbolic trend shows that $\frac{dU_{ZERO}}{dU_{ENV}}$ is zero outside of the envelope and asymptotically approaches a minimum slope of -1 after the envelope is sufficiently large. Due to this trend, even very large background velocities

may not result in a turning point, since $U_{ZERO}$ may be shifted at about the same rate as the opening of the envelope, canceling the effect of the negative background velocities. The rate at which $U_{ZERO}$ is shifted depends on the properties of the small waves and inertial wave.

Figure 3.33 and Figure 3.34 show the same interactions as displayed in Figure 3.31 and Figure 3.32, respectively. The value of $U_{ZERO}$ oscillates as the small waves propagate through the phases of the inertial wave, indicated by the black lines in (b), but the average change is regular, shown by the dashed red line. For larger values of *L*, the magnitude of the oscillations of $U_{ZERO}$ diminishes, because the inertial envelope opens and closes more slowly. Because the magnitude of the oscillations is inversely related to *L*, or rather the magnitude is related to $\frac{\partial U_{ENV}}{\partial z}$, waves may be slightly more likely to experience a Jones' critical level or turning point sooner when interacting with inertial waves with small values of *L*. For a Gaussian envelope, $\frac{\partial U_{ENV}}{\partial z}$ is near zero at locations near the center of the envelope, and the $U_{ZERO}$ oscillations diminish in these regions, as indicated by Figure 3.33b and Figure 3.34b. This indicates that the total probability of small waves reaching a Jones' critical level or turning point does not significantly change with different values of *L*, but the Jones' critical level or turning point may occur at slightly smaller background velocities for smaller values of *L*.

The value of $U_{ZERO}$ may change significantly for inertial wave interactions but is dependent on initial small wave frequencies and wavenumbers, inertial wavenumbers and background velocities. Also, the value of $U_{ZERO}$ may not be realistically determined after a wave experiences a turning point or critical level, yet $U_{ZERO}$ will have an impact on whether these outcomes occur.

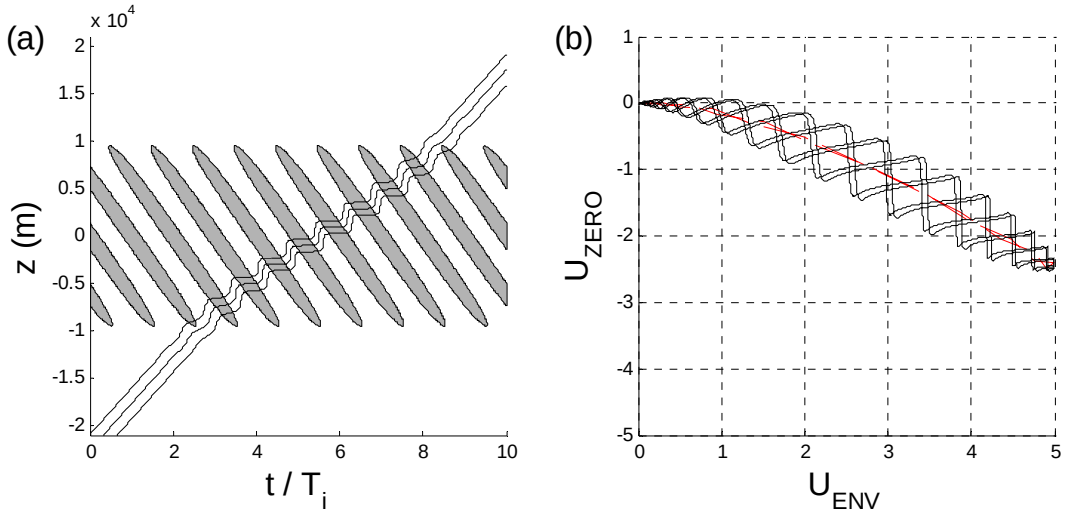


**Figure 3.33 (a) shows ray trajectories with shaded regions representing horizontal velocities exceeding time-independent critical level velocity. (b) shows how $U_{ZERO}$ changes with the envelope. Black lines show $U_{ZERO}$ for each ray, one as each ray propagates into the center of the envelope, and the other as it propagates out of the envelope. The dashed red line shows the average $U_{ZERO}$ during propagation through the envelope.**

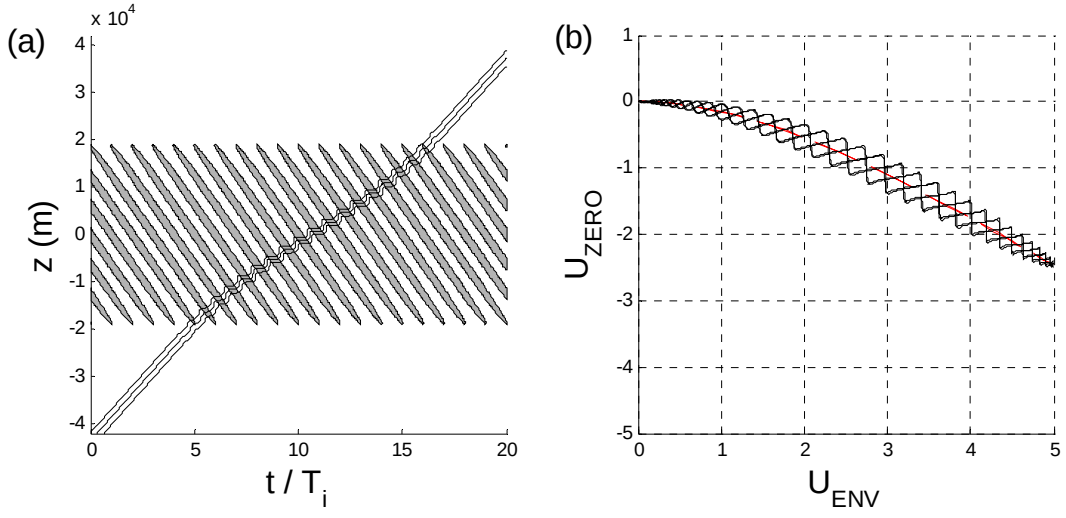


**Figure 3.34 Plots identical to Figure 3.33 but with a larger value of *L*. Larger envelope sizes result in smaller oscillations about the average $U_{ZERO}$, but the same average value of $U_{ZERO}$.**

Figure 3.35 illustrates the shift that occurs with numerous interactions with an inertial wave packet with maximum background velocities of 5 m/s, and the vertical wavenumber of the inertial wave packet is $M = -0.001\, m^{-1}$. The small waves may experience magnitudes of $U_{ZERO}$ up to about 4 m/s, or 80% of the total amplitude, but this only occurs for large initial wavenumbers of the small waves in the mid-frequency region. Waves with small initial wavenumbers, where $m < \mu$, experienced little or no offset. These waves also had large initial group speeds and required large velocities for reaching a critical level, so it is not expected that they would experience large changes in $U_{ZERO}$. The blackened portions of the figure represent areas without valid offset data, the upper right portion representing the region where the short waves experienced reflection before a maximum offset value could be obtained, and the far right portion representing a region where the small waves were initialized in a Jones' critical level.

The results change significantly between an inertial wave train and an inertial packet. Figure 3.36 shows how $U_{ZERO}$ will affect the outcome of the interaction. For these simulations,

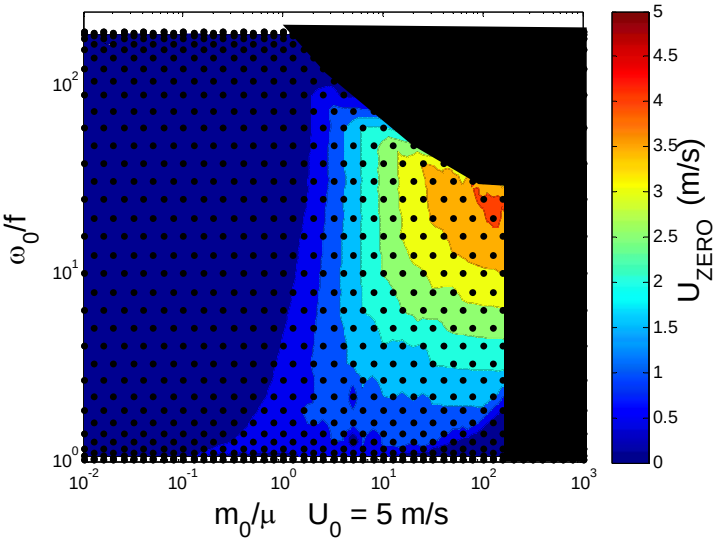


**Figure 3.35 Maximum change in $U_{ZERO}$ for an interaction with an inertial wave with 5 m/s maximum horizontal velocities.**

the chances of reflection have diminished and no waves with initial frequencies lower than about $30f$ were capable of reaching a turning point. Other waves reached a Jones' critical level during the interaction with an inertial wave packet, but these waves would have required background velocities larger than 5 m/s to reach a critical level interacting with an infinite wave train. For all the waves tested in this interaction, the inertial envelope caused the number of waves that reached a critical to increase by about 4% and the number of reflections decreased by about 21%. The number of freely propagating waves stayed constant at about 60% of all waves tested.

In all these simulations, the inertial wave packet is contained within a Gaussian envelope, yet the shape of the packet does is not very important. Other scenarios were run using triangular or parabolic envelopes and the average values of $U_{ZERO}$ were identical. Only the oscillating values of $U_{ZERO}$, illustrated in Figure 3.33b and Figure 3.34b, changed with the shape of the envelope. For the opening and closing of the envelope, equation 3.31 shows that a change in the envelope size corresponds to a specific change in $U_{ZERO}$, and this governed the magnitudes of the oscillations.

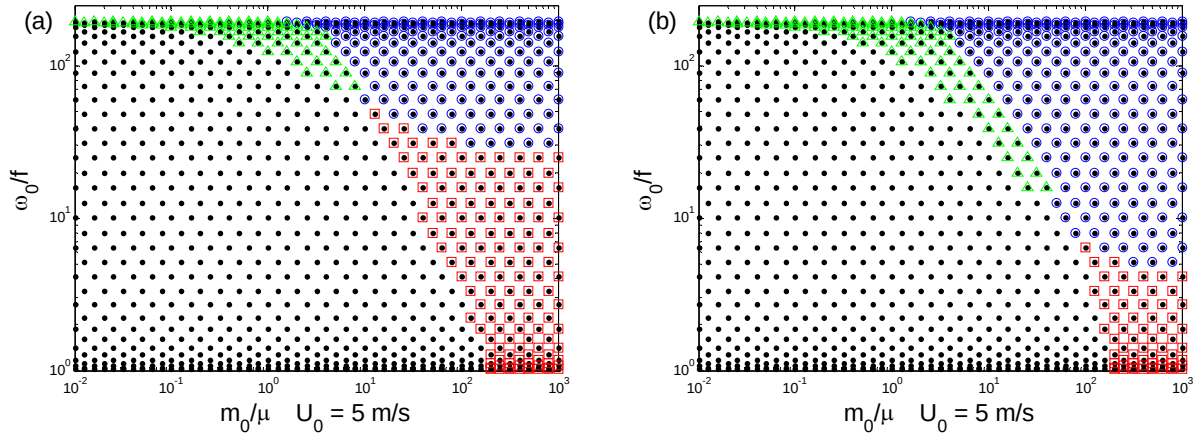


**Figure 3.36 Effect of inertial wave envelope on internal wave interactions result. Plot (a) shows results from an internal wave interaction with an inertial wave packet. Plot (b) shows interaction with an infinite inertial wave train. Green triangles depict waves that reach a turning point, red squares represent waves that reach critical levels, and blue circles represent waves that reach either a turning point or critical level.**

If the inertial envelope is not much larger than the inertial waves, containing at least three or four distinct inertial wavelengths, wave rays will experience dissimilar interactions. If fewer wavelengths exist in the packet, the small waves may never interact with a significant background crest or trough, and the results of the interaction become dependent on where the small waves approach the inertial wave. To this point, the outcomes of the interactions with an inertial wave packet are not dependent on how the small waves approach the packet. Hence, the results discussed here are not valid if the inertial wave packet is not sufficiently large.

$U_{ZERO}$ has been defined by comparing the vertical wavenumber or frequency of the small wave to equation 3.24 during the interaction, effectively comparing $m$ to $m_0$ or $\omega$ to $\omega_0$. However, if instead of $m$ or $\omega$, $A$ is used to calculate the offset, slightly different results occur. This involves calculating $U_{ZERO}$ based on divergence from equation 3.27 during the interaction. Figure 3.37 - Figure 3.39 are recreations of Figure 3.30 - Figure 3.32, except that $A$ is used instead of $m$.

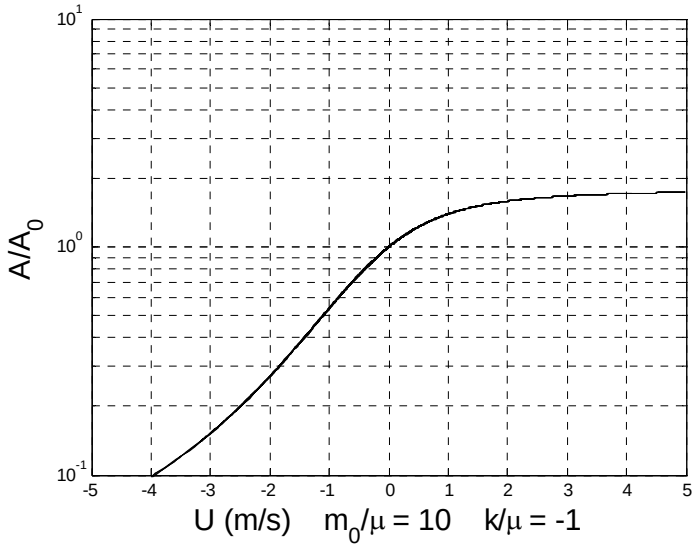


**Figure 3.37 Plot of wave action density against local background velocity for internal wave propagating through an infinite inertial wave train. This plot agrees with equation 3.27.**

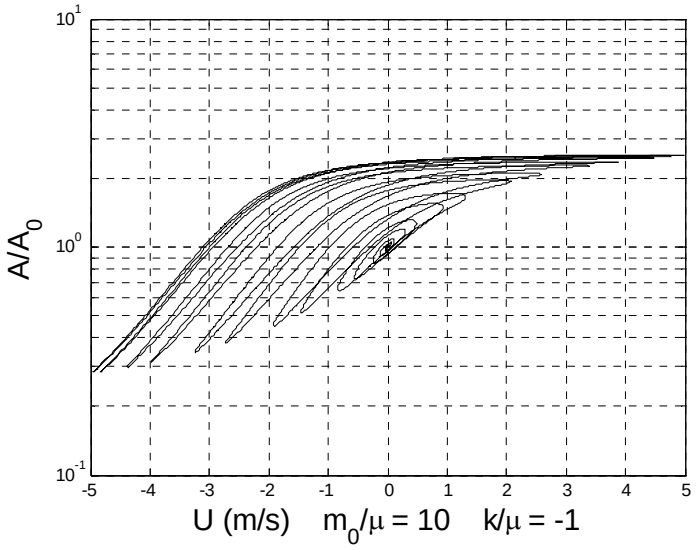


**Figure 3.38 Plot of wave action density against local background velocity for internal wave propagating through an inertial wave packet. This plot diverges from equation 3.27. Inertial envelope contains about four or five distinct wave crests and troughs.**

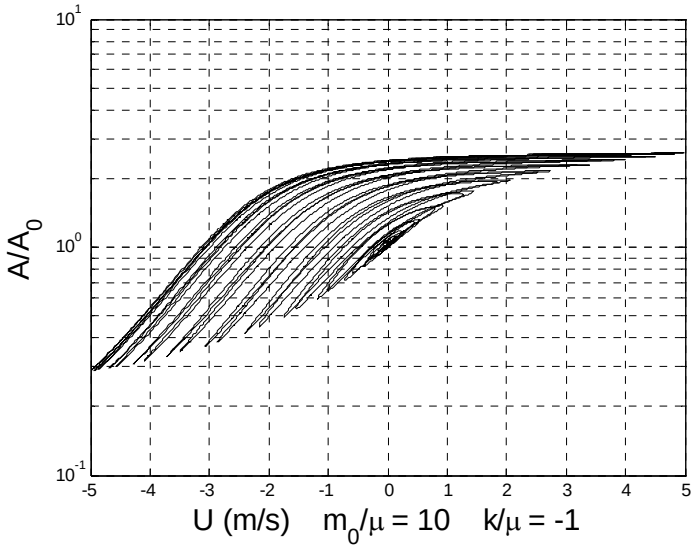


**Figure 3.39 Plot of wave action density against local background velocity for internal wave propagating through an inertial wave packet. Like $U_{ZERO}$ based on *m* or $\omega$, the size of the envelope does not affect the value of $U_{ZERO}$. Inertial envelope contains about nine or ten distinct wave crests and troughs.**

Figure 3.37 shows how $A$ changes when waves interacts with an infinite wave train, which agrees with equation 3.27. The other figures show the interaction with an inertial wave packet. The trends are similar to $U_{ZERO}$ based on $m$, in that the curves interacting with a wave packet are parallel to the curves of the infinite wave train simulation. $U_{ZERO}$ also shifts downward, indicating the small waves "see" different oscillations at the center of the envelope, where the maximum shift occurs.

Although the offset is still not affected by the length of the envelope, the values of $U_{ZERO}$ differ when defined by $A$ as compared to $m$ or $\omega$. While the maximum offset based on $m$ was about 2.5 m/s, the maximum offset as defined by $A$ is about 3.0 m/s for the same interaction. This is because different equations may define $U_{ZERO}$ when based on $A$. It was explained previously that the small wave encounters accelerating winds during the interaction, and these accelerations cause $U_{ZERO}$ to change. However, $A$ is not only influenced by the background velocity, but also by the background shear as shown by equation 3.15. In order to understand the behavior of $A$ during the interaction, it may be beneficial to define a "zero shear shift", or $\partial U/\partial z_{ZERO}$ in the same way that $U_{ZERO}$ was defined. This new variable is defined in equation 3.34.

$$\frac{\partial\left(\partial U/\partial z_{ZERO}\right)}{\partial t} = \frac{\partial U_{ENV}}{\partial z} f \sin\theta \tag{3.34}$$

This added equation makes it more difficult to describe the behavior analytically, yet the same qualitative result ensues. This shift causes the waves to experience larger positive background velocities, where the wave action, and subsequently wave steepness, rise and the wave may potentially overturn. Comparing Figure 3.37 and Figure 3.38 show that waves interacting with an inertial packet have larger maximum values of wave action density compared to an infinite wave train, and for this interaction the increase is about 20%. The minimum values

of wave action density are also larger for interactions with an inertial packet. Because the wave action density affects wave steepness, the waves may be more likely to overturn and break due to wave steepness, in addition to being more likely to encountering a Jones' critical level when interacting with an inertial wave packet when compared to an infinite inertial wave train.

This shift may also be defined by the wave steepness, $\zeta_Z$ in order to more accurately measure the difference in instability. Because $\zeta_Z$ is a function of both $A$ and $\omega$, it will experience an offset between the offset values defined by $A$ and $\omega$. This offset is related by equation 3.18, and Figure 3.40 shows that the interaction displayed in Figure 3.31 based on $\zeta_Z$. The resultant shift based on $\zeta_Z$ is about 2.8 m/s

For this simulation, the small waves will obtain a maximum wave steepness increase of about 400% for the interaction with an inertial wave packet and about 300% for the interaction with an infinite wave train. Waves are therefore more likely to overturn and break when interacting with an inertial wave packet due to wave steepness. In addition to reaching larger changes in wave steepness, the waves will also spend more time during the interaction at a larger

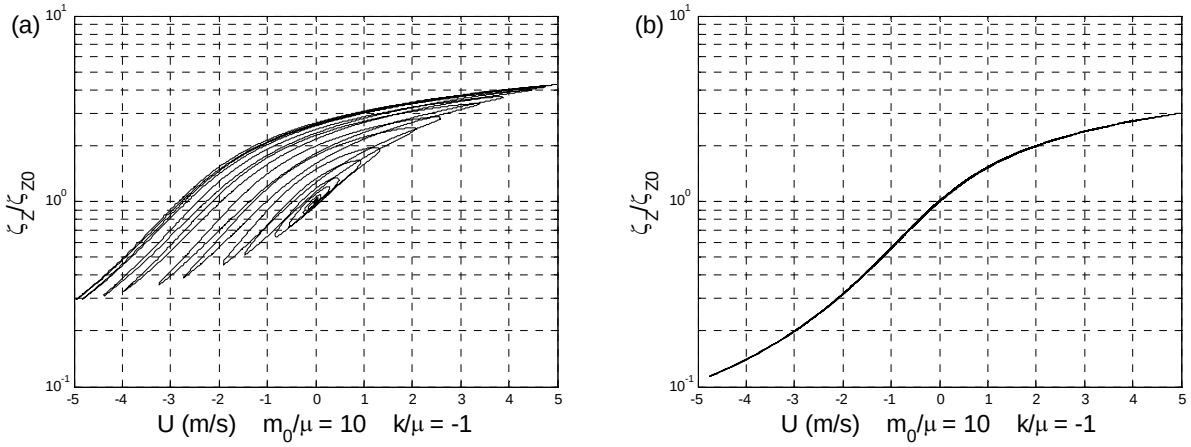


**Figure 3.40 Plot of wave steepness against local background velocity for internal wave propagating through (a) an inertial wave packet and (b) infinite inertial wave train. Both reach a maximum steepness at the largest local background velocity.**

relative steepness. Because the likelihood of wave breaking may be influenced by the time duration of instability, the envelope may have an even larger impact in increasing the likelihood of wave breaking, due to prolonged periods of instability.

The interaction of waves with infinite wave trains has been previously studied, but the different results that occur from an interaction with an inertial wave packet have not been discussed. The envelope that contains an inertial wave packet increases the likelihood of wave instability due to Jones' critical levels or excessive wave steepness. Waves are also much less likely to experience turning points and become reflected.

The interaction between small internal waves and an inertial wave packet is much more realistic than propagating through an infinite wave train, for no waves are ever infinite. Also, the results in this section are not limited to only two dimensions, but apply also to three dimensions. For all simulations discussed, the horizontal wavenumber *k* of the small wave has had the same sign and *l* has been constant at 0. Within the atmosphere, many types of internal waves are propagating vertically upwards in all horizontal directions and interact with inertial waves. These inertial waves contain oscillating wind velocities in both the x and y directions, as noted in the introduction. Internal waves with negative *k* values or any *l* values will still interact with inertial waves in the same format as discussed in this section, only that values of *k* may be replaced with $k_H$, where $k_H = \sqrt{k^2 + l^2}$, and the background wind velocities must be aligned with the horizontal phase speed of the small waves. This means that Jones' critical levels and turning points may occur for waves independent of their horizontal propagation directions. In this way, small waves experiencing a Jones' critical level while interacting with an inertial wave packet may strengthen the inertial wave in all horizontal directions, due to the energy transfer.

### 3.3.2 Caustic Interactions

In the previous scenarios, the inertial wave phases propagated downward, in the opposite direction as the small internal wave group velocity. Inertial waves may also have phases that propagate upward, in the same direction as the small internal wave group velocity. This type of interaction, shown in Figure 3.41, is more prevalent in the oceans whereas the first interaction is more common in the atmosphere, yet both may exist in either region. The results differ significantly for this type of interaction.

The caustic regions will not be discussed in this paper, as they are discussed in others' work where this type of interaction was analyzed for principally oceanic applications (Vanderhoff 2007, Broutman and Young 1986, Bruhwiler and Kaper 1995). Some major points include that these interactions may permanently alter the small waves, in that two possible

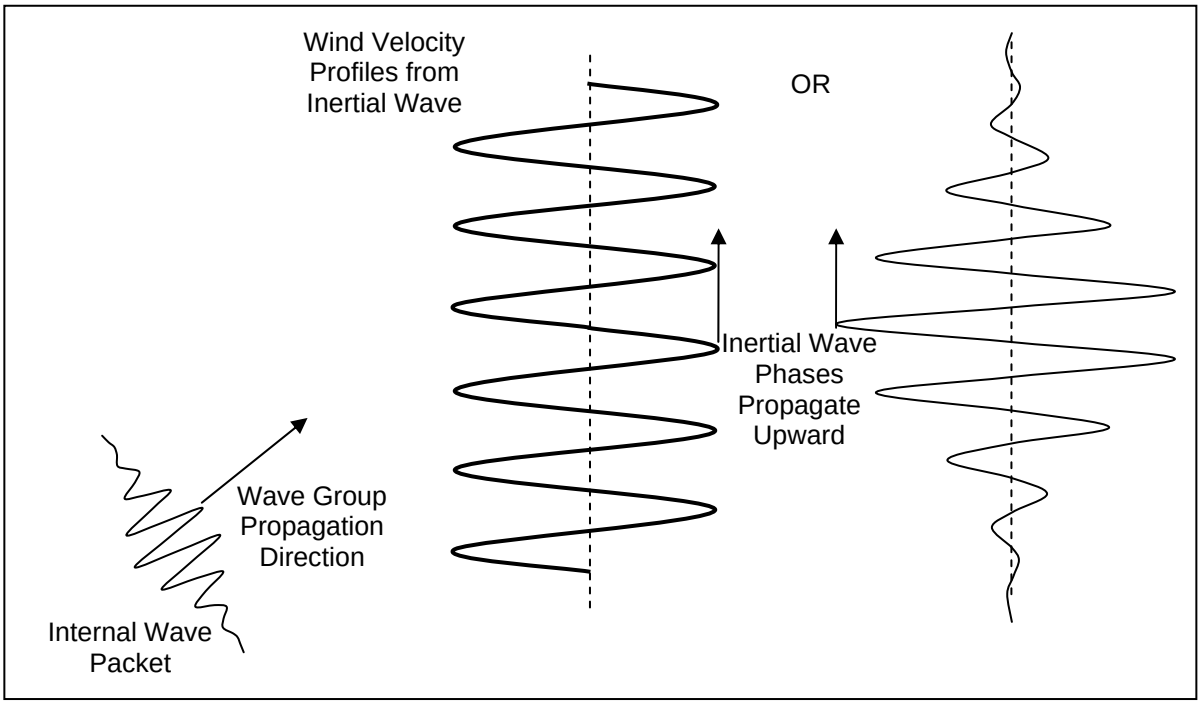


**Figure 3.41 Internal wave packet approaching either an inertial wave train or inertial wave packet with the inertial phases moving upward, signifying that *M* is positive.**

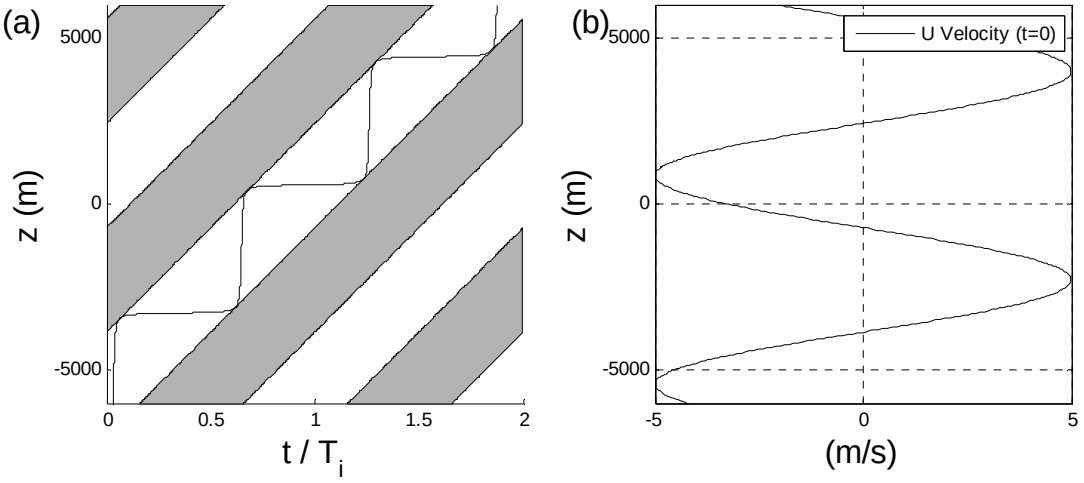


**Figure 3.42 Internal wave ray propagating through an infinite wave train, trapped between caustic regions and mostly in regions of negative horizontal velocity. Shaded regions indicated positive horizontal velocity.**

solutions may satisfy the conservation of total frequency or equation 3.24. According to linear ray theory, at the caustics, the vertical wavenumber of the small waves experiences a sudden jump and the wave action density and steepness rise toward infinity due to the relative volume of the ray tubes changing sign, and the researchers have been able account for this through an Airy function matching technique. In this region, the basic wave motion prescribed by linear theory remains valid.

Figure 3.42 illustrates a wave ray (all ray trajectories are identical in shape) propagating through an infinite wave train of this type. The wave is trapped between regions of specific background velocities bounded by a value where equation 3.24 becomes undefined. This value is referred to as the caustic. For this scenario, the properties are identical to those in Figure 3.11 except that *M* is positive instead of negative. The value of the caustic is near 0.01 m/s, meaning that the wave is confined to background velocities below about 0.01 m/s, as is shown by Figure 3.43, and the wave will never propagate through background velocities larger than this value. This agrees with equation 3.24.

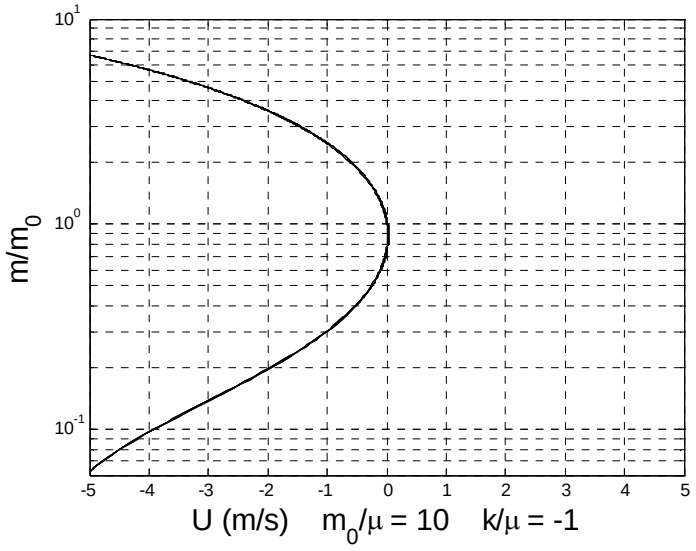


**Figure 3.43 Plot of vertical wavenumber against background velocity. This plot agrees with equation 3.24.**

The shift from $U_{ZERO}$ is important to the caustic interactions as well as the previously discussed interactions. In fact, $U_{ZERO}$ is even more severe in these interactions because the small waves may become trapped in regions of negative background velocity. For the previous inertial wave packet simulations the small waves spend more time in regions of positive background velocity, whereas in these simulations, the waves may spend most or nearly all their time in negative background velocities, and as such experience a stronger shift during the opening and closing of the inertial envelope. Because the inertial phases propagate in the opposite direction as the previous scenarios, the net value of $U_{ZERO}$ is negative according to equation 3.33, and a maximum magnitude occurs at the center of the inertial envelope. The shift has the same sign as previously discussed simulations because the inertial phase speed has a different sign and the rays spend more time in negative background velocities instead of positive velocities. Because this shift causes the waves to "see" larger background velocities, and the waves become trapped

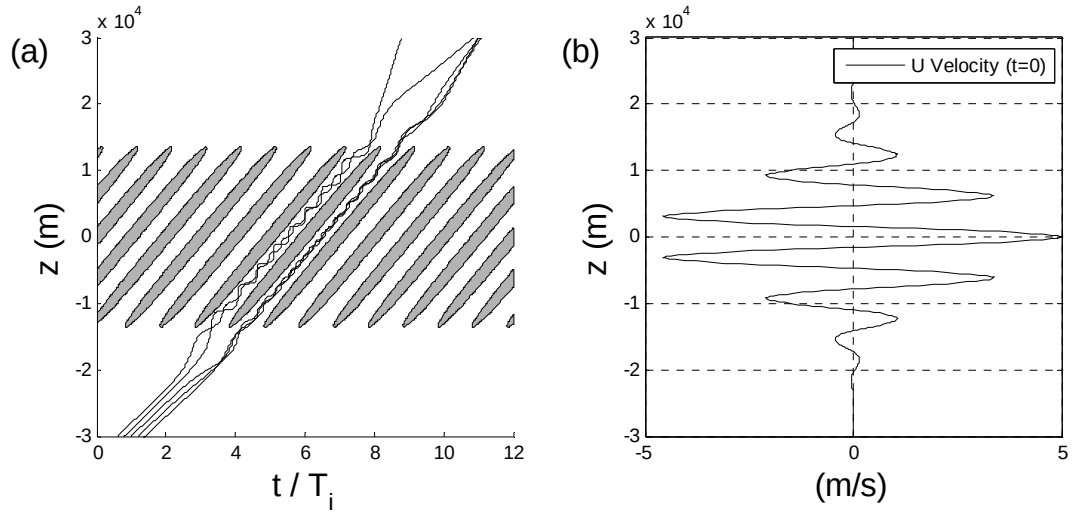


**Figure 3.44 Single internal wave propagating through an inertial wave packet contained within a Gaussian envelope, with inertial phases propagating upward. Shaded regions show local background velocity that exceeds time-independent critical level velocities.**

in velocities lower than the caustic velocity, the net effect of the shift is that the waves see smaller background velocity oscillations.

Figure 3.44 and Figure 3.45 show how the rays are trapped within the negative phases of the inertial wave packet, and become shifted during the opening and closing of the inertial envelope. Figure 3.44a shows the trajectories of five wave rays approaching the inertial wave. The rays become trapped in regions of negative background velocities and remain within a single trough of the inertial wave. When the waves exit the interaction, the vertical group velocity is not identical to the initial velocity, which is typical of caustic interactions.

Figure 3.45 shows how the wavenumbers of the waves change during the interaction, and illustrates that the waves will not pass through regions of positive background velocity. Not all rays are shifted the same amount, which is generally true for previous simulations where the inertial phases propagated downward. Of the five rays in this interaction, shown in different colors in Figure 3.45, the green ray is shifted to about -3.0 m/s, the magenta ray is shifted to -4.7

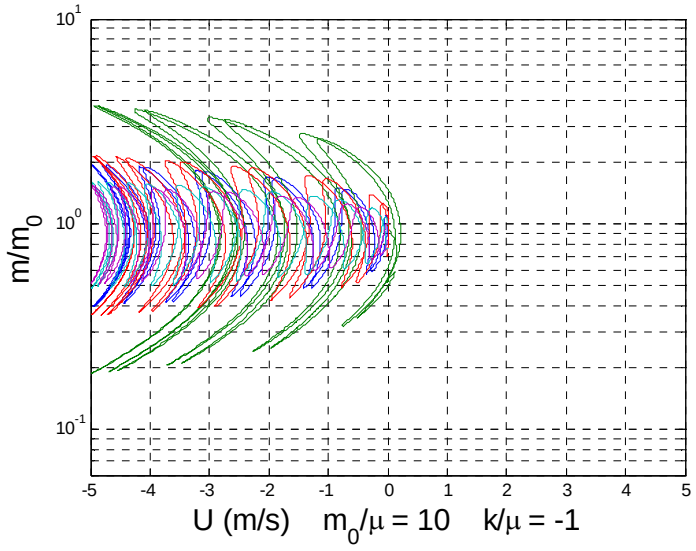


**Figure 3.45 Vertical wavenumber plotted against background velocity for five rays, each shown in a different color. This plot significantly diverges from equation 3.24. Not all rays are shifted the same amount.**

m/s, or about 94% of the total background velocity, and the other rays are shifted to values in between. The differences between the shifts depend on how the small waves approach the inertial wave packet, and the local phase of the inertial wave with which the small waves initially interact. The variance in shifting amounts is more pronounced for small waves that have initial vertical group velocities similar to the phase speed of the inertial wave, yet all waves may be significantly shifted. Broutman and Young (1986) stated that the rays that approach and settle into a trough, or negative background velocities of the inertial wave, will experience smaller changes in $m$ or $\omega$. This is shown in Figure 3.45, and these rays experience a large change in $U_{ZERO}$. Small waves that approach a crest, with positive background velocities, will experience larger changes in $m$ or $\omega$, due to a smaller change in $U_{ZERO}$.

It is interesting to note that the background velocity required for a caustic also shifts with $U_{ZERO}$, as is shown in Figure 3.45. At the center of the envelope, the rays are confined to

background velocities well below the original caustic velocity, specifically below the sum of $U_{ZERO}$ and the original caustic velocity.

With the infinite wave train interaction, the vertical wavenumber oscillates between two full orders of magnitude for these types of waves, as is shown in Figure 3.43. With an inertial wave envelope, the wavenumber only oscillates by a factor between about 4 and 20 at the center of the inertial envelope. Hence, these waves are not likely to experience either a turning point or a critical wavenumber.

At the center of the envelope, with maximum background velocities of 5 m/s, the wavenumber oscillations were only slightly larger than the oscillations when the envelope magnitude was 1 m/s. In other words, $U_{ZERO}$ changes only slightly during the initial opening of the envelope, and then changes at nearly the same rate as the envelope magnitude. This is similar to the inertial wave packet interaction in Figure 3.33, which shows that the relation between $U_{ZERO}$ and the magnitude of the inertial envelope is nearly hyperbolic in form, where $U_{ZERO}$

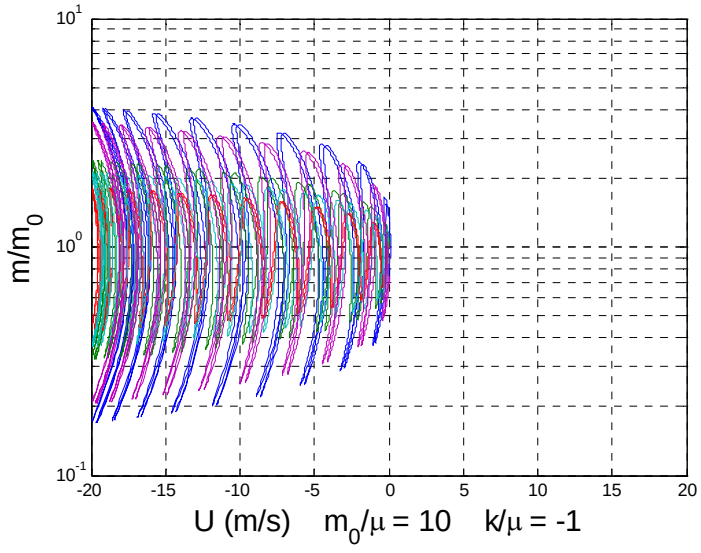


**Figure 3.46 Vertical wavenumber plotted against background velocity, indentical to Figure 3.45 but with larger maximum background velocities.**

changes at about the same rate as the envelope for larger amplitudes. This indicates that the interaction between internal waves and an inertial envelope from Figure 3.44 may have results that are not very different than if the inertial envelope had background velocities of 1.0 m/s or 20 m/s, for $U_{ZERO}$ reduces the oscillations in wavenumber or frequency magnitude. This is shown in Figure 3.46, indicating that some internal waves may be able to propagate through inertial wave packets of this type with much larger background velocities without experiencing large frequency oscillations that would otherwise cause a turning point or critical wavenumber. However, this depends on the velocity required for a caustic, based on the initial conditions of the small waves. It should be remembered that the internal waves may also become unstable due to shear or excessive wave steepness, or effects due to the caustic regions themselves, which are not discussed for this type of simulation.

# 4 DISCUSSION AND CONCLUSIONS

Internal waves are constantly generated in the atmosphere and, as they propagate, are interacting with other flows. The interactions discussed in this paper are similar to those which have been observed to frequently occur. The results of internal waves propagating through background winds show that outcomes vary significantly depending on whether the background flow is time-dependent or time-independent, as well as the special variation of that time-dependence.

The total frequency of internal waves is conserved for internal waves propagating through time-independent flows or interacting with non-deforming infinite wave trains, and may be useful in predicting internal wave propagation until turning points or instability occur. Ray theory is valid for predicting wave propagation behavior and whether waves will reach turning points or critical levels, but cannot accurately predict the behavior of waves with the onset of instability.

Conserving the total frequency for these types of interactions allows for the determining background velocities that will cause internal waves to reach a critical level or turning point. Alternatively, the range of waves that will experience a critical level or turning point may be determined for any given background velocities. The probability of experiencing a critical level (or Jones' critical level) or turning point is dependent on background velocities, inertial phase speeds, and the initial wavenumbers and frequencies of the small waves. The results section shows these velocities through equations and graphics, which have not been extensively

discussed for atmospheric interactions in other work. For interactions with inertial wave trains, atmospheric internal waves may reach turning points, become unstable, or continue free propagation. Higher frequency waves are more likely to reach turning points, and waves with large wavenumbers are more likely to reach critical levels or Jones' critical levels. The probability of reaching Jones' critical levels or turning points is lower for time-dependent background flows when compared to time-independent flows for the same velocities.

The outcomes of a critical level include absorption into the background flow or instability and overturning. These outcomes may be caused by the internal waves approaching a critical level, wavenumbers that reach a critical value, a wave steepness that approaches unity, or low Richardson numbers due to strong background shear. The initial amplitude of internal waves has no impact on whether the waves will approach a critical level or critical wavenumber, but it does influence whether the waves will become absorbed by the background or overturn at these locations. It has been shown that critical wavenumbers, excessive wave steepness, and strong shear occur for different ranges of internal waves and possibly at different locations of the interaction. Hence, all cases must be considered in order to accurately predict the outcome of the interaction.

Because inertial wave trains are never infinite, results from internal wave interactions with an inertial wave packet, bounded by an envelope, are more realistic. Internal waves interacting with inertial wave packets do not maintain a constant total frequency, which has been concluded previously in other work but has not been measured or parameterized for these types of atmospheric internal wave interactions. As discussed in the results section, the changes in total frequency are minimal for a wide range of waves, but are significant for mid-frequency waves with large initial wavenumbers. These waves are more affected by the inertial envelope due to

how much time the internal waves spend in positive or negative background velocities of the inertial wave during the opening and closing of the envelope. The deviance from a constant total frequency affects the probability of internal waves reaching a critical wavenumber or turning point, and changes the amount of steepening that the wave will experience. This change is comparable to a shift in velocity from that experienced by internal waves interacting with an infinite wave train, and this velocity shift may be a significant fraction of the maximum background velocities. The influence of the wave packet, and the velocity shift that arises because of it, increases the likelihood of wave instability due to Jones' critical levels or excessive wave steepness, and reduces the likelihood of turning points.

The velocity shift that arises due to the inertial packet envelope follows a regular trend. The average shift follows a hyperbolic curve relative to the maximum background velocities, and becomes more pronounced for larger background velocities. The shape and length of the envelope only slightly affect the probabilities of internal waves reaching a turning point or critical level instability, and generally only have an effect if there are few inertial wavelengths contained within the packet. This effect slightly increases the probability of critical level instability or turning points at background velocities smaller than predicted when accounting for the velocity shift and conservation of total frequency.

Except in cases of instability or turning points, or caustic interactions where the inertial phases propagate in the same direction as the small waves' group velocity, the internal waves will not be permanently affected after interactions with time-independent or time-dependent background waves. Any change in total frequency for internal waves interacting with an inertial wave packet is reduced as the waves propagate out of the packet, although minimal changes may

occur if few inertial wavelengths exist within the packet. Even in these cases, the properties of the internal waves are close to their initial conditions

For interactions with caustics, the conservation of total frequency indicates two possible outcomes for the vertical wavenumber and the waves may therefore be permanently altered after the interaction. The changes in total frequency during a caustic inertial wave packet interaction may considerably reduce the changes in vertical wavenumber or frequency of the small waves.

The factors that will influence the outcome of internal waves interacting with inertial waves, from most influential to least, are as follows:

- Larger background velocity magnitudes increase the probability of turning points or instability, meaning that a larger range of waves will reach turning points or become unstable with larger velocities.
- Time-dependence reduces the probability of turning points or instability, and increased inertial phase speeds further reduce the probability. As the phase speed decreases, the results approach the time-independent results.
- The inertial envelope increases the probability of the internal waves' wavenumber reaching a critical value and increases the maximum wave steepness during the interaction, but reduces the probability of turning points. The envelope thus decreases an expectation of vertical flux of horizontal momentum in the atmosphere. For an interaction with caustics, changes in vertical wavenumber and frequency are reduced.
- The length of the inertial wave envelope, if small relative to the inertial wavelength, may cause the internal waves to reach a critical wavenumber value, excessive wave steepness, or a turning point at slightly lower velocities.

## 4.1 Contributions

The research in this thesis discusses results that are not discussed in previous work. This includes the following list.

- When interacting with an inertial wave train, the relative change in internal waves' wave action density is large when the initial vertical wavenumber and frequency exist between the lines that designate the time-independent critical level velocity and inertial wave phase speed, as shown in Figure 3.21.
- Differences in the interaction results between an infinite waves train and inertial wave packet may be analyzed as a velocity shift experienced by the small waves. This shift is dependent on inertial velocities, inertial phase speeds, and initial conditions of the small waves. The shift becomes more pronounced with larger background velocities. (See equation 3.33)
- Atmospheric waves interacting with an inertial wave packet are more likely to experience a Jones' critical level and less likely to reach a turning point when compared with interactions with an infinite inertial wave train. (See Figure 3.36)
- Atmospheric waves interacting with an inertial wave packet will reach a larger wave steepness value and remain in larger steepness values for longer periods of time when compared with interactions with an infinite inertial wave train. (See Figure 3.38)
- The shape and length of the inertial wave packet does not significantly matter for the interaction, but rather only the maximum velocities of the envelope. (See Figure 3.34)

Internal waves, and interactions involving internal waves and other flows, affect numerous fields, such as meteorology, environmental sciences, and aerospace applications. For example, these results may be beneficial for global climate models. Because global climate

models analyze the dynamics of the atmosphere over the entire earth, they are not sufficiently resolved for individual internal waves. Although ray tracing is computationally cheap, it may be difficult to account for waves due to length scales that are much smaller than the smallest resolution of the climate models. These models must therefore make estimations about where waves are generated, where they propagate, and where their energy or momentum is deposited. This research improves the accuracy of that estimation. Climate models may predict where internal waves are generated, and have an estimation of where they propagate. The models may know practically where mean winds or inertial waves exist that may cause critical levels or turning points. If the models do not account for time-dependence, they may incorrectly predict critical level locations or turning points where none exist. Alternatively, if time-dependence is included by conserving the total frequency of waves, fewer waves will be predicted to encounter critical levels or turning points, which may be more accurate, but not as accurate if the inertial wave envelope is taken into account. If the envelope of the inertial waves is included, the models may more accurately predict more critical level instabilities and fewer turning points. This results in improved estimations of where internal wave energy and momentum is transported or deposited in these global models.

## 4.2 Future Work

These results and conclusions assume simplified and idealized scenarios, which inherently indicate a degree of error. Naturally, there are many avenues that may be pursued to acquire more accurate results, such as accounting for or eliminating the assumptions that have been made for all of the interactions discussed. Of these avenues, some have been or are currently being pursued. The assumptions are:

- Buoyancy frequency remains constant in time and elevation.
- The average fluid density is assumed constant.
- The Coriolis frequency is assumed constant, although the frequency changes with latitude.
- There are no vertical background velocities.
- The background inertial wave is perfectly defined without any noise or deformations.

Other methods, such as fully non-linear, three-dimensional simulations are required to eliminate the following assumptions.

- Internal waves are small enough to remain linear prior to breaking or reflection.
- Small waves do not affect the background or other waves.
- Nonlinear effects of wave propagation are ignored

Eliminating these assumptions may improve the accuracy of these simulations and provide higher order effects for the outcomes. However, this work provides a more accurate model for the dynamics of internal wave interactions and their general effects on the atmosphere while remaining computationally cheap.

## REFERENCES


Broutman, D., Young, W. R. (1986) "On the interaction of small-scale oceanic internal waves with near-inertial waves." *J. Fluid Mech.*, 166, 341-358.

Bruhwiler, D. L., Kaper, T. J., (1995) "Wavenumber transport: scattering of small-scale internal waves by large-scale wavepackets." *J. Fluid Mech.*, 289, 379-405.

Eckermann, S., (1997) "Influence of Wave Propagation on the Doppler Spreading of Atmospheric Gravity Waves." *J. Atmos. Sci.*, 54, 2554-2573.

Fritts, D. C., Alexander, M. J., (2003) "Middle Atmosphere Gravity Wave Dynamics." Review of Geophysics, 41, 1/1003

Javam, A., Redekopp, L. G. (1998) "The transmission of spatially-compact internal wave packets through a critical level." *Dynamics of Atmospheres and Oceans*, 127-128

Godoy-Diana, R., Chomaz, J-M. Donnadieu, C., (2006) "Internal gravity waves in a dipolar wind: a wave-vortex interaction experiment in a stratified fluid." *J. Fluid Mech.*, 548, 281-308.

Guest, Reeder, Marks, and Karoly, (2000) "Inertia-Gravity Waves Observed in the Lower Stratosphere over MacQuerie Island." *J. Atmos. Sci.*, 57, 737-752.

Jones, W. L., (1967) "Propagation of internal gravity wave in fluids with shear and rotation." *J. Fluid Mech.,***30,** 439–448.

Lighthill, J., (1978) *Waves in Fluids* Cambridge University Press

Nappo CJ, (2002) "An Introduction to Atmospheric Gravity Waves," Vol.85 of *International Geophysics Series*. Academic Press, San Diego, 276 pp

Pedlosky, J., (2003) *Waves in the Atmosphere and Ocean*, Springer-Verlag Berlin Heidelberg New York

Sartelet, K. N., (2003) "Wave Propagation inside an Inertia Wave. Part I: Role of Time Dependence and Scale Separation." *J. Atmospheric Sciences*, 60, 1448-1455.

Sartelet, K. N., (2003) “Wave Propagation inside an Inertia Wave. Part II: Wave Breaking.” *J. Atmospheric Sciences*, 60, 1448-1455.

Sato, O’Sullivan, and Dunkerton, (1997) “Low-frequency inertia-gravity waves in the stratosphere revealed by three-week continuous observation with the MU radar.” *Geophysical Research Letters*, 24, 1739-1742

Thompson, R. O. R. Y., (1978) “Observation of inertial waves in the stratosphere.” *Quart. J. R. Met. Soc.,* 104, 691-698

Thorpe, S. A. (1981) “An Experimental Study of Critical Layers.” *Journal of Fluid Mechanics, 195*, 321-344.

Vanderhoff, J. C., K. K. Nomura, J. W. Rottman, and D Broutman (2007), “Statistical analysis of short wave packets interacting with near inertial waves.” to be submitted to *J. Geophys. Res.*

Vanderhoff, J. C., K. K. Nomura, J. W. Rottman, and C. Macaskill (2008), “Doppler Spreading of internal gravity waves by an inertia-wave packet.” *J. Geophys. Res.* 113, C05018, doi:10.1029/2007JC004390

Winters, K. B., D’Asaro, E. A., (1989) “Two-Dimensional Instability of Finite Amplitude Internal Gravity Wave Packets Near a Critical Level.” *Journal of Geophysical Research, 94*, 12 709-12,719.

Winters, K. B., D’Asaro, E. A., (1994) “Three-Dimensional Instability Wave Instability Near a Critical Level.” *Journal of Fluid Mechanics, 272*, 255-284.

## APPENDIX A POLARIZATION RELATIONS

The polarization relations, which define the perturbation density, pressure, and particle velocities, are determined from the linear Boussinesq equations, dispersion relation, and continuity.

$$\frac{\partial u'}{\partial x}+\frac{\partial v'}{\partial y}+\frac{\partial w'}{\partial z}=0$$

$$\frac{\partial u'}{\partial t}=\frac{-\partial p'}{\partial x}\frac{1}{\rho_0} \tag{2-2}$$

$$\frac{\partial v'}{\partial t}=\frac{-\partial p'}{\partial y}\frac{1}{\rho_0} \tag{2-3}$$

$$\frac{\partial w'}{\partial t}=\frac{-\partial p'}{\partial z}\frac{1}{\rho_0}+\frac{\rho'}{\rho_0}g_z \tag{2-4}$$

$$0=\frac{\partial \rho'}{\partial t}+w\frac{\partial \overline{\rho}}{\partial z} \tag{2-5}$$

$$w'=w_o\cos\left(kx+ly+mz-\omega t\right) \tag{2-6}$$

$$\frac{\partial \rho'}{\partial t}+w\frac{\partial \rho}{\partial z}=0$$

$$N^2=-\frac{g}{\rho_0}\frac{\partial \rho}{\partial z} \tag{2-1}$$

$$-N^2\frac{\rho_0}{g}=\frac{\partial \rho}{\partial z}$$

$$\frac{\partial \rho'}{\partial t}+w_oN^2\frac{\rho_0}{g}\cos\left(kx+ly+mz-\omega t\right)=0$$

$$\partial\rho'=w_oN^2\frac{\rho_0}{g}\cos\left(kx+ly+mz-\omega t\right)\partial t$$

Integrate both sides

$$\rho' = -\frac{w_o N^2}{\omega}\frac{\rho_0}{g}\sin(kx + ly + mz - \omega t) \tag{A-1}$$

$$\frac{\partial w'}{\partial t} = \frac{-1}{\rho_0}\frac{\partial p'}{\partial z} - \frac{\rho'}{\rho_0}g$$

Plug in equation A-1

$$\frac{\partial w}{\partial t} = \frac{-1}{\rho_0}\frac{\partial p'}{\partial z} + \frac{w_o}{\omega}N^2\sin(kx + ly + mz - \omega t)$$

$$w_o\omega\sin(kx + ly + mz - \omega t) = \frac{-1}{\rho_0}\frac{\partial p'}{\partial z} + \frac{w_o}{\omega}N^2\sin(kx + ly + mz - \omega t)N^2$$

$$\left(w_o\omega - \frac{w_o}{\omega}N^2\right)\sin(kx + ly + mz - \omega t) = \frac{-1}{\rho_0}\frac{\partial p'}{\partial z}$$

$$\partial p' = -\rho_0 w_o\left(\omega - \frac{N^2}{\omega}\right)\sin(kx + ly + mz - \omega t)\partial z$$

$$p' = \frac{\rho_0}{m}w_o\left(\omega - \frac{N^2}{\omega}\right)\cos(kx + ly + mz - \omega t)$$

$$p' = \frac{\rho_0}{m}w\omega\left(1 - \frac{N^2}{\omega^2}\right)$$

$$p' = \frac{\rho_0}{m}w\omega\left(1 - \frac{N^2}{N^2\dfrac{k^2 + l^2}{k^2 + l^2 + m^2}}\right)$$

$$p' = \frac{\rho_0}{m}w\omega\left(1 - \frac{k^2 + l^2 + m^2}{k^2 + l^2}\right)$$

$$p' = \frac{\rho_0}{m}w\omega\left(\frac{-m^2}{k^2 + l^2}\right)$$

$$p' = -\rho_0 w \omega \frac{m}{k^2 + l^2}$$

$$p' = -\rho_0 \omega \frac{m}{k^2 + l^2} w_0 \cos(kx + ly + mz - \omega t) \tag{A-2}$$

$$\frac{\partial u'}{\partial t} = \frac{-1}{\rho_0} \frac{\partial p'}{\partial x}$$

$$\frac{\partial u'}{\partial t} = \frac{-1}{\rho_0} \rho_0 \omega \frac{m}{k^2 + l^2} k w_0 \sin(kx + ly + mz - \omega t)$$

$$\partial u' = \frac{-1}{\rho_0} \rho_0 \omega \frac{m}{k^2 + l^2} k w_0 \sin(kx + ly + mz - \omega t) \partial t$$

$$u' = -\frac{mk}{k^2 + l^2} w_0 \cos(kx + ly + mz - \omega t) \tag{A-3}$$

$$\frac{\partial v'}{\partial t} = \frac{-1}{\rho_0} \frac{\partial p'}{\partial y}$$

$$\frac{\partial v'}{\partial t} = \frac{-1}{\rho_0} \rho_0 \omega \frac{m}{k^2 + l^2} l w_0 \sin(kx + ly + mz - \omega t)$$

$$\partial v' = \frac{-1}{\rho_0} \rho_0 \omega \frac{m}{k^2 + l^2} l w_0 \sin(kx + ly + mz - \omega t) \partial t$$

$$v' = -\frac{lm}{k^2 + l^2} w_0 \cos(kx + ly + mz - \omega t) \tag{A-4}$$

## APPENDIX B DERIVATION OF THE LINEAR DISPERSION RELATION

Take the x – momentum and y – momentum equations and add them in this manner.

$$\frac{\partial}{\partial x}(x-mom)+\frac{\partial}{\partial y}(y-mom)$$

$$\frac{\partial}{\partial t}\left(\frac{\partial u'}{\partial x}+\frac{\partial v'}{\partial y}\right)=\frac{-1}{\rho_0}\left(\frac{\partial^2}{\partial x^2}+\frac{\partial^2}{\partial y^2}\right)p'$$

Through continuity $\frac{\partial u'}{\partial x}+\frac{\partial v'}{\partial y}=-\frac{\partial w'}{\partial z}$

$$\frac{\partial}{\partial t}\left(\frac{-\partial w'}{\partial z}\right)=\frac{-1}{\rho_0}\nabla_H^2 p'$$

Apply $\nabla_H^2\left(\frac{\partial}{\partial t}\left[\frac{\partial w'}{\partial t}=\frac{-\partial p'}{\partial z}\frac{1}{\rho_0}+\frac{\rho'}{\rho_0}g_z\right]\right)$

$$\frac{\partial}{\partial t}\left(\nabla_H^2\frac{\partial w'}{\partial t}\right)=\frac{-1}{\rho_0}\frac{\partial^2}{\partial t\partial z}\left(\nabla_H^2 p'\right)-\frac{\partial}{\partial t}\nabla_H^2\left(\frac{\rho'}{\rho_0}g_z\right)$$

Because $\frac{\partial\rho'}{\partial t}\frac{g_z}{\rho_0}=N^2 w$, the equation simplifies to

$$\frac{\partial}{\partial t}\left(\nabla_H^2\frac{\partial w'}{\partial t}\right)=\frac{-1}{\rho_0}\frac{\partial^2}{\partial t\partial z}\left(\nabla_H^2 p'\right)-\nabla_H^2\left(N^2 w'\right)$$

Because $\nabla_H^2 p'=\frac{\partial^2 w'}{\partial t\partial z}\rho_0$, the equation changes to

$$\frac{\partial}{\partial t}\left(\nabla_H^2\frac{\partial w'}{\partial t}\right)=-\frac{\partial^2}{\partial t\partial z}\left(\frac{\partial^2 w'}{\partial t\partial z}\right)-\nabla_H^2\left(N^2 w'\right)$$

$$\frac{\partial}{\partial t}\left(\nabla^2\frac{\partial w'}{\partial t}\right)+\nabla_H^2\left(N^2 w'\right)=0$$

## APPENDIX C DERIVATION OF WAVE ACTION DENSITY EQUATION

$$c_{gz0} = \frac{\partial z_0}{\partial t} = \frac{\partial \omega_0}{\partial m_0}$$

$$\frac{\partial\left(\partial m / \partial z_0\right)}{\partial t} = -k \frac{\partial^2 U}{\partial z^2} \frac{\partial z}{\partial z_0} \frac{1}{c_{gz0}} \frac{\partial z_0}{\partial t}$$

$$\frac{\partial\left(\partial m / \partial z_0\right)}{\partial t} = \frac{-k}{c_{gz0}} \frac{\partial^2 U}{\partial z \partial t}$$

Integrating both sides with respect to time yields

$$\partial m / \partial z_0 = \frac{-k}{c_{gz0}} \frac{\partial U}{\partial z} \tag{3.15}$$

Rearrange equation 2.21 and substitute back into equation 3.15

$$\frac{\partial U}{\partial z} = \frac{1}{-k} \frac{\partial m}{\partial t}$$

$$\partial m / \partial z_0 = \frac{1}{c_{gz0}} \frac{\partial m}{\partial t}$$

Substitute into equation 3.10 and simplify

$$\frac{\partial\left(\partial z / \partial z_0\right)}{\partial t} = \frac{\partial^2 \omega}{\partial m^2} \frac{1}{c_{gz0}} \frac{\partial m}{\partial t}$$

$$\partial\left(\partial z / \partial z_0\right) = \frac{\partial^2 \omega}{\partial m} \frac{1}{c_{gz0}}$$

Integrating both sides results in

$$\partial z / \partial z_0 = \frac{\partial \omega}{\partial m} \frac{1}{c_{gz0}} + Cst$$

$$\partial z / \partial z_0 = \frac{c_{gz}}{c_{gz0}} + Cst$$

At the initial part of the simulation, $\partial z / \partial z_0 = 1$, and $Cst = 0$

$$\partial z / \partial z_0 = \frac{c_{gz}}{c_{gz0}}$$

$$\frac{A}{A_0} = \frac{c_{gz0}}{c_{gz}} \tag{3.14}$$

## APPENDIX D RAY TRACING CODE

```
%Ray Tracing -Brian Casaday (adapted from JV ray codes)
%Interactions with Critical Levels
%Began May 4, 2009

tic
close all
clear
clc

%for run = 1:41  %---movie

%Initial parameters

f = 0.0001;             % inertia frequency (0 - 0.00014)
g = -9.8;               % gravity
rho = 0.0340;           % density of the fluid (0.1 for air (stratosphere),
1000 for water)
rho_z = -.0001386*rho; %dp/dz (rho_z/rho = -.000139 for air,
N = f*200;              %Buoyancy frequency or brunt Vaisala frequency (100f
- 360?f)
%N = sqrt(g/rho*rho_z); %Buoyancy frequency
Tn = 2*pi/N;            % buoyancy period


% Define background flow
bflow = 0; % (0 for wave, 1 for wind, 2 for wind and wave, 3 for accelerating
wind, 4 for moving wind, 5 for stationary wave, 6 for moving stationary wave)

% define time span
t0 = 0;
Ti = 2*pi/f;             % inertial period
tfin = 10 * Ti;          % Time of evaluation
ntimes = tfin/Ti * 3000;         % number of time steps
tspan = linspace(t0, tfin, ntimes);
dt = (tfin-t0)/ntimes;

% SHORT WAVES
k = 2*pi*.0005;     % horizontal wavenumber (k = .0005 - .003 c/m for
Stratosphere
l = 0;

% INERTIA WAVE
z0env = 0;        % center of envelope
Lenv = 10000;%1000*pi*3.5/5.5;      % envelope scale
M = 2*pi/6280;    % vertical wavenumber
%U0 = N/(2.4*M);  % mean velocity
U0 = 5;         % Inertial Wave velocity amplitude

mu = 2*pi/2500;   %eckerman Normalization
muc = -200*mu;
```

```
% Calculate wave steepness
zeta_0 = abs(0.1); %Initial wave steepness

nztot = 3;       % number of initial z values  total number of rays traced

nMtot = 1;
nktot = 1;%31%19
nutot = 1;
nmtot = 1;%51
nMtot*nktot*nutot*nmtot;

graphic = 0; % 0 is on, 1 is off
run = 0;

% main ray-tracing loop-------------------------------------
%Dat = zeros(4,nMtot);
Data = zeros(14,nMtot);

for Mdif = 1:nMtot
    M = 2*pi/(2*pi*1000+(Mdif-1)*1000);
for udif = 1:nutot
    U0 = 5 + (udif-1) * .5;
for mdif = 1:nmtot
%     mratio = 1 + (mdif-1)*.1;
    mratio = 10^1;%((mdif-1)/10-0);%((mdif-1)/10-2);%((mdif+kdif*2-3)/10-
3.5);
    m0 = (-mratio)*mu;
for kdif = 1:nktot

cgz0 = -(N^2-
f^2)*(k^2+l^2)*m0/(sqrt(f^2*m0^2+N^2*(k^2+l^2))*(k^2+l^2+m0^2)^(3/2));
dz = Ti*cgz0/nztot; %set up space between rays so that all fill one inertial
period
czlw = f/M;


% memory allocation-----------------------------------------
mkeep = zeros(ntimes+1, nztot);    xkeep  = mkeep;   A2keep = mkeep;
ykeep = mkeep;                  zkeep = mkeep;    wpkeep = mkeep;
zz0keep = mkeep;                mz0keep = mkeep;  Akeep = mkeep;
uzkeep = mkeep;                 mmzkeep = mkeep;  thetakeep = mkeep;
zetakeep = mkeep;               Ekeep = mkeep;    E2keep = mkeep;
zeta2keep = mkeep;              ukeep = mkeep;    clkeep = mkeep+0.00001;
Rigkeep = mkeep;                Rig2keep = mkeep; Rig3keep = mkeep;
wpcheck = mkeep;                breakkeep = mkeep;cgzkeep = mkeep;
breakkeep = breakkeep + Lenv*10;coskeep = mkeep;  sinkeep = mkeep;
uzzkeep = mkeep;                uenvkeep = mkeep; cgxkeep = mkeep;

    run = run+1;
    dt;

    ncase = 0;
       for nz = 1:nztot
```

```
        ncase = ncase + 1;
%       disp(['case ' num2str(ncase)]);


% x0, y0, and z0 define where the short wave will begin (and in
%  z0 how closely others will follow)

        x0 = 0;
        y0 = 0;
        z0 = -Lenv*3.5 - dz*(nz-1);

        %Dispersion Relation
        kh2 = k^2 + l^2;
        wp0 = sqrt( (kh2 * N^2 + m0^2 * f^2) / (kh2 + m0^2) );

       disp(['     wp0/N = ', num2str(wp0/N)])

        zz0 = 1;      % Hayes quantity dz/dz0
        mz0 = 0;      % Hayes quantity dm/dz0

        Y0 = [x0 y0 z0 m0 wp0 zz0 mz0]';


        % Replace ode45 with 4th order Runge-Kutta
        xkeep(1,ncase) = Y0(1);
        ykeep(1,ncase) = Y0(2);
        zkeep(1,ncase) = Y0(3);
        mkeep(1,ncase) = Y0(4);
        wpkeep(1,ncase) = Y0(5);
        zz0keep(1,ncase) = Y0(6);
        Akeep(1,ncase) = abs(1/Y0(6));
        A2keep(1,ncase) = 1;
        Ekeep(1,ncase) = 1;
        E2keep(1,ncase) = 1;
        zetakeep(1,ncase) = k*(2/rho)^.5*wpkeep(1,ncase)^(-
.5)*Akeep(1,ncase)^(.5);
        zeta2keep(1,ncase) = zeta_0*wpkeep(1,ncase)^(-
.5)*Akeep(1,ncase)^(.5)/((wp0)^(-.5)*Akeep(1,ncase)^(.5));
        ukeep(1,ncase) = 0;
        Y = Y0;



        i = 1;
        while i <= ntimes + 0

            i = i + 1;

            t = t0 + (i-1)*dt;
            k1 = dt * rhs(t,Y,k,l,N,f,U0,z0env,Lenv,M,bflow) ;
            k2 = dt * rhs(t+dt/2,Y+k1/2,k,l,N,f,U0,z0env,Lenv,M,bflow) ;
            k3 = dt * rhs(t+dt/2,Y+k2/2,k,l,N,f,U0,z0env,Lenv,M,bflow) ;
            k4 = dt * rhs(t+dt,Y+k3,k,l,N,f,U0,z0env,Lenv,M,bflow) ;
```

```
            Y = Y +1/6*(k1 + 2*k2 + 2*k3 + k4) ;

        xkeep(i,ncase) = Y(1);
        ykeep(i,ncase) = Y(2);
        zkeep(i,ncase) = Y(3);
        mkeep(i,ncase) = Y(4);
        wpkeep(i,ncase) = Y(5);
        zz0keep(i,ncase) = Y(6);
        Akeep(i,ncase) = abs(1/Y(6));
        mz0keep(i,ncase) = Y(7);


        Ekeep(i,ncase) = Akeep(i,ncase)*wpkeep(i,ncase)/wp0;
%       E2keep(i,ncase) =
(1+(f*mkeep(i,ncase)/N/k)^2)/(1+(f*m0/N/k)^2);%*(wp0/wpkeep(i,ncase));
%       A2keep(i,ncase) = E2keep(i,ncase)/wpkeep(i,ncase);
        zetakeep(i,ncase) = wpkeep(i,ncase)^(-
.5)*Akeep(i,ncase)^(.5)/(wpkeep(1,ncase)^(-.5)*Akeep(1,ncase)^(.5));
        zeta2keep(i,ncase) = zeta_0*(wpkeep(i,ncase)^(-
.5)*Akeep(i,ncase)^(.5))/(wpkeep(1,ncase)^(-.5)*Akeep(1,ncase)^(.5));

        wpcheck(i,ncase) = sqrt( (kh2 * N^2 + mkeep(i,ncase)^2 * f^2) / (kh2
+ mkeep(i,ncase)^2) );


A0 =(1+(m0^2*f^2/(N*k)^2))*0.5*rho*N^2*zeta_0^2/wp0;
uzkeep(i,ncase)  = N*k*((2/rho)^(1/2))*(wpkeep(i,ncase).^(-1/2)).*((1-
f^2./(wpkeep(i,ncase).^2)).^(-1/2)).*(A0*Akeep(i,ncase)).^(1/2);
%uzkeep2(i,ncase) = (wpkeep(i,ncase).^(-1/2)).*(abs((1-
(f^2)./(wpkeep(i,ncase).^2))).^(-1/2)).*(Akeep(i,ncase).^(1/2));


        % Determine the Gradient Richardson Number
        [U,V, Uz,Uzz, Vz,Vzz, env] =
bgd(zkeep(i,ncase),t,N,f,U0,z0env,Lenv,M, bflow);
        Rigkeep(i,ncase) = g/rho*rho_z / Uz^2;
%Richardson number from background wind
        Rig2keep(i,ncase) = g/rho*rho_z*(1+zeta2keep(i,ncase)) /
(Uz+uzkeep(i,ncase))^2;                          %Richardson number from
background wind and wave induced shear
        Rig3keep(i,ncase) = g/rho*rho_z*(1-zeta2keep(i,ncase)) /
(Uz+uzkeep(i,ncase))^2;     %Richardson number from background wind and wave
induced shear

%         thetakeep(i,ncase) = atan2(.25*(Uz+uzkeep(i,ncase))^2,
g/rho*rho_z*(1-zeta2keep(i,ncase)));
        ukeep(i,ncase) = U;
        uenvkeep(i,ncase) = env;
        uzkeep(i,ncase) = Uz;
        uzzkeep(i,ncase) = Uzz;
        coskeep(i,ncase) = cos(M*zkeep(i,ncase) + f*t);
        sinkeep(i,ncase) = sin(M*zkeep(i,ncase) + f*t);
```

```
     % Critical Level Velocity
     UCL = wp0/k;

     % Find where does the ray pass the critical Level

     if (ukeep(i,ncase)/UCL-1 >= 0)
     clkeep(i,ncase) = 1;
     end

     %Find areas of instability
     if(abs(mkeep(i,ncase)) > abs(muc))
%      if (zeta2keep(i,ncase) > 1.0)
        breakkeep(i,ncase) = zkeep(i,ncase);
     end

     %Dat(:,ntimes*(mdif-1)+i) = [mratio U/UCL Akeep(i,ncase)
zetakeep(i,ncase)/zetakeep(1,ncase)];

%         end

        end

%Find zero offset
cgzkeep = -(N^2-f^2)*k^2*mkeep ./ ((f^2*mkeep.^2 + N^2*k^2).^0.5 .* (k^2 +
mkeep.^2).^(3/2));
cgxkeep = (N^2-f^2)*k*mkeep.^2 ./ ((f^2*mkeep.^2 + N^2*k^2).^0.5 .* (k^2 +
mkeep.^2).^(3/2)) + ukeep;
q = 0;
a = 0;
Uzero = 0;
for i = 2:ntimes
    if (mkeep(i,1)/m0 > 1 && mkeep(i-1,1)/m0 < 1)
        q = q+1;
        a(q,1) = i-1;
        a(q,2) = i;
    end
    if (mkeep(i-1,1)/m0 > 1 && mkeep(i,1)/m0 < 1)
        q = q+1;
        a(q,1) = i;
        a(q,2) = i-1;
    end

end

for i = 1:q
    Uzero(i) = ukeep(a(i,1)) + (1-mkeep(a(i,1))/m0)*...
        (ukeep(a(i,2))-ukeep(a(i,1)))/(mkeep(a(i,2))/m0-mkeep(a(i,1))/m0);
    Uzeroenv(i) = uenvkeep(a(i,1)) + (1-mkeep(a(i,1))/m0)*...
        (uenvkeep(a(i,2))-uenvkeep(a(i,1)))/(mkeep(a(i,2))/m0-
mkeep(a(i,1))/m0);
end
U0diff = min(Uzero);
```

```
       wpcheck(1,ncase) = sqrt( (kh2 * N^2 + mkeep(1,ncase)^2 * f^2) / (kh2 +
mkeep(1,ncase)^2) );
       wperr = (wpkeep(:,ncase) - wpcheck(:,ncase))'/N;
       if ncase == 1
       disp(['     maxerr = '   num2str(max(abs(wperr)))])
       end

       end

       %Define Jones Critical Level and Reflection Velocities
Uturn = wp0/k - N/k;
UCLjones = wp0/k - 1/k*sqrt((N^2*k^2 + f^2*muc^2)/(k^2+muc^2)) - f/k/M*(muc-
m0);


for i = 1:ntimes + 1
    t(i) = dt*(i-1);
end

%Set up Critical Level Visual graph and Richardson number graph
Cgraph = 300;
Ugraph = zeros(Cgraph,Cgraph);
Rigraph = zeros(Cgraph,Cgraph);
Ut = zeros(Cgraph,Cgraph);
Uzgraph = zeros(Cgraph,Cgraph);

for i = 1:Cgraph+1
    for j = 1:Cgraph+1
        Ut(i,j) = (i-1)*tfin/Cgraph;
        Uzgraph(i,j) = (j-1-Cgraph/2)/Cgraph*Lenv*6;
        [UU,V, Uz,Uzz, Vz,Vzz] = bgd(Uzgraph(i,j),Ut(i,j),N,f,
U0,z0env,Lenv,M,bflow);
        Ugraph(i,j) = UU;       % Velocity in space and time
        if (abs(Uz) >=0)
        Rigraph(i,j) = g/rho*rho_z/(Uz*(Uz)); % Rig in space and time
        else
        Rigraph(i,j) = 1000;
        end
    end
end

function F = rhs(t,Y,k,l,N,f,U0,z0env,Lenv,M,bflow)

% Here we find the time derivative of the values stored in
%  the Y array by using ray theory and some manipulation.

x = Y(1);
y = Y(2);
z = Y(3);
m = Y(4);
wp = Y(5);
zz0 = Y(6);
mz0 = Y(7);
```

```
%%----
[U,V, Uz,Uzz, Vz,Vzz] = bgd(z,t,  N,f,U0,z0env,Lenv,M, bflow);

%------------ Group Velocity

  kh = sqrt(k^2 + l^2);
  f2=f^2;
  N2=N^2;
  denom =  sqrt(f2 * m^2 + N2 * kh^2) * (kh^2 + m^2)^(3/2);

  cgx =  (N2 - f2) * k * m^2 / denom;
  cgy =  (N2 - f2) * l * m^2 / denom;
  cgz = - (N2 - f2) * kh^2 * m / denom;

%-------------

kmag = sqrt(kh^2 + m^2);
denom = sqrt(kh^2 * N^2 + m^2 * f^2) * (kmag^2)^1.5;
numer = kh^2 * (f^2 - N^2) * (1 - m^2 * (f^2/(kh^2 * N^2 + m^2 * f^2) +
3/(kmag^2)));
omm = numer/denom;


F = [cgx + U;      cgy + V;     cgz;   ...
    -k*Uz-l*Vz;    -k * cgz * Uz - l * cgz*Vz;  ...
     omm*mz0;      (-k * Uzz - l * Vzz)*zz0];

function [U,V, Uz,Uzz, Vz,Vzz,env] = bgd(z,t,N,f,U0,z0env,Lenv,M, bflow)


if bflow == 0

    % Inertia wave packet with Gaussian envelope

    zz = z - z0env;

    env =  U0* exp(- z.^2 / Lenv^2);

    cphase = cos(M*z + f*t);
    sphase = sin(M*z + f*t);

    env_z =  -2 * (zz./Lenv^2) .* env;
    env_zz = -2 * (zz./Lenv^2) .* env_z - 2 /Lenv^2 .* env;

    U =  env .* cphase;
    Uz = env_z .* cphase - env .* M .* sphase;
    Uzz = env_zz .* cphase - 2 * env_z .* M .* sphase -  M^2 .* U;%

    V =  env .* sphase;
    Vz = env_z .* sphase + env .* M .* cphase;
    Vzz = env_zz .* sphase + 2 .* env_z .* M .* cphase -  M^2 .* V;
    end
```

```
    if bflow == 1

    % Background wind with Gaussian envelope

    zz = z - z0env;

    env =  U0* exp(- zz.^2 / Lenv^2);

    cphase = 1;
    sphase = 0;

    env_z =  -2 * (zz/Lenv^2) .* env;
    env_zz = -2 * (zz/Lenv^2) .* env_z - 2 /Lenv^2 .* env;

    U =  env .* cphase;
    Uz = cphase .* env_z;
    Uzz = cphase .* env_zz;

    V =  0;
    Vz = 0;
    Vzz = 0;
    End
end
```